A Cubic Spline Approximation for Fusion-Welding Problem in the Presence of Natural Convection

Weiliang Dai

A Thesis

in

The Department

of

Mechanical Engineering

Presented in Partial Fulfillment of the Requirements
for the Degree of Master of Mechanical Engineering at
Concordia University
Montréal, Quebéc, Canada

August 1986

ISBN 0-315-32250-0

ABSTRACT

A Cubic Spline Approximation for Fusion-Welding Problem in the Presence of Natural Convection

Weiliang Dai

A study of the characteristics of a fusion-welding problem with natural convection in the liquid region, involving melting and solidification processes, is conducted. The governing equations that describe the behaviour of the problem are formulated, and a cubic spline numerical approximation technique is developed and applied to solve such problems.

Results were obtained from aluminium and lead fusion welding processes for the moving interface, the temperature distribution in the liquid and solid regions, and the stream line pattern in the liquid region. The effect of dimensionless parameters, such as the Biot number, the superheating coefficient, the subcooling coefficient, and the aspect ratio on the average moving interface, was also studied. It has been found that the position of the moving interface varied considerablely along the vertical direction. These findings indicate that the effects of natural convection should be considered in metal fusion welding processes. It also reveals that the temperature in the liquid region was uniformly distributed at the melting point shortly after the moving interface reaches its maximum position. Therefore a pseudo one-dimensional model could be adopted, and the time consumption in calculation would be reduced dramatically.

ACKNOWLEDGEMENT

The author wishes to express his gratitude and deep appreciation to his thesis supervisors, Dr. S. Lin and Dr. C.K. Kwok, for initiating this project and providing continued guidance and financial support throughout the investigation.

The author also wishes to thank Michael Gregory for his valuable criticism in English.

Finally, the patient typing of Miss Xin Cao is gratefully acknowledged.

v

TABLE OF CONTENTS

LIST OF FIGURES

LIST OF TABLES

Fig. 13

Fig. 1

Fi

NOMENCLATURE

B_i	Biot number $= hD/k_s$	
c	specific heat	kJ/kg^oC
d_1	half width of the liquid region	m
d_2	width of the metal sheet	m
D	width of half system $= d_1+d_2$	m
g	acceleration of gravity	m/s^2
Gr	Grashof number $= g\beta(T_m-T_a)d_1^3/\nu^2$	
h	heat transfer coefficient of environment	$W/m^{2o}C$
H	height of the metal sheet	m
k	thermal conductivity	W/m^oC
k_r	dimensionless thermal conductivity $= k_s/k_\ell$	
Lq	latent heat of the fusion	kJ/kg
Nu	Nusselt number $= hH/k$	
p	pressure	N/m^2
Pr	Prandtl number $= \nu/\alpha_\ell$	
R	aspect ratio $= H/D$	
Ra	Rayleigh number $=$ GrPr	
Rs	ratio of liquid width to total width $= d_1/D$	
s	position of liquid-solid interface	m
Sp	Cubic Spline notation	
Ste	Stefan number $= Lq/c_p(T_m-T_a)$	
t	dimensional time	s
T	temperature	^oC

T_m	melting temperature of the material	^oC
T_a	ambient temperature	^oC
$T_{\ell o}$	initial temperature of the liquid region	^oC
T_{so}	initial temperature of the solid region	^oC
u	velocity component in x-direction	m/s
v	velocity component in y-direction	m/s

Greek Symbols

α	thermal diffusivity $= k/\rho c$	m^2/s
α_r	dimensionless thermal diffusivity $= \alpha_s/\alpha_\ell$	
β	thermal volumetric expansion coefficient of the liquid region	$1/^oC$
η	dimensionless moving boundary interface $= s/D$	
μ	dynamic viscosity	kg/ms
ν	kinematic viscosity $= \mu/\rho_o$	m^2/s
ρ	density	kg/m^3
ρ_o	density of the material at the melting temperature T_m	kg/m^3
τ	dimensionless time	
ϕ_c	coefficient of subcooling $= (T_{so}-T_a)/(T_m-T_a)$	
ϕ_h	coefficient of superheating $= (T_{\ell o}-T_a)/(T_m-T_a)$	
ψ	stream function	m^2/s
ω	vorticity	1/s

Subscripts

ℓ location within liquid region

s location within solid region

Superscripts

k k-th derivative

n n-th time interval

r r-th time interval

* dimensionless representation

CHAPTER ONE

INTRODUCTION

Fusion welding involves the welding together of two sheets of metal through the infusion of molten metal [1]. Depending on such factors as the welding set-up and the physical properties of the metal, there are two possible outcomes of a fusion welding heat transfer process [2]. One outcome is solidification of the molten metal only, usually a process akin to common soldering. Another outcome which is more desirable, however, is solidification following the melting of a small portion of the parent plate. This thesis proposes to examine the heat transfer behaviour of just such a fusion-welding process.

As is the case with phase-change problems, the most notable characteristic of the fusion-welding process is the existence of a moving interface between the liquid and solid phases. Prediction of the maximum moving interface position, as well as the temperature distribution and the rates of melting and solidification is a critical aspect of the control of the fundamental parameters of the fusion-welding process. It is such predictive ability that the thesis attempts to develop.

During the heat transfer process in phase-change problem, the intense heat possessed by molten metal is transferred to the surrounding material through conduction, and to lesser extents, convection and radiation [1]. As shown in [3], a review paper on the previous heat transfer literature, conduction is considered to be the only mode of heat transfer in the analysis of the most phase-change problems. A series of analytical solutions has been reported in the literature. A list of references for various analytical and numerical methods, when only the conduction is considered, has been provided by Wang et al.[2].

In recent years, more attention has been focused upon the associated convection flow developed in the liquid region during the heat transfer process. However, due to mathematical complexities, few numerical results have been produced. The natural convection flow developed in the liquid region due to the thermal gradient is very important as it can have a great effect on the moving interface [4]. Work pertaining to the phase-change problem involving natural convection can be found in Sparrow et al.[4], Ramachandran et al.[5], and Rieger et al.[6].

Sparrow et al.[4] developed an implicit finite difference scheme to solve a melting problem with a solid maintained at the fusion temperature. Rather than dealing with a transformed non-orthogonal computation grid, assumptions were made to drop terms related to the curvature of the phase boundary to obtain a solution with reasonable computational efforts. The phase position was determined at the end of each time step during the numerical computation, thus requiring adjustment of the dependent variables.

Following Sparrow's lead, Ramachandran et al.[5] carried out an analysis for the solidification in a rectangular enclosure with a subcooled solid region. A finite difference numerical analysis based on the same assumptions made in [4] was used to ease the computation. However instead of calculating the phase position at the end of each time step with a concomitant adjustment of the other dependent variables, Ramachandran et al. proposed a scheme to determine the phase position at the beginning of each time step without adjustment.

Rieger et al.[6] attempted to solve the melting process around a heated horizontal cylinder. The solid region was assumed to be at the melting temperature, and the difficulties of the handling of the moving interface were overcome by applying the so called "body-fitted coordinates numerical mapping" technique.

Fusion welding involves even greater complexities than those of the previously described cases. In fusion-welding problem, both melting and solidification processes appear, one following the other. In addition the superheating in liquid region and subcooling in solid region must also be considered. Unfortunately there appears to be a complete lack of published information to fusion welding problem with natural convection in the liquid region involving melting and solidification processes.

As formulated in [4,5,6], fusion-welding problem involving natural convection incorporates two spatial coordinates, as well as time. The complexity of the two-dimensional unsteady flow and heat transfer problem calls for the use of a numerical solution procedure. In this thesis, a cubic spline approximation numerical procedure was derived and adopted to solve the present fusion-welding problem.

The cubic spline approximation numerical technique has been applied to fluid mechanics by Rubin and Graves [7], Panton and Sallee [8], and Wang and Kahawita [9]. It has also been used in fusion welding analysis, but without consideration of the natural convection [2]. The principle advantages of using cubic spline approximation are as follows [2,7]:

1) High order accuracy for the first and second derivatives even with a non-uniform mesh. It is expected that for a uniform mesh, the spline approximation provides fourth order accuracy for the first derivative, with third order accuracy for a non-uniform grid. The second order accuracy for the second derivative is maintained for both uniform and non-uniform mesh.

2) The governing matrix system, obtained with the implicit formulation, will contain either the values of the functoin, its first derivative, or its second derivative at the node points. Such matrix system is always tridiagonal, thus facilitating any efficient inversion procedure.

3) A direct evaluation of spatial derivatives leads to an accurate determination of the gradient boundary conditions.

4) It is easy to adopt the non-uniform grids.

To employ the cubic spline approximation numerical procedure in solving the fusion-welding problem, a further study for the mixed boundary conditions has been made. A study of previously developed solution procedure using cubic spline techniques in [2], has shown that the tridiagonal matrix system is limited to the solution of transient problems. In the direct evaluation of the steady-state solution using cubic spline numerical techniques, a band matrix having six diagonals, two above the main diagonal and three below, has found.

In chapter two, a mathematical model of the fusion-welding problem is presented. A brief introduction to the cubic spline approximation technique is presented in chapter three. Chapter four presents the cubic spline approximation numerical procedure as employed in the solution of the fusion-welding problem. The numerical results of the fusion-welding problem under investigation are presented and discussed in chapter five. In the final chapter, the concluding remarks and suggestions for extension of the work done in this thesis are presented.

CHAPTER TWO

MATHEMATICAL FORMULATION OF THE FUSION-WELDING PROBLEM

The subject of this chapter is to derive the mathematical formulation of the fusion-welding problem with natural convection in the liquid region. Section 2.1 contains a description of the fusion-welding problem. In section 2.2, the governing differential equations relating to the conservation of mass, momentum, and energy are given. A vorticity and stream function representation is adopted to simplify the mathematical formulation. In the last section of this chapter, section 2.3, a dimensionless representation is made to generalize the derived model.

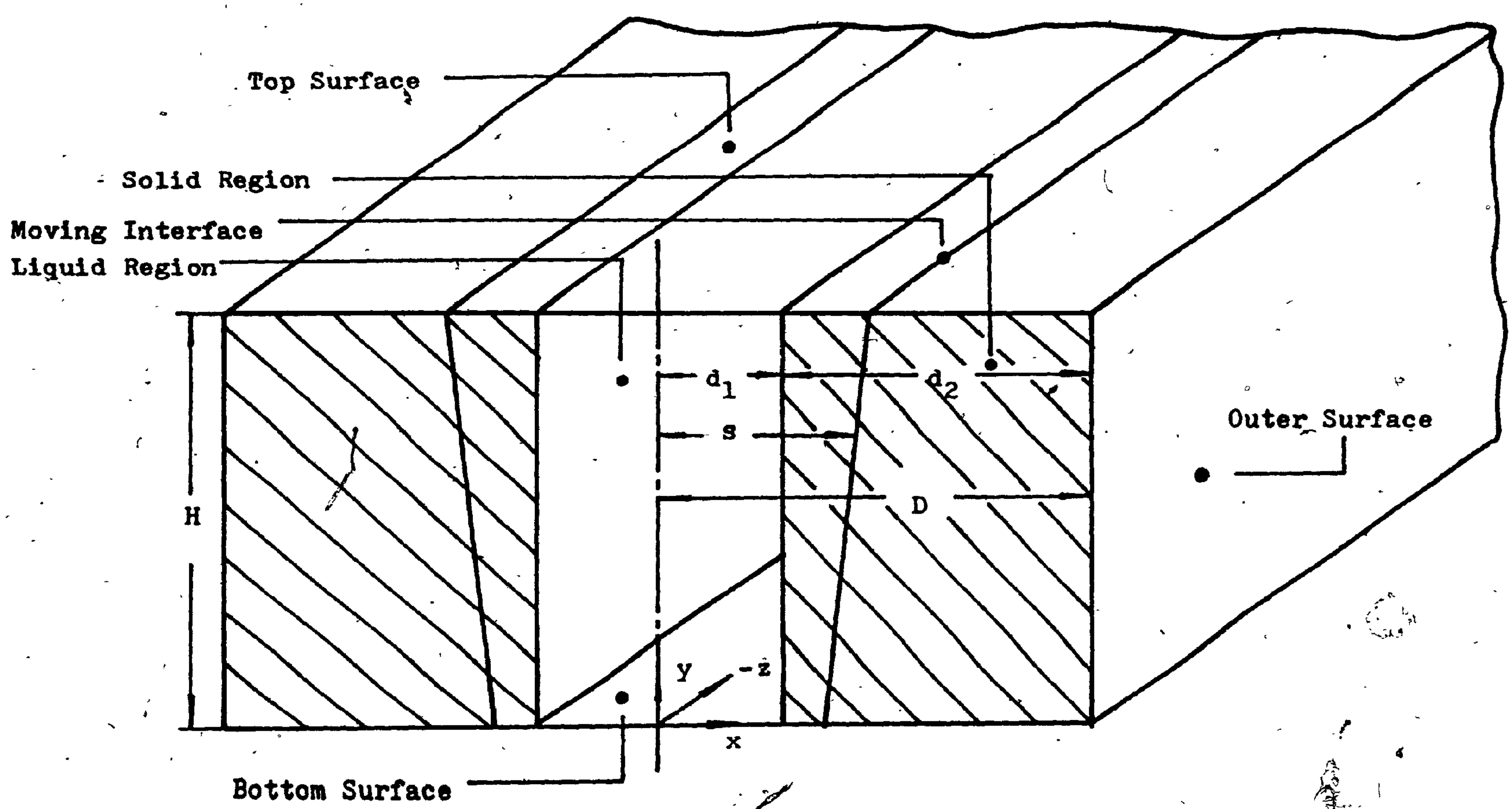

Figure 1. Schematic diagram of the fusion-welding problem

2.1. Problem Statement And Assumptions

As shown in Figure 1, consider two metal sheets formed of the same material of thickness d_2, height H, and infinity in z-direction, having identical dimensions. They are separated by a distance of $2d_1$. s is the position of the moving interface.

Initially, the solid metal is kept at a temperature T_{so} which is lower than the melting temperature T_m of that material. These two sheets are welded together by infusing molten metal of the same material having a uniform initial temperature $T_{\ell o}$ ($>T_m$). If the $T_{\ell o}$ is high enough, a thin layer of melting on the parent metal sheets will occur during the fusion-welding process. Under the influence of the buoyancy forces, there is a recirculating flow within the liquid region. As the melting and solidification processes progress, the liquid-solid interface becomes more sloped (as indicated schematically in figure 1).

In the analysis, the top and the bottom surfaces of the two metal sheets, and the top and bottom surfaces of the gap between those sheets are kept adiabatic. The outer vertical surfaces of the two metal sheets are exposed to an environment of temperature T_a ($<T_{so}$) with a heat transfer coefficient h.

The analyses and solutions were carried out according to the following objectives:

(1) Determination of the position of the moving interface during the melting and solidification.

(2) Determination of the rate of the melting and solidification.

(3) Determination of the time required to cool down the liquid region to solid state.

(4) Investigation of the effects of the natural convection in the fusion-welding problem.

(5) Investigation of the fluid flow in the liquid phase and the temperature distributions in the liquid and solid phases.

In the formulation of the fusion-welding problem, the following assumptions were made:

(1) All thermophysical properties, i.e. thermal conductivity, specific heat and viscosity, with the exception of the density of the liquid, were assumed to be independent of the temperature in the liquid and solid regions. The density variations in the liquid region were considered only insofar as they contributed to the buoyancy forces, but were otherwise neglected in accordence with the Boussinesq model [10]. Consequently, the fluid was considered to be incompressible.

(2) The density difference between the liquid and solid regions was neglected.

(3) The fluid in the liquid region was assumed to follow a Newtonian flow (i.e. shearing stress is linearly proportional to the rate of strain).

(4) Radiation in both liquid and solid regions was negligible.

Due to the symmetry of the problem shown in Fig. 1, only one half of it was studied.

2.2. Derivation of the Governing Equations Based on Temperature Model

Literature dealing with phase changes in heat transfer problems can be divided into two groups depending on the variables selected in the formulation of the problems [11,12]. In one group, based on the enthalpy model, the specific enthalpy is chosen as one of the dependent variables. An energy conservation equation is written for both liquid and solid regions, and the position of the liquid-solid interface is not determined explicitly but only approximately, by an examination of the enthalpy distribution. In the second group, the formulation is based on a temperature model, where the energy conservation equations are written separately for the liquid and solid regions in terms of the dependent variable, namely temperature. The liquid-solid interface is explicitly determined by making an energy balance on it.

In the problem statement in the last section, one of the main objectives was to determine the position of the moving interface. A temperature model was therefore used to formulate the fusion-welding problem in order to render an explicit determination of this position.

Using the Cartesian coordinate system, with the origin, x, y, and z axes are located as shown in figure 1, and note the system is extended from $-\infty$ to ∞ in z direction. The system of equations governing fluid flow and heat transfer in two-dimensional liquid-solid fusion-welding problems (with assumptions as per preceeding), is given as follows [13].

In the solid region, only the temperature distribution needs be considered, as conduction is the only mode of heat transfer in this region. The temperature distribution is governed by the energy equation,

$$\frac{\partial T_s}{\partial t} = \alpha_s\left(\frac{\partial^2 T_s}{\partial x^2} + \frac{\partial^2 T_s}{\partial y^2}\right) \qquad (2.2.1)$$

Where

T_s = temperature within the solid (^oC)

$\alpha_s = \frac{k_s}{\rho_o c_s}$, thermal diffusivity of the solid (m^2/s)

k_s = thermal conductivity of the solid (W/m^oC)

ρ_o = density of the material at the melting temperature (kg/m^3)

c_s = specific heat of the solid (kJ/kg^oC)

Equation 2.2.1 is subject to the following initial and boundary conditions :

$$\text{at } t = 0,\ T_s = T_{so} \qquad (2.2.2)$$

$$\text{at } x = s,\ T_s = T_m \qquad (2.2.3)$$

$$\text{at } x = D,\ -k_s \frac{\partial T_s}{\partial x} = h(T_s - T_a) \qquad (2.2.4)$$

$$\text{at } y = 0, \ \frac{\partial T_s}{\partial y} = 0 \tag{2.2.5}$$

$$\text{at } y = H, \ \frac{\partial T_s}{\partial y} = 0 \tag{2.2.6}$$

Where

s = position of liquid-solid interface (m)

$D = d_1+d_2$, width of half system (m)

H = height of the system (m)

T_m = melting temperature of the material (^oC)

T_a = ambient temperature (^oC)

h = heat transfer coefficient of environment ($W/m^{2o}C$)

T_{so} = initial temperature of solid region (^oC)

In the liquid region, with the Boussinesq approximation [10], the effect of temperature on density is confined to the bouyancy force term of the momentum equation. It is assumed to vary linearly with temperature:

$$\rho = \rho_0[1-\beta(T_\ell-T_m)] \tag{2.2.7}$$

Where,

β = thermal volumetric expansion coefficient of the liquid region ($1/^oC$)

T_ℓ = temperature within the liquid (^oC)

The equations, which govern the fluid flow and heat transfer in the liquid region, are as follows,

Continuity equation:

$$\frac{\partial u}{\partial x} + \frac{\partial v}{\partial y} = 0 \tag{2.2.8}$$

Momentum equations:

in the x-direction,

$$\frac{\partial u}{\partial t} + u\frac{\partial u}{\partial x} + v\frac{\partial u}{\partial y} = -\frac{1}{\rho_o}\frac{\partial p}{\partial x} + \nu\left(\frac{\partial^2 u}{\partial x^2} + \frac{\partial^2 u}{\partial y^2}\right) \tag{2.2.9}$$

and in the y-direction,

$$\frac{\partial v}{\partial t} + u\frac{\partial v}{\partial x} + v\frac{\partial v}{\partial y} = -\frac{1}{\rho_o}\frac{\partial p}{\partial y} + \nu\left(\frac{\partial^2 v}{\partial x^2} + \frac{\partial^2 v}{\partial y^2}\right) - g[1-\beta(T_\ell - T_m)] \tag{2.2.10}$$

Energy equation:

$$\frac{\partial T_\ell}{\partial t} + u\frac{\partial T_\ell}{\partial x} + v\frac{\partial T_\ell}{\partial y} = \alpha_\ell\left(\frac{\partial^2 T_\ell}{\partial x^2} + \frac{\partial^2 T_\ell}{\partial y^2}\right) \tag{2.2.11}$$

where,

u = velocity component in x direction (m/s)

v = velocity component in y direction (m/s)

p = pressure $[N/m^2]$

$\alpha_\ell = \dfrac{k_\ell}{\rho_o c_\ell}$ thermal diffusivity of the liquid (m^2/s)

k_ℓ = thermal conductivity of the liquid $(W/m\,^oC)$

c_ℓ = specific heat of the liquid (kJ/kg^{o}C)

μ = dynamic viscosity of the liquid (kg/ms)

$\nu = \frac{\mu}{\rho_o}$ kinematic viscosity of liquid (m^2/s)

The boundary and initial conditions for equation (2.2.8) to (2.2.11) are:

at $t = 0$, $u = v = 0$ (2.2.12)

$T_\ell = T_{\ell o}$ (2.2.13)

at $x = 0$, $u = 0,\ \frac{\partial v}{\partial x} = 0$ (2.2.14)

$\frac{\partial T_\ell}{\partial x} = 0$ (2.2.15)

at $x = s$, $v = 0,\ u = 0$ (2.2.16)

$T_\ell = T_m$ (2.2.17)

at $y = 0$, and $y = H$

$u = 0$,

$v = 0$ or $\frac{\partial v}{\partial x} = 0$ (2.2.18)

$\frac{\partial T_\ell}{\partial y} = 0$ (2.2.19)

where $T_{\ell o}$ represents initial temperature of the liquid region (^{o}C).

The second condition in eq.(2.2.18), $\frac{\partial v}{\partial x}$=0, is purely due to the consideration in the simplifications in later stream and vorticity representations. Mathematically speaking, the conditions v=0 and $\frac{\partial v}{\partial x}$=0 differs from a constant. However, by specifying initially v=0 and applying $\frac{\partial v}{\partial x}$=0 as boundary condition, the result will be the same as given v=0 as the boundary condition.

The energy balance at the liquid-solid interface can be described as follows[5],

$$\left(k_s \frac{\partial T_s}{\partial x} - k_\ell \frac{\partial T_\ell}{\partial x}\right) \left[1+\left(\frac{\partial s}{\partial y}\right)^2\right] = \rho_o Lq \frac{\partial s}{\partial t} \qquad (2.2.20)$$

where Lq represents the latent heat of fusion (kJ/kg), and the initial value of s is equal to d_1.

Note that the term $[1+(\frac{\partial s}{\partial y})^2]$ is necessitated by the curvilinear liquid-solid interface. If the initial temperature in the liquid region is higher than the melting temperature, during fusion welding, the liquid region will release heat to the solid region through the liquid-solid interface, at which the temperature remains at the melting temperature. Thus the temperature in the liquid region near the interface will decrease. According to the Boussinesq model [10], the density of the material in the liquid region near the interface will be increased. As a result, there is a natural convection in the liquid region. This natural convection produces a vertical temperature gradient, in which the temperature bordering the interface is higher at the top than at the bottom. Consequently, more molten metal will be formed at the top. These factors culminate in the formation of a curvilinear interface.

The formulation of the problem can be simplified by employing vorticity ω and stream function ψ. By first derivating equations (2.2.9) and (2.2.10) with respect to y and x respectively, and then combining them by employing equation (2.2.8), a vorticity equation can be derived as follows,

$$\frac{\partial\omega}{\partial t} + u\frac{\partial\omega}{\partial x} + v\frac{\partial\omega}{\partial y} = g\beta\frac{\partial T_\ell}{\partial x} + \nu\left(\frac{\partial^2\omega}{\partial x^2} + \frac{\partial^2\omega}{\partial y^2}\right) \tag{2.2.21}$$

where,

$$\omega = -\left(\frac{\partial^2\psi}{\partial x^2} + \frac{\partial^2\psi}{\partial y^2}\right) \tag{2.2.22}$$

$$u = \frac{\partial\psi}{\partial y}, \qquad v = -\frac{\partial\psi}{\partial x} \tag{2.2.23}$$

The boundary and initial conditions for equations (2.2.21)-(2.2.23) may be written as,

$$\text{at } t = 0, \qquad \psi = 0, \qquad \omega = 0 \tag{2.2.24}$$

$$\text{at } x = 0, \qquad \frac{\partial^2\psi}{\partial x^2} = 0, \qquad \omega = -\frac{\partial^2\psi}{\partial y^2} \tag{2.2.25}$$

$$\text{at } x = s, \qquad \frac{\partial\psi}{\partial x} = 0, \qquad \omega = -\left(\frac{\partial^2\psi}{\partial x^2} + \frac{\partial^2\psi}{\partial y^2}\right) \tag{2.2.26}$$

at $y = 0$ and $y = H$,

$$\frac{\partial\psi}{\partial y} = 0, \qquad \omega = -\frac{\partial^2\psi}{\partial y^2} \tag{2.2.27}$$

Therefore equations (2.2.1)-(2.2.6), (2.2.11), (2.2.13), (2.2.15), (2.2.17), (2.2.19) together with equations (2.2.20)-(2.2.27), form the mathematical representations of the fusion-welding problem concerned.

2.3. Dimensionless Representations of Governing Equations

To make the results more general, the following quantities are used,

$$x_\ell^* = \frac{x}{s}, \qquad x_s^* = \frac{x-s}{D-s}$$

$$t^* = \frac{\alpha_\ell t}{D^2}, \qquad y^* = \frac{y}{H}$$

$$u^* = \frac{uH}{\alpha_\ell}, \qquad v^* = \frac{vH}{\alpha_\ell} \tag{2.3.1}$$

$$\psi^* = \frac{\psi}{\alpha_\ell}, \qquad \omega^* = \frac{\omega D^2}{\alpha_\ell}$$

$$T_\ell^* = \frac{T_\ell - T_a}{T_m - T_a}, \qquad T_s^* = \frac{T_s - T_a}{T_m - T_a}$$

$$\phi_h = \frac{T_{\ell o} - T_a}{T_m - T_a}, \qquad \phi_c = \frac{T_{so} - T_a}{T_m - T_a}$$

Based on above transformation, the coordinate variables x, y, t are replaced by x_ℓ^*, x_s^*, y^*, t^*. Thus

$$\frac{\partial}{\partial t} = \frac{\alpha_\ell}{D^2}\frac{\partial}{\partial t^*} - \frac{x_\ell^*}{s}\frac{\partial s}{\partial t}\frac{\partial}{\partial x_\ell^*} \tag{2.3.2a}$$

$$\frac{\partial}{\partial x} = \frac{1}{s}\frac{\partial}{\partial x_\ell^*} \quad \text{or} \quad \frac{\partial}{\partial x} = \frac{1}{D-s}\frac{\partial}{\partial x_s^*} \tag{2.3.2b}$$

$$\frac{\partial}{\partial y} = \frac{1}{H}\frac{\partial}{\partial y^*} - \frac{x_\ell^*}{s}\frac{\partial s}{\partial y}\frac{\partial}{\partial x_\ell^*} \tag{2.3.2c}$$

Sparrow et al. [4] pointed out that in making the first approximation in a phase-change problem with natural convection, the terms $\partial s/\partial t$ and $\partial s/\partial y$ can be neglected. His reasoning follows from the assumptions listed below,

(1) The liquid-solid interface remains stationary for the time interval Δt, in which heat is extracted from it in the numerical solution procedure. Therefore $\partial s/\partial t$ appeared in equation (2.3.2a) can be neglected.

(2) The change of slope of the moving interface along y-direction in the time interval Δt is minimal. Therefore $\partial s/\partial y$ can be neglected.

Consideration of the above assumptions results in the following relations,

$$\frac{\partial}{\partial t} = \frac{\alpha_\ell}{D^2}\frac{\partial}{\partial t^*} \tag{2.3.3a}$$

$$\frac{\partial}{\partial x} = \frac{1}{s}\frac{\partial}{\partial x_\ell^*}, \quad \text{or} \quad \frac{\partial}{\partial x} = \frac{1}{D\text{-}s}\frac{\partial}{\partial x_s^*} \tag{2.3.3b}$$

$$\frac{\partial}{\partial y} = \frac{1}{H}\frac{\partial}{\partial y^*} \tag{2.3.3c}$$

The following dimensionless parameters are used in the late system of equations,

$Pr = \frac{\nu}{\alpha_\ell}$ Prandtl number

$Ra = GrPr$, Rayleigh number

$Gr = g\beta(T_m - T_a)\frac{d_1^3}{\nu^2}$ Grashof number

$Ste = \frac{Lq}{c_p(T_m - T_a)}$ Stefan number

$B_i = \frac{hD}{k_s}$ Biot number

$\eta = \frac{s}{D}$ dimensionless position of the liquid-solid interface

$R = \frac{H}{D}$ aspect ratio

$\alpha_r = \frac{\alpha_s}{\alpha_\ell}$ ratio of thermal diffusivities

$k_r = \frac{k_s}{k_\ell}$ ratio of thermal conductivities

$Rs = \frac{d_1}{D}$ ratio of liquid width to total width

Substituting equations (2.3.3a) to (2.3.3c) into the governing system of equations derived from the last section, the transformed dimensionless system of equations are expressed as follows.

In the solid region,

the energy equation,

$$\frac{\partial T_s^*}{\partial t^*} = \alpha_r [(\frac{1}{1-\eta})^2 \frac{\partial^2 T_s^*}{\partial x_s^{*2}} + \frac{1}{R^2} \frac{\partial^2 T_s^*}{\partial y^{*2}} \tag{2.3.4}$$

with the initial condition,

$$\text{at } t^* = 0, \quad T_s^* = \phi_c \tag{2.3.4a}$$

and the boundary conditions,

$$\text{at } x_s^* = 0, \quad T_s^* = 1 \tag{2.3.4b}$$

$$\text{at } x_s^* = 1, \quad \frac{\partial T_s^*}{\partial x_s^*} = -Bi(1-\eta)T_s^* \tag{2.3.4c}$$

at $y^* = 0$ and $y^* = 1$,

$$\frac{\partial T_s^*}{\partial y^*} = 0 \tag{2.3.4d}$$

In the liquid region,

the energy equation,

$$\frac{\partial T_\ell^*}{\partial t^*} + u^* \frac{1}{\eta R} \frac{\partial T_\ell^*}{\partial x_\ell^*} + v^* \frac{1}{R^2} \frac{\partial T_\ell^*}{\partial y^*} = \frac{1}{\eta^2} \frac{\partial^2 T_\ell^*}{\partial x_\ell^{*2}} + \frac{1}{R^2} \frac{\partial^2 T_\ell^*}{\partial y^{*2}} \tag{2.3.5}$$

the vorticity equation,

$$\frac{\partial \omega^*}{\partial t^*} + u^* \frac{1}{\eta R} \frac{\partial \omega^*}{\partial x_\ell^*} + v^* \frac{1}{R^2} \frac{\partial \omega^*}{\partial y^*} =$$

$$+ \mathrm{RaPr} \frac{1}{Rs^3 \eta} \frac{\partial T_\ell^*}{\partial x_\ell^*} + \Pr\left(\frac{1}{\eta^2} \frac{\partial^2 \omega^*}{\partial x_\ell^{*2}} + \frac{1}{R^2} \frac{\partial^2 \omega^*}{\partial y^{*2}}\right) \qquad (2.3.6)$$

where,

$$u^* = \frac{\partial \psi^*}{\partial y^*}, \qquad v^* = -\frac{R}{\eta} \frac{\partial \psi^*}{\partial x_\ell^*} \qquad (2.3.6a)$$

and the stream function equation,

$$\omega^* = -\left[\frac{1}{\eta^2} \frac{\partial^2 \psi^*}{\partial x_\ell^{*2}} + \frac{1}{R^2} \frac{\partial^2 \psi^*}{\partial y^{*2}}\right] \qquad (2.3.7)$$

with initial conditions,

$$\text{at } t^* = 0, \quad \psi^* = \omega^* = 0, \quad T_\ell^* = \phi_h \qquad (2.3.8a)$$

and boundary conditions,

at $x_\ell^* = 0$,

$$\frac{\partial^2 \psi^*}{\partial x_\ell^{*2}} = 0, \quad \omega^* = -\frac{1}{R^2} \frac{\partial^2 \psi^*}{\partial y^{*2}}, \quad \frac{\partial T_\ell^*}{\partial x_\ell^*} = 0 \qquad (2.3.8b)$$

at $x_\ell^* = 1$,

$$\frac{\partial \psi^*}{\partial x_\ell^*} = 0, \quad \omega^* = -\left(\frac{1}{\eta^2} \frac{\partial^2 \psi^*}{\partial x_\ell^{*2}} + \frac{1}{R^2} \frac{\partial^2 \psi^*}{\partial y^{*2}}\right), \quad T_\ell^* = 1 \qquad (2.3.8c)$$

at $y^* = 0$ and $y^* = 1$,

$$\frac{\partial \psi^*}{\partial y^*} = 0, \quad \omega^* = -\frac{1}{R^2}\frac{\partial^2 \psi^*}{\partial y^{*2}}, \quad \frac{\partial T_\ell^*}{\partial y^*} = 0 \qquad (2.3.8d)$$

In the liquid-solid interface,

$$\left(k_r \frac{1}{1-\eta}\frac{\partial T_s^*}{\partial x_s^*} - \frac{1}{\eta}\frac{\partial T_\ell^*}{\partial x_\ell^*}\right) = \mathrm{Ste}\,\frac{\partial \eta}{\partial t^*} \qquad (2.3.9)$$

The initial condition for the position of liquid-solid interface is $\eta(0) = d_1/D = Rs$.

Having derived the mathematical formulation, attention is now turned to the numerical method to be used in the solution of the fusion-welding problem.

CHAPTER THREE

CUBIC SPLINE APPROXIMATION METHOD

The finite difference and finite element numerical techniques are extensively used in the solution of engineering problems. In dealing with high order accuracy of solutions, lower cost in computer storage and computational time, derivative boundary conditions, irregular boundary, and so on, various different finite difference schemes were developed to satisfy different requirements. It is difficult to design one finite difference scheme which can satisfy all of these requirements. With the aid of the finite element technique, derivative boundary conditions are more easily solved, and the choice of non-uniform elements leads to the easy treatment of the irregular boundaries. However, as the complexity of the problem increases, the number of elements should also increase leading to a treatment of a very large coefficient matrix which contains many more non-zero entries than the usual finite difference technique. Therefore, it is also difficult to obtain such a finite element scheme which satisfies all those requirements stated above.

More recently, the cubic spline interpolation technique is introduced into the numerical solutions of partial differential equations [7,8,9]. A tridiagonal coefficient matrix, which is diagonal dominant, can be derived by applying cubic spline technique in solving the transient problems of any kind of specified boundary conditions. This allows a use of an efficient inversion algorithm. And the cubic spline technique is of high order accuracy even with a non-uniform mesh. As studied by Rubin et al. in [7], an overall second order accuracy will be easily obtained in solving partial differential equations (PDE) regardless the type of mesh and the boundary conditions. Hence, a well designed scheme, which leads to a high order accuracy , lower cost, easy treatment of derivative boundary and irregular boundary, can be expected by using cubic spline technique.

In this chapter, a brief introduction to cubic spline theory is made first in section 3.1. Followed in section 3.2, a cubic spline approximation procedures for solving the PDE of different prescribed boundary conditions are derived. In section 3.3, a spline alternating direction implicit (SADI) procedure is given for solving the two-dimensional problems. In the section 3.4, steady state solution of one-dimensiondal PDE by using cubic spline technique is discussed. And a tridiagonal coefficient matrix derived from the solution procedure of the transient problem no longer exists, instead a band coefficient matrix having width of six is found. A truncation error analysis and the improvement of accuracy for uniform mesh are made in the section 3.5 and section 3.6, respectively. In section 3.7, the cubic spline approximation for solution of a simple phase-change problem is presented. And its numerical result is compared with the exact solution. For more numerical examples, refer to Rubin et al. [7] and Wang et al. [9].

3.1. Basic Cubic Spline Theory

As mentioned in chapter one, Cubic Spline is a polynomial which is continuous, together with its first and second derivatives, over the entire region interested, i.e., it is a cubic polynomial on each subinterval, but it may discontinue for higher derivatives on the nodes connecting two subintervals [14].

In mathematical expression, consider a region [a,b], and

$$a = x_1 < x_2 \ldots\ldots < x_N < x_{N+1} = b$$

where $x_1, x_2, \ldots, x_{N+1}$ are nodal points inside region [a,b], and

$$h_i = x_i - x_{i-1} > 0.$$

And consider function $u(x) \in [a,b]$, such that at the nodal point x_i.

$$u(x_i) = u_i$$

Therefore, the cubic spline is defined as a function, Sp(x), which satisfies

$$Sp(x_i) = u_i \qquad 1 \leq i \leq N+1$$

Sp(x) is a cubic polynomial on each interval $[x_{i-1}, x_i]$, such that

$$Sp^k(x_i^-) = Sp^k(x_i^+) \qquad 1 \leq i \leq N+1$$

where the superscript k denotes the k-th derivative, and with $0 \leq k \leq 2$.

Then, in general, if $Sp(x)$ is a cubic polynomial on $[x_{i-1}, x_i]$, then

$$Sp''(x) = M_{i-1}\left(\frac{x_i - x}{h_i}\right) + M_i\left(\frac{x - x_{i-1}}{h_i}\right)$$

Where $M_i = Sp''(x_i)$

Integrating twice and evaluating the constants of integration by considering $Sp(x_i) = u_i$, $Sp(x_{i-1}) = u_{i-1}$, a useful spline interpolation formula can be obtained as follows:

$$Sp(x) = M_{i-1}\frac{(x_i - x)^3}{6h_i} + M_i\frac{(x - x_{i-1})^3}{6h_i} +$$

$$\left(u_{i-1} - \frac{M_{i-1}h_i^2}{6}\right)\frac{x_i - x}{h_i} + \left(u_i - \frac{M_i h_i^2}{6}\right)\frac{x - x_{i-1}}{h_i} \qquad (3.1.1)$$

By considering $Sp'(x_i^-) = Sp'(x_i^+)$, a relation between the second derivative and function is obtained [14],

$$\frac{h_i}{6}M_{i-1} + \frac{h_i + h_{i+1}}{3}M_i + \frac{h_{i+1}}{6}M_{i+1} = \frac{u_{i+1} - u_i}{h_{i+1}} - \frac{u_i - u_{i-1}}{h_i}$$

$$2 \leq i \leq N \qquad (3.1.2)$$

Additional relations obtained from equation (3.1.1) and (3.1.2) by using the compatibility on them, are listed below [14]:

$$\frac{1}{h_i}m_{i-1} + 2\left(\frac{1}{h_i} + \frac{1}{h_{i+1}}\right)m_i + \frac{1}{h_{i+1}}m_{i+1} = 3\,\frac{u_i - u_{i-1}}{h_i^2} + 3\,\frac{u_{i+1} - u_i}{h_{i+1}^2}$$

$$2 \le i \le N \tag{3.1.3}$$

where $m_i = Sp'(x_i)$

$$m_{i+1} - m_i = \frac{h_{i+1}}{2}(M_i + M_{i+1}), \qquad 1 \le i \le N \tag{3.1.4}$$

$$m_i = \frac{h_i}{3}M_i + \frac{h_i}{6}M_{i-1} + \frac{u_i - u_{i-1}}{h_i} \qquad 2 \le i \le N+1 \tag{3.1.5}$$

or $$m_i = -\frac{h_{i+1}}{3}M_i - \frac{h_{i+1}}{6}M_{i+1} + \frac{u_{i+1} - u_i}{h_{i+1}} \quad 1 \le i \le N \tag{3.1.6}$$

$$M_i = \frac{2m_{i-1}}{h_i} + \frac{4m_i}{h_i} - 6\,\frac{u_i - u_{i-1}}{h_i^2} \qquad 2 \le i \le N+1 \tag{3.1.7}$$

or $$M_i = -\frac{4m_i}{h_{i+1}} - \frac{2m_{i+1}}{h_{i+1}} + 6\,\frac{u_{i+1} - u_i}{h_{i+1}^2} \qquad 1 \le i \le N \tag{3.1.8}$$

With the above relation of equations (3.1.2) - (3.1.8), a development of the numerical solution procedure by using cubic spine is introduced in the next section.

3.2. Cubic Spline Approximation for Solving Partial Differential Equations

Consider a one-dimensional Quasi-linear second-order partial differential equation,

$$u_t = f(u, u_x, u_{xx}) \tag{3.2.1}$$

An approximate solution for u_i may be obtained by considering the solution of,

$$(u_t)_i = f(u_i, m_i, M_i) \qquad 2 \leq i \leq N \tag{3.2.2}$$

where the time derivative can be discretized in a manner as in the finite difference scheme, i.e.

$$\frac{u_i^{n+1} - u_i^n}{\Delta t} = (1-\theta)f_i^n + \theta f_i^{n+1} \tag{3.2.3}$$

It has to be noted that this is not the only way to discretize the time derivative, some other schemes may also be taken when one considers the accuracy or stability, etc. This will be discussed briefly in section 3.6. And here if $\theta = 0$, an explicit scheme is obtained, $\theta = 1$ will result in a fully implicit scheme, and while $\theta = 1/2$ a Crank-Nicolson scheme will be obtained [9].

Equation (3.2.3) may be rewritten as follows,

$$u_i^{n+1} = u_i^n + \Delta t(1-\theta)f_i^n + \Delta t\theta f_i^{n+1}$$

$$= F_i + R_i m_i^{n+1} + Q_i M_i^{n+1} \tag{3.2.4}$$

where,

$$F_i = g_1(u_i^n,\ m_i^n,\ M_i^n,\ x,\ t,\ \Delta t,\ \theta) \tag{3.2.4a}$$

$$R_i = g_2(\ x,\ t,\ \Delta t,\ \theta) \tag{3.2.4b}$$

$$Q_i = g_3(\ x,\ t,\ \Delta t,\ \theta) \tag{3.2.4c}$$

For a given function of f, the functions of F_i, R_i, and Q_i can be defined.

Since i is equal to 1 to N+1 in equation (3.2.2), there are 3(N+1) unknowns to be determined. However, from equations (3.2.4), (3.1.2) and (3.1.3), a system of 3(N-1) equations can be obtained. To close this system, another six conditions are necessary. Two of these can be derived from the given boundary conditions. The remaining four conditions can be obtained by making use of the spline relations of equation (3.1.4) to (3.1.8) and the governing equation (3.2.4). The following example will explain the discretization of a given system.

Example 1

Consider a one-dimensional heat conduction equation,

$$\frac{\partial u}{\partial t} = \frac{\partial^2 u}{\partial x^2}$$

A possible discritization of this equation is,

$$\frac{u_i^{n+1} - u_i^n}{\Delta t} = (1-\theta)M_i^n + \theta M_i^{n+1}$$

or $$u_i^{n+1} = u_i^n + \Delta t[(1-\theta)M_i^n + \theta M_i^{n+1}]$$

This results in the following values for the coefficients of equation (3.2.4),

$$F_i = u_i^n + \Delta t(1-\theta)M_i^n$$

$$R_i = 0$$

$$Q_i = \Delta t\theta$$

If an implicit scheme is considered, i.e. $\theta = 1$, it follows that

$$F_i = u_i^n, \quad R_i = 0, \quad Q_i = \Delta t$$

If an explicit scheme is used, i.e. $\theta = 0$, it follows that

$$F_i = u_i^n + \Delta t M_i^n, \quad R_i = 0, \quad Q_i = 0$$

When the Crank-Nicolson scheme is adopted, it follows,

$$F_i = u_i^n + \Delta t M_i^n/2, \quad R_i = 0, \quad Q_i = \Delta t/2$$

In section (3.2.1), a compact equation is given for u_i represented in a single tridiagonal system. It can be directly solved, together with the prescribed boundary conditions for u_i. In sections (3.2.2), (3.2.3), and (3.2.4), the solution procedures for a given system of equations are derived for the prescribed boundary conditions given in the forms of m_i, M_i, and mixed, respectively.

3.2.1. Prescribed Boundary Conditions for u_i

A single tridiagonal system for u_i can be derived by first using governing equation (3.2.4) and the spline relations (3.1.5) and (3.1.6) to obtain the expressions for M_{i-1}, M_i, and M_{i+1} in terms of u_{i-1}, u_i, and u_{i+1}. Substituting these expressions into equation (3.1.2) gives following results [15],

$$A_i u_{i-1}^{n+1} + B_i u_i^{n+1} + C_i u_{i+1}^{n+1} = D_i, \qquad 2 \leq i \leq N \tag{3.2.5}$$

where

$$A_i = \frac{e_i h_i}{6c_i} - \frac{1}{h_i}$$

$$B_i = \frac{d_i h_i}{6c_i} + \frac{e_{i+1}(h_i+h_{i+1})}{3c_{i+1}} -$$

$$\frac{R_{i+1}(h_{i+1}^2+3R_i h_{i+1}-6Q_i)}{36c_{i+1}} + \frac{h_i+h_{i+1}}{h_i h_{i+1}}$$

$$C_i = \frac{d_{i+1}(h_i+h_{i+1})}{3c_{i+1}} - \frac{1}{h_{i+1}} -$$

$$\frac{R_i(2h_{i+1}-3R_{i+1})h_{i+1}-6Q_i(h_{i+1}-R_{i+1})}{36c_{i+1}}$$

$$D_i = \frac{a_i h_i}{6c_i} + \frac{a_{i+1}(h_i+h_{i+1})}{3c_{i+1}} -$$

$$\frac{F_{i+1}(2R_i h_{i+1} - 6Q_i) + F_i R_{i+1} h_{i+1}}{36 c_{i+1}} \, h_{i+1}$$

$$a_i = \frac{F_i R_{i-1} h_i}{6} + F_{i-1}\left(\frac{R_i h_i}{3} + Q_i\right)$$

$$c_i = \frac{R_i R_{i-1} h_i^2}{36} - \frac{(R_i h_i + 3Q_i)(R_{i-1} h_i - 3Q_{i-1})}{9}$$

$$d_i = R_{i-1}\left(\frac{h_i}{6} - \frac{R_i}{2} - \frac{Q_i}{h_i}\right)$$

$$e_i = R_i\left(\frac{h_i}{3} + \frac{R_{i-1}}{2}\right) + Q_i\left(1 + \frac{R_{i-1}}{h_i}\right)$$

$$h_i = x_i - x_{i-1} .$$

Equation (3.2.5) can be solved together with the prescribed boundary conditions for u_i by any efficient inversion algorithm.

To determine m_i after solving for u_i, the governing equation (3.2.4) may be employed by replacing M_i with equation (3.1.7) for $i \neq 1$, or equation (3.1.8) for $i = 1$. The following relation is obtained,

$$[A][m]^T = [D]^T \qquad (3.2.6)$$

where

$$[A] = \begin{bmatrix} a_1, & b_1, & 0, & 0, & \ldots, & 0, & 0 \\ a_2, & b_2, & 0, & 0, & \ldots, & 0, & 0 \\ 0, & a_3, & b_3, & 0, & \ldots, & 0, & 0 \\ 0, & 0, & a_4, & b_4, & \ldots, & 0, & 0 \\ .. & .. & .. & .. & \ldots & .. & .. \\ 0, & 0, & 0, & 0, & a_N, & b_N, & 0 \\ 0, & 0, & 0, & 0, & \ldots, & a_{N+1}, & b_{N+1} \end{bmatrix}$$

$$[m] = [m_1, m_2, m_3, \ldots, m_{N+1}]^{n+1}$$

$$[D] = [d_1, d_2, d_3, \ldots, d_{N+1}]$$

where,

$$a_1 = -R_1 + \frac{4Q_1}{h_2}$$

$$b_1 = \frac{2Q_1}{h_2}$$

$$d_1 = F_1 - u_1^{n+1} + 6Q_1 \frac{u_2^{n+1} - u_1^{n+1}}{h_2^2}$$

$$a_i = -\frac{2Q_i}{h_i}$$

$$b_i = -R_i - \frac{4Q_i}{h_i} \qquad 2 \leq i \leq N+1$$

$$d_i = F_i - u_i^{n+1} - 6Q_i \frac{u_i^{n+1} - u_{i-1}^{n+1}}{h_i^2}$$

Thus equation (3.2.6) can be solved by following recursive relations.

$$m_1^{n+1} = \frac{d_1 b_2 - d_2 b_1}{a_1 b_2 - a_2 b_1}$$

$$m_i^{n+1} = \frac{d_i - a_i m_{i-1}^{n+1}}{b_i} \qquad 2 \leq i \leq N+1 \qquad (3.2.6a)$$

And it is easy to obtain M_i for given known values for both u_i and m_i, by directly evaluating equation (3.1.7) for $i \neq 1$, and equation (3.1.8) for $i=1$.

3.2.2. Prescribed Boundary Conditions for m_i

By first using equations (3.1.7) and (3.1.8) to eliminate M_i from the governing equation (3.2.4), the expressions for $(u_i - u_{i-1})$ and $(u_{i+1} - u_i)$ in terms of m_{i-1}, m_i and m_{i+1} can be obtained. Substituting these expressions into equation (3.1.3), permits the derivation of a single tridiagonal system, as shown below [15],

$$A_i m_{i-1}^{n+1} + B_i m_i^{n+1} + C_i m_{i+1}^{n+1} = D_i, \qquad 2 \leq i \leq N \qquad (3.2.7)$$

where,

$$A_i = \frac{1}{3h_i} - \frac{2Q_i + 4Q_{i-1} - R_{i-1} h_i}{h_i^3 e_i}$$

$$B_i = \frac{2}{3}\left(\frac{1}{h_i} + \frac{1}{h_{i+1}} \right) - \frac{2Q_{i+1} + 4Q_i - R_i h_{i+1}}{h_{i+1}^3 e_{i+1}}$$

$$- \frac{2Q_{i-1} + 4Q_i - R_i h_i}{h_i^3 e_i}$$

$$C_i = \frac{1}{3h_{i+1}} - \frac{2Q_i + 4Q_{i+1} + R_{i+1} h_{i+1}}{h_{i+1}^3 e_{i+1}}$$

$$D_i = \frac{F_{i+1} - F_i}{h_{i+1}^2 e_{i+1}} + \frac{F_i - F_{i-1}}{h_i^2 e_i}$$

$$e_i = 1 + 6\,\frac{Q_i + Q_{i-1}}{h_i^2}$$

Equation (3.2.7) can be solved together with the prescribed boundary conditions for m_i using any efficient inversion algorithm.

When m_i is known, determination of u_i may be accomplished by means of a simple relation between u_i and m_i. This involves replacing M_i in the governing equation (3.2.4) with equation (3.1.7) for $i \neq 1$, or equation (3.1.8) for $i = 1$. The relation can be stated in the matrix form as follows,

$$[A]\ [U]^T = [D]^T \tag{3.2.8}$$

where

$$[A] = \begin{bmatrix} a_1, & b_1, & 0, & 0, & \ldots, & 0, & 0 \\ a_2, & b_2, & 0, & 0, & \ldots, & 0, & 0 \\ 0, & a_3, & b_3, & 0, & \ldots, & 0, & 0 \\ 0, & 0, & a_4, & b_4, & \ldots, & 0, & 0 \\ .. & .. & .. & .. & \ldots & .. & .. \\ 0, & 0, & 0, & 0, & a_N, & b_N, & 0 \\ 0, & 0, & 0, & 0, & \ldots, & a_{N+1}, & b_{N+1} \end{bmatrix}$$

$$[U] = [u_1,\ u_2,\ u_3,\ \ldots,\ u_{N+1}]^{n+1}$$

$$[D] = [d_1,\ d_2,\ d_3,\ \ldots,\ d_{N+1}]$$

where,

$$a_1 = 1 + \frac{6Q_1}{h_2^2}$$

$$b_1 = -\frac{6Q_1}{h_2^2}$$

$$d_1 = F_1+R_1 m_1^{n+1}-Q_1 \frac{2m_2^{n+1}+4m_1^{n+1}}{h_2}$$

$$a_i = -\frac{6Q_i}{h_i^2}$$

$$b_i = 1 + \frac{6Q_i}{h_i^2} \qquad 2\leq i\leq N+1$$

$$d_i = F_i + R_i m_i^{n+1} + Q_i \frac{2m_{i-1}^{n+1}+4m_i^{n+1}}{h_i}$$

Equation (3.2.8) can be solved by using the following simple series of recursive relations,

$$u_1^{n+1} = \frac{d_1 b_2 - d_2 b_1}{a_1 b_2 - a_2 b_1}$$

$$u_i^{n+1} = \frac{d_i - a_i u_{i-1}^{n+1}}{b_i} \qquad 2\leq i\leq N+1 \qquad (3.2.8a)$$

In the determination of M_i, equation (3.1.7) for $i\neq 1$, and equation (3.1.8) for $i=1$, can be directly evaluated for M_i without complication.

3.2.3. Prescribed Boundary Conditions for M_i

As was done in arriving at equation (3.2.7), elimination of m_i from the governing equation (3.2.4) through the employment of the spline relation of equations (3.1.5) and (3.1.6), permits the derivation of the expressions for $(u_{i+1}-u_i)$ and (u_i-u_{i-1}). Substituting them into (3.1.2), gives a tridiagonal system containing only the second derivatives, and is derived as follows [15],

$$A_i M_{i-1}^{n+1} + B_i M_i^{n+1} + C_i M_{i+1}^{n+1} = D_i, \quad 2 \leq i \leq N \qquad (3.2.9)$$

where,

$$A_i = \frac{h_i}{6} + \frac{R_i + 2R_{i-1}}{6e_i} - \frac{Q_{i-1}}{h_i e_i}$$

$$B_i = \frac{h_i + h_{i+1}}{3} - \frac{R_{i+1} + 2R_i}{6e_{i+1}} +$$

$$\frac{2R_i + R_{i-1}}{6e_i} + Q_i\left(\frac{1}{e_{i+1} h_{i+1}} + \frac{1}{e_i h_i}\right)$$

$$C_i = \frac{h_{i+1}}{6} - \frac{2R_{i+1} + R_i}{6e_{i+1}} - \frac{Q_{i+1}}{h_{i+1} e_{i+1}}$$

$$D_i = \frac{F_{i+1} - F_i}{e_{i+1} h_{i+1}} - \frac{F_i - F_{i-1}}{e_i h_i}$$

$$e_i = 1 - \frac{R_i - R_{i-1}}{h_i}$$

Equation (3.2.9) can be solved together with the prescribed boundary conditions for M_i by any efficient inversion algorithm.

Having obtained values for M_i, it is possible to determine u_i by means of a simple relation between u_i and M_i which can be derived by replacing m_i in the governing equation (3.2.4) with equation (3.1.5) for $i \neq 1$, or equation (3.1.6) for $i=1$. The result can be given in the matrix form as follows,

$$[A]\,[U]^T = [D]^T \tag{3.2.10}$$

where

$$[A] = \begin{bmatrix} a_1, & b_1, & 0, & 0, & ..., & 0, & 0 \\ a_2, & b_2, & 0, & 0, & ..., & 0, & 0 \\ 0, & a_3, & b_3, & 0, & ..., & 0, & 0 \\ 0, & 0, & a_4, & b_4, & ..., & 0, & 0 \\ .. & .. & .. & .. & .. & .. & .. \\ 0, & 0, & 0, & 0, & a_N, & b_N, & 0 \\ 0, & 0, & 0, & 0, & ..., & a_{N+1}, & b_{N+1} \end{bmatrix}$$

$$[U] = [u_1,\ u_2,\ u_3,\ ...,\ u_{N+1}]^{n+1}$$

$$[D] = [d_1,\ d_2,\ d_3,\ ...,\ d_{N+1}]$$

Where,

$$a_1 = 1 + \frac{R_1}{h_2}$$

$$b_1 = \frac{R_1}{h_2}$$

$$d_1 = F_1 - R_1\left(\frac{h_2}{6} M_2^{n+1} + \frac{h_2}{3} M_1^{n+1}\right) + Q_1 M_1^{n+1}$$

$$a_i = \frac{R_i}{h_i}$$

$$b_i = 1 - \frac{R_i}{h_i}$$

$$d_i = F_i + R_i\left(\frac{h_i}{3} M_i^{n+1} + \frac{h_i}{6} M_{i-1}^{n+1}\right) + Q_i M_i^{n+1}$$

A simple recursive relation can then be derived to solve equation (3.2.10) as follow,

$$u_1^{n+1} = \frac{d_1 b_2 - b_1 d_2}{a_1 b_2 - b_1 a_2}$$

$$u_i^{n+1} = \frac{d_i - a_i u_{i-1}^{n+1}}{b_i} \qquad 2 \leq i \leq N+1 \qquad (3.2.10a)$$

The values of m_i may then be evaluated directly from equation (3.1.5) for $i \neq 1$, and equation (3.1.6) for $i = 1$.

3.2.4. Prescribed Mixed Boundary Conditions

In previous sections, the prescribed boundary conditions are the same at both ends, either both in u_i, or both in m_i, and or both in M_i. However, there are also other kinds of boundary conditions. For example, if one end of the boundary condition is specified in u_i with the other end in m_i, or M_i, or even at the same end, a function of u_i and m_i is specified. Hereafter, such kinds of boundary conditions will be referred to as mixed boundary conditions.

In this section, we introduce a method to transfer a given mixed boundary condition to u_i. The procedure specified in section (3.2.1) can then be adopted to solve the given system. Two types of mixed boundary conditions will be discussed as follows.

Mixed boundary condition 1.

Consider the following form of mixed boundary condition,

$$\frac{\partial u}{\partial x} + pu = q \qquad \text{at } x = a \tag{3.2.11}$$

where p and q can be functions of time.

The corresponding discretization of equation (3.2.11) by using cubic spline approximation may be in following form,

$$m_1 + pu_1 = q \tag{3.2.12}$$

To transfer the above boundary condition to a relation in u_i only, the governing equation (3.2.4) is employed. First, spline relations (3.1.7) and (3.1.8) are substituted into the governing equation (3.2.4) for i=2 and i=1, respectively. Two equations can be obtained which only contain u_1, u_2, m_1, and m_2. Eleminating m_2 from these two equations produces a relation between u_1, u_2 and m_1. Finally, substituting equation (3.2.12) into this relation, gives a relation between u_1 and u_2, as shown below.

$$B_1 u_1 + C_1 u_2 = D_1 \tag{3.2.13}$$

where,

$$B_1 = \frac{6Q_2}{h_2^2} - d_1\left(\frac{h_2}{2Q_1} + \frac{3}{h_2}\right) + e_1 p$$

$$C_1 = d_1 \frac{3}{h_2} - \left(1 + \frac{6Q_2}{h_2^2}\right)$$

$$D_1 = -\frac{h_2}{2Q_1} d_1 F_1 - F_2 + e_1 q \tag{3.2.13a}$$

$$d_1 = R_2 + \frac{4Q_2}{h_2}$$

$$e_1 = -d_1\left(\frac{R_1 h_2}{2Q_1} - 2\right) - \frac{2Q_2}{h_2}$$

If the boundary condition (3.2.11) is given at $x=b$, the discretized form of the condition (3.2.11) can be as follows,

$$m_{N+1} + p u_{N+1} = q \tag{3.2.14}$$

In the same fashion as that used to derive the equation (3.2.13), a relation between u_N and u_{N+1} is obtained as follows,

$$A_{N+1}u_N + B_{N+1}u_{N+1} = D_{N+1} \tag{3.2.15}$$

where,

$$A_{N+1} = -d_2 \frac{3}{h_{N+1}} - (1+ \frac{6Q_N}{h^2_{N+1}})$$

$$B_{N+1} = \frac{6Q_N}{h^2_{N+1}} + d_2(\frac{h_{N+1}}{2Q_{N+1}} + \frac{3}{h_{N+1}}) + e_2 p$$

$$D_{N+1} = \frac{h_{N+1}}{2Q_{N+1}} d_2 F_{N+1} - F_N + e_2 q \tag{3.2.15a}$$

$$d_2 = R_N - 4 \frac{Q_N}{h_{N+1}}$$

$$e_2 = \frac{2Q_N}{h_{N+1}} + d_2(\frac{h_{N+1}R_{N+1}}{2Q_{N+1}} + 2)$$

Mixed boundary condition 2.

Consider the following form of the boundary condition,

$$\frac{\partial^2 u}{\partial x^2} = q, \qquad \text{at } x=a \tag{3.2.16}$$

where q can be a function of time.

The discretized form of (3.2.16) can be,

$$M_1 = q, \tag{3.2.17}$$

To transfer above boundary condition to a relation in u_1 only, the governing equation (3.2.4) is employed. First the spline relations (3.1.5) and (3.1.6) are substituted into the governing equation (3.2.4) for i=2 and i=1, respectively. The resulting two equations contain only u_1, u_2, M_1, and M_2. Elimination of M_2 from these two equations gives a relation between u_1, u_2 and M_1. Finally, substituting equation (3.2.17) into this relation, produces a further relation between u_1 and u_2, obtained as follows,

$$B_1u_1 + C_1u_2 = D_1 \tag{3.2.18}$$

where,

$$B_1 = -d_1(1 + \frac{R_1}{R_2}) - \frac{R_2}{h_2}$$

$$C_1 = d_1 \frac{R_1}{h_2} - 1 + \frac{R_2}{h_2}$$

$$D_1 = -d_1F_1 - F_2 + e_1q$$

$$d_1 = \frac{2R_2}{R_1} + \frac{6Q_2}{R_1h_2}$$

$$e_1 = d_1(\frac{R_1h_2}{3} - Q_1) - \frac{R_2h_2}{6}$$

If the boundary condition, equation (3.2.16), is given at x=b, we may have

$$M_{N+1} = q \tag{3.2.19}$$

Using the same procedure used to derive equation (3.2.18), a relation between u_N and u_{N+1} can be obtained as follows,

$$A_{N+1}u_N + B_{N+1}u_{N+1} = D_{N+1} \tag{3.2.20}$$

where,

$$A_{N+1} = d_2 \frac{R_{N+1}}{h_{N+1}} - (1+ \frac{R_N}{h_{N+1}})$$

$$B_{N+1} = d_2(1- \frac{R_{N+1}}{h_{N+1}})+ \frac{R_N}{h_{N+1}}$$

$$D_{N+1} = d_2F_{N+1} - F_N + e_2q$$

$$d_2 = \frac{6Q_N}{R_{N+1}h_{N+1}} - \frac{2R_N}{R_{N+1}}$$

$$e_2 = d_2(Q_{N+1} + \frac{R_{N+1}h_{N+1}}{3}) + \frac{R_N h_{N+1}}{6}$$

Having demonstrated the method of transferring a boundary condition other than specified for u_i to u_i, we will now provide an example showing how to use it in the solution of a given problem.

Example 2

Consider a one-dimensional heat conduction equation,

$$\frac{\partial u}{\partial t} = \frac{\partial^2 u}{\partial x^2} \qquad 0<x<1,\ t>0 \tag{3.2.21}$$

together with the boundary conditions,

$$u = u_a, \qquad \text{at } x=0 \tag{3.2.21a}$$

$$\frac{\partial u}{\partial x} = h(u-u_b), \qquad \text{at } x=1 \tag{3.2.21b}$$

Equation (3.2.21) can be discretized in the implicit form,

$$u_i^{n+1} = F_i+R_i m_i^{n+1} + Q_i M_i^{n+1} \qquad 2\leq i\leq N \tag{3.2.22}$$

where,

$$F_i = u_i^n, \quad R_i = 0, \quad \text{and } Q_i = \Delta t$$

Using equation (3.2.15), the boundary condition at x=1 may be discretized as,

$$A_{N+1}u_N^{n+1} + B_{N+1}u_{N+1}^{n+1} = D_{N+1} \tag{3.2.23}$$

where A_{N+1}, B_{N+1} and D_{N+1} are defined as in equation (3.2.15a), which are functions of time.

By using boundary conditions equation (3.2.21a) and (3.2.23) together with equations (3.2.5), a system of equations in the matrix form is produced as follows,

$$\begin{bmatrix} 1, & 0, & 0, & 0, & \dots, & 0, & 0, & 0 \\ A_2, & B_2, & C_2, & 0, & \dots, & 0, & 0, & 0 \\ 0, & A_3, & B_3, & C_3, & \dots, & 0, & 0, & 0 \\ .. & .. & .. & .. & ... & .. & .. & .. \\ 0, & 0, & 0, & 0, & \dots, & A_N, & B_N, & C_N \\ 0, & 0, & 0, & 0, & \dots, & 0, & A_{N+1}, & B_{N+1} \end{bmatrix} \begin{bmatrix} u_1 \\ u_2 \\ u_3 \\ .. \\ u_N \\ u_{N+1} \end{bmatrix} = \begin{bmatrix} u_a \\ D_2 \\ D_3 \\ .. \\ D_N \\ D_{N+1} \end{bmatrix}$$

This tridiagonal system can be solved for u_i, allowing m_i and M_i to be calculated as in section (3.2.1).

From this example it can be seen that, a given mixed boundary condition can be transferred to a relation in u_i by using the governing equation (3.2.4), with the corresponding spline relations, equations (3.1.5) to (3.1.8). Hence the solution procedure given in section (3.2.1) can be used to solve u_i, m_i, and M_i sequentially. Thus, this method appears to be very advantageous in the solution of problems having mixed boundary conditions.

3.3. Two-Dimensional Problem Using SADI Procedure

As is well known, the Alternating Direction Implicit (ADI) method can be used in the solution of two-dimensional numerical problems. Rubin et al. [7] and Wang [9], the first two to use ADI in Cubic Spline Approximation in two-dimensional problems, have developed a Spline Alternating Direction Implicit (SADI) method. It can be briefly introduced here.

For a equation with two spatial dimensions, such that

$$u_t = f(u, u_x, u_y, u_{xx}, u_{yy})$$

a two step SADI formulation is of the following form,

step 1:

$$u_{ij}^{n+1/2} = u_{ij}^{n} + \frac{\Delta t}{2} f(u_{ij}^{n}, m_{ij}^{n+1/2}, M_{ij}^{n+1/2}, \ell_{ij}^{n}, L_{ij}^{n})$$

step 2:

$$u_{ij}^{n+1} = u_{ij}^{n+1/2} + \frac{\Delta t}{2} f(u_{ij}^{n+1/2}, m_{ij}^{n+1/2}, M_{ij}^{n+1/2}, \ell_{ij}^{n+1}, L_{ij}^{n+1})$$

where ℓ_{ij} and L_{ij} are the spline approximations to the first and second derivatives of u with respect to y, respectively. The cubic spline relations (equations (3.1.2)-(3.1.8)), may be directly expanded to the above two-dimensional case.

3.4. Steady State Problems Using Cubic Spline Approximation

In a manner similar to that used in section 3.2, a tridiagonal system can be derived to solve a system of equations through the use of cubic spline approximation. It could be observed that the solution procedures of those tridiagonal systems derived in section 3.2, are all need to have the knowledge of the values of function, its first and second derivatives from the previous time step. In other words, the solution procedures so derived as in section 3.2, are recursive ones. If only steady state solutions are sought, a direct method outlined below is preferable.

Consider the steady state solution of a one-dimensional second order PDE ,

$$f(u, u_x, u_{xx}) = 0 \tag{3.4.1}$$

An approximate solution using cubic spline interpolation can be constructed by considering the solution of,

$$f(u_i, m_i, M_i) = 0 \tag{3.4.2}$$

Where u_i, m_i and M_i are the spline function, and its first and second derivatives, respectively.

To solve equation (3.4.2), m_i or M_i can be transferred to a relation containinging u_i and M_i (or u_i and m_i) by using basic spline relations of equations (3.1.5) and (3.1.6) (or equations (3.1.7) and (3.1.8)).

Case 1.

If equations (3.1.5) and (3.1.6) are incorporated, equation (3.4.2) can be reduced to,

$$g(u_i, M_i) = 0 \qquad 2 \leq i \leq N \qquad (3.4.3)$$

equation (3.4.3) can be solved together with equation (3.1.2) and the proper boundary conditions. It is obvious that the system under consideration is a $2(N+1)\times 2(N+1)$ spare matrix. After carefully arranging the variables, a band matrix having 6 diagonals(2 above the main diagonal, 3 below it) is found rather than a tridiagonal one.

Case 2.

If equations (3.1.7) and (3.1.8) are used, equation (3.4.2) is reduced to,

$$g(u_i, m_i) = 0 \qquad (3.4.4)$$

Equation (3.4.4) can be solved together with the equation (3.1.3) and the proper boundary conditions. The following example shows how to use the cubic spline technique to obtain steady state solutions.

Example 3

Consider the solution of the following equation,

$$\frac{\partial^2 u}{\partial x^2} + a(x)\frac{\partial u}{\partial x} + b(x) = 0 \qquad (3.4.5)$$

or in the discretized form,

$$M_i + a_i m_i + b_i = 0 \tag{3.4.6}$$

The boundary conditions, which are the same as in equations (3.2.21a) and (3.2.21b), in the discretized forms are,

$$u_1 = u_a \tag{3.4.7}$$

and
$$m_{N+1} = hu_{N+1} - hu_b \tag{3.4.8}$$

Substituting (3.4.6) into equation (3.1.7) for $i \neq 1$, and into equation (3.1.8) for $i = 1$, together with the cubic spline relation, equation (3.1.3), and the given boundary conditions, equations (3.4.7) and (3.4.8), a $2(N+1) \times 2(N+1)$ band matrix having 6 diagonals is found as follows,

$$[A]\ [Y]^T = [D]^T \tag{3.4.9}$$

where

$$[A] = \begin{bmatrix}
1, & 0, & 0, & 0, & 0, & 0, & 0, & 0, & \ldots, & 0, & 0, & 0, & 0 \\
c_2, & -d_2, & a_2, & -b_2, & 0, & 0, & 0, & 0, & \ldots, & 0, & 0, & 0, & 0 \\
a_2, & b_2, & c_2, & d_2, & 0, & 0, & 0, & 0, & \ldots, & 0, & 0, & 0, & 0 \\
e_2, & f_2, & g_2, & i_2, & j_2, & k_2, & 0, & 0, & \ldots, & 0, & 0, & 0, & 0 \\
0, & 0, & a_3, & b_3, & c_3, & d_3, & 0, & 0, & \ldots, & 0, & 0, & 0, & 0 \\
0, & 0, & e_3, & f_3, & g_3, & i_3, & j_3, & k_3, & \ldots, & 0, & 0, & 0, & 0 \\
\ldots, & \ldots, & \ldots, & \ldots, & \ldots, & \ldots, & \ldots, & \ldots, & \ldots, & \ldots, & \ldots & & \\
0, & 0, & 0, & 0, & 0, & 0, & 0, & 0, & \ldots, & a_{N+1}, & b_{N+1}, & c_{N+1}, & d_{N+1} \\
0, & 0, & 0, & 0, & 0, & 0, & 0, & 0, & \ldots, & 0, & 0, & -h, & 1
\end{bmatrix}$$

$$[Y]=[u_1,\ m_1,\ u_2,\ m_2,\ \ldots,\ u_{N+1},\ m_{N+1}]^{n+1}$$

$$[D]=[u_o,\ -b_1,\ -b_2,\ 0,\ -b_3,\ 0,\ \ldots\ldots,\ 0,\ -b_{N+1},\ -hu_o]$$

and with

$$a_i = \frac{6}{h_i^2}, \qquad b_i = \frac{2}{h_i}$$

$$c_i = -\frac{6}{h_i^2}, \qquad d_i = \frac{4}{h_i} + a_i$$

$$e_i = \frac{3}{h_i^2}, \qquad f_i = \frac{1}{h_i}$$

$$g_i = -\left(\frac{3}{h_i^2} - \frac{3}{h_{i+1}^2}\right), \qquad i_i = 2\left(\frac{1}{h_i} + \frac{1}{h_{i+1}}\right)$$

$$j_i = -\frac{3}{h_{i+1}^2}, \qquad k_i = \frac{1}{h_{i+1}}$$

Any efficient inversion algorithm can be used to solve the equation (3.4.9). As discussed in the next section, a second order accuracy can be expected not only for u_i, but also for m_i and M_i. However, as the number of the node points is very large, the direct evaluation of equation (3.4.9) is rather time-consuming. An alternative scheme is considered in chapter four.

3.5. Truncation Error

To examine the accuracy of the cubic spline approximation, expanding u_i, m_i and M_i in a Taylor series with the assumption of the necessary continuity of derivatives for u, the spatial accuracy of the cubic spline approximation for interior points can be directly estimated from the spline relations, equations (3.1.2) and (3.1.3), as follows [8],

$$M_i = (u_{xx})_i - \frac{h_{i+1}^3 + h_i^3}{h_{i+1} + h_i} (u_{xxxx})_i / 12 -$$

$$(u_{xxxxx})_i \left[\frac{7(h_{i+1} - h_i)(h_{i+1}^2 - h_i^2)}{90} + \right.$$

$$\left. \frac{(h_{i+1} - h_i)(h_{i+1}^3 + h_i^3)}{36(h_{i+1} + h_i)} \right] + O(h_i^4) \tag{3.5.1}$$

$$m_i = (u_x)_i - \frac{(h_{i+1} - h_i) h_{i+1} h_i}{72} (u_{xxxx})_i + O(h_i^4) \tag{3.5.2}$$

where u_x denotes the first exact derivative of u with respect to x, and u_{xx} the second exact derivative of u with respect to x, and so on.

It is obvious that the cubic spline approximation is third-order accuracy for m_i with a non-uniform mesh and fourth-order for m_i with a uniform mesh. And regardless of the choice of mesh, a second order accuracy can be always achieved for M_i by using cubic spline interpolation.

Truncation error associated with the time discretization can be obtained by using the same technique outlined above.

Consider

$$u_i' = f(u_i, m_i, M_i) \tag{3.5.3}$$

A possible discritization using implicit scheme can be of following form,

$$u_i^{n+1} = u_i^n + f_i^{n+1}\Delta t$$

A Taylor series expansion leads to,

$$(u_t)_i = f_i + O[\Delta t \; f_t] \tag{3.5.4}$$

i.e. a first-order accuracy will result when employing an implicit scheme.

3.6. High-Order Accuracy Cubic Spline Approximation

In the last section, it was shown that with a uniform mesh the cubic spline interpolation is fourth order accuracy for m_i and second order accuracy for M_i. Non-uniform mesh produces third order accuracy for m_i and second order accuracy for M_i. From section 3.2, we may observe that when a cubic spline interpolation is applied to a system of equations, the function u_i, its first derivative m_i, and the second derivative M_i are all included in the solution procedure. Therefore an overall second order accuracy can be expected. The main bottleneck of this procedure is the accuracy of the second derivative.

In this section, we will present techniques to improve the accuracies of the spatial second-derivative with a uniform mesh, and the time derivative approximation [16].

Consider a standard three point finite-difference approximations of the second derivative for a uniform mesh,

$$\frac{\partial^2 u}{\partial x^2} = \frac{u_{i-1}-2u_i+u_{i+1}}{h^2}$$

The accuracy of this scheme can be found by applying Taylor expansion on it. The result is,

$$\frac{u_{i-1}-2u_i+u_{i+1}}{h^2} = (u_{xx})_i + (u_{xxxx})_i\frac{h^2}{12} + O(h^4) \qquad (3.6.1)$$

Combining equation (3.5.1) with (3.6.1), it gives

$$\frac{1}{2}[M_i + \frac{u_{i-1}-2u_i+u_{i+1}}{h^2}] = (u_{xx})_i + O(h^4) \qquad (3.6.2)$$

Substituting equation (3.1.2) into above equation, it yields

$$\frac{1}{2}[M_i + (\frac{1}{6}M_{i-1} + \frac{2}{3}M_i + \frac{1}{6}M_{i+1})] = (u_{xx})_i + O(h^4)$$

or

$$(u_{xx})_i = \frac{M_{i-1}+10M_i+M_{i+1}}{12} - O(h^4) \qquad (3.6.3)$$

Equation (3.6.3) demonstrates that an overall fourth order accuracy can be achieved with a uniform mesh.

To improve the accuracy of the time derivative, the Crank-Niclson scheme used in the finite-difference approximation can be adopted. Applying Crank-Niclson scheme, the discretised form of equation (3.5.3) can be written as follows,

$$u_i^{n+1} = u_i^n + \frac{\Delta t}{2}(f_i^{n+1} + f_i^n)$$

It can be shown that, after Taylor series expansion about $(n+1/2)\Delta t$,

$$(u_t)_i = f_i + O[\Delta t^2 f_{tt}]_i \qquad (3.6.4)$$

This provides second order accuracy for the time derivative.

In section 3.7, the cubic spline approximation for the solution of a simple phase-change problem is presented. And the numerical result is compared with the exact solution.

3.7 Numerical Example

In this section, we consider a simple case of solidification of metal which is initially at its melting temperature, $T=T_m$. It is assumed that at a certain time, $t=0$, the temperature at $x=d_1$ drops to T_o $(<T_m)$ and remains constant thereafter. The system of equation, the initial and boundary conditions can be stated as follows,

$$\frac{\partial T}{\partial t} = \alpha \frac{\partial^2 T}{\partial x^2} \tag{3.7.1}$$

$$\text{at} \quad t=0, \qquad T = T_m \tag{3.7.2}$$

$$\text{at} \quad x=s, \qquad T = T_m \tag{3.7.3}$$

$$x=d_1, \qquad T = T_o \tag{3.7.4}$$

The energy balance at the phase front is,

$$\rho L q \frac{ds}{dt} = k \frac{\partial T}{\partial x} \tag{3.7.5}$$

and initially the liquid-solid interface s is located at $x=d_1$.

If the following transformations are employed,

$$x^* = \frac{x-s}{d_1-s} \qquad T^* = \frac{T-T_m}{T_o-T_m}$$

$$t^* = \frac{\alpha t}{d_1^2} \qquad \eta = \frac{s}{d_1}$$

$$\text{Ste} = -\frac{c(T_o - T_m)}{Lq}$$

The system of equations, eqs.(3.7.1)-(3.7.5) can be rewritten in the dimensionless forms as below.

$$\frac{\partial T^*}{\partial t^*} = \frac{1-x^*}{1-\eta}\frac{\partial \eta}{\partial t^*}\frac{\partial T^*}{\partial x^*} + \frac{\partial^2 T^*}{\partial x^{*2}}\frac{1}{(1-\eta)^2} \tag{3.7.6}$$

$$t^* = 0,\ T^* = 0 \tag{3.7.7}$$

$$x^* = 0,\ T^* = 0 \tag{3.7.8}$$

$$x^* = 1,\ T^* = 1 \tag{3.7.9}$$

$$\frac{d\eta}{dt^*} = \frac{\text{Ste}}{1-\eta}\frac{\partial T^*}{\partial x^*} \tag{3.7.10}$$

By using cubic spline approximation technique stated in this chapter, the descritized form of above system is as follows,

$$T^{*n+1} = T^{*n} + \Delta t^*[\frac{x^*-1}{1-\eta}\frac{\partial \eta}{\partial t^*}m^{n+1} + \frac{1}{(1-\eta)^2}M^{n+1}]$$

$$= F + Rm^{n+1} + QM^{n+1} \tag{3.7.11}$$

where

$$F = T^{*n}$$

$$R = \Delta t^* \frac{x^*-1}{1-\eta}\frac{\partial \eta}{\partial t^*} \tag{3.7.11a}$$

$$Q = \frac{\Delta t^*}{(1-\eta)^2}$$

The exact solution of this solidification process is given by [17],

$$T^* = -1 + \frac{\mathrm{erf}[\lambda(1-\eta)]}{\mathrm{erf}(\lambda)}$$

and $\eta = 2\lambda\sqrt{t^*}$

with the Gauss error function defined as,

$$\mathrm{erf}(x) = \frac{2}{\sqrt{\pi}} \int_0^x e^{-y^2} dy.$$

where the value of λ is determined from

$$\sqrt{\pi} e^{\lambda^2} \mathrm{erf}(\lambda) = Ste$$

Table 1 shows the comparison of the results obtained from the cubic spline numerical approximation with those obtained from the exact solution for the location of the moving phase front. The data used in obtaining the numerical results in Table 1, except specified in Table 1, are as follows,

Δt^*=0.001

Space Ratio=1.5 (see chapter 5 foot note for detail)

Ste = 0.5

number of grids N = 5.

The results indicate that, the maximum relative error is less than 1% for the case of Ste=0.1 and 0.5 while less than 3.4% for the case of Ste=1.0.

Table 1 Comparison of position of moving front computed by cubic spline numerical approximation with that by analytical solution.

t^*	Ste=0.5					Ste=0.1		Ste=1.0	
	Analytic Solution	Numerical Solution Δt=.001	Numerical Solution Δt=.0001	Numerical Solution N=10	Numerical Solution $h_{\xi+1}/h_\xi=1$	Analytic Solution	Numeric Solution	Analytic Solution	Numeric Solution
0.05	0.792141	0.790510	0.791933	0.790550	0.790521	0.901606	0.901289	0.722700	0.719356
0.10	0.706044	0.705097	0.705826	0.705153	0.705112	0.860850	0.860745	0.607838	0.605637
0.20	0.584283	0.583730	0.584048	0.583809	0.583751	0.803211	0.803221	0.445399	0.443845
0.30	0.490853	0.490435	0.490600	0.490582	0.490461	0.758984	0.758978	0.320755	0.319409
0.40	0.412087	0.411713	0.411819	0.411825	0.411743	0.721699	0.721667	0.215676	0.214414
0.50	0.342693	0.342282	0.342410	0.342408	0.342316	0.688850	0.688803	0.123099	0.121832
0.60	0.279957	0.279518	0.279659	0.279655	0.279554	0.659152	0.659096	0.039403	0.038074
0.70	0.222264	0.221803	0.221952	0.221951	0.221842	0.631842	0.631779		
0.80	0.168566	0.168085	0.168240	0.168243	0.168127	0.606423	0.606355		
0.90	0.118131	0.117633	0.117793	0.117801	0.117678	0.582549	0.582476		
1.00	0.070428	0.069916	0.070078	0.070093	0.069963	0.559968	0.559892		
2.00						0.377700	0.377615		
3.00						0.237841	0.237754		
4.00						0.119935	0.119848		
5.00						0.016057	0.015970		
Computation Time (Second)	----	3.2	30.5	5.9	3.1	----	13.7	----	1.8

CHAPTER FOUR

CUBIC SPLINE APPROXIMATION FOR SOLVING FUSION-WELDING PROBLEM

In this chapter, the spline alternating direction implicit procedure is applied to solve a two-dimensional fusion-welding problem involving natural convection in the liquid region, as formulated in chapter two. Section 4.1 gives the entire reformulation in the discretized form. A numerical solution methodology is introduced to solve the problem (section 4.2). The stability consideration and truncation error analysis are made for this problem in sections 4.3 and 4.4, respectively.

4.1. Cubic Spline Approximation for Solving Fusion-Welding Problem

In this section, the governing equations for the fusion-welding problem derived in chapter 2 are discretized by using the two step SADI cubic spline approximation technique presented in chapter 3.

Energy equation in solid

Using the two step SADI procedure, the energy equation (2.3.4) in solid can be discretized as follows,

Step 1, at $t^* = n+1/2$,

$$(T_s{}^*)_{ij}^{n+1/2} - (T_s{}^*)_{ij}^{n} + \frac{\Delta t^*}{2}[(\frac{1}{1-\eta_i^{n+1}})^2 G_{ij}^{n} + \frac{1}{R^2} K_{ij}^{n+1/2}]\alpha_r$$

$$= F_{ij}^{n+1/2} + R_{ij}^{n+1/2} k_{ij}^{n+1/2} + Q_{ij}^{n+1/2} K_{ij}^{n+1/2} \qquad (4.1.1)$$

where

$$F_{ij}^{n+1/2} = (T_s{}^*)_{ij}^{n} + \frac{\Delta t^*}{2}[(\frac{1}{1-\eta_i^{n+1}})^2 G_{ij}^{n}]\alpha_r$$

$$R_{ij}^{n+1/2} = 0 \qquad (4.1.1a)$$

$$Q_{ij}^{n+1/2} = \frac{\Delta t^*}{2R^2}\alpha_r$$

Step 2, at $t^* = n+1$,

$$(T_s{}^*)_{ij}^{n+1} - (T_s{}^*)_{ij}^{n+1/2} + \frac{\Delta t^*}{2}[(\frac{1}{1-\eta_i^{n+1}})^2 G_{ij}^{n+1} + \frac{1}{R^2} K_{ij}^{n+1/2}]\alpha_r$$

$$= F_{ij}^{n+1} + R_{ij}^{n+1} g_{ij}^{n+1} + Q_{ij}^{n+1} G_{ij}^{n+1} \qquad (4.1.2)$$

where

$$F_{ij}^{n+1} = (T_s^*)_{ij}^{n+1/2} + \frac{\Delta t^*}{2}\left(\frac{1}{R^2} K_{ij}^{n+1/2}\right)\alpha_r$$

$$R_{ij}^{n+1} = 0 \qquad (4.1.2a)$$

$$Q_{ij}^{n+1} = \frac{\Delta t^*}{2}\left(\frac{1}{1-\eta_i^{n+1}}\right)^2 \alpha_r$$

and where

$$g = \frac{\partial T_s^*}{\partial x_s^*} \qquad G = \frac{\partial^2 T_s^*}{\partial x_s^{*2}} \qquad k = \frac{\partial T_s^*}{\partial y^*} \qquad K = \frac{\partial^2 T_s^*}{\partial y^{*2}}$$

The initial and boundary conditions, eqs.(2.3.4a)-(2.3.4d), are discretized as follows,

$$(T_s^*)_{ij}^{o} = \phi_c, \qquad (4.1.3a)$$

$$(T_s^*)_{1,j}^{n+1} = 1 \qquad (4.1.3b)$$

$$g_{N+1,j}^{n+1} = -B_i \,(1-\eta_i^{n+1})(T_s^*)_{N+1,j}^{n+1} \qquad (4.1.3c)$$

$$k_{i,1}^{n+1/2} = 0, \qquad k_{i,N+1}^{n+1/2} = 0 \qquad (4.1.3d)$$

The solution of eq.(4.1.1), the first time step in y^* direction, can now be considered. Since the boundary conditions, eq.(4.1.3d), are specified in the values of the first derivatives in both ends, the solution procedure given in section (3.2.2) can be employed. By evaluating eq.(3.2.7) together with the prescribed boundary conditions, where the values of F, R and Q used in the solution of eq.(3.2.7) are given in eq.(4.1.1a), the values of the first derivative of T_s^* can then be solved. Following this, the values of T_s^* and its second derivative K can be obtained in a manner similar to that described in section (3.2.2). For the second time step in the x^* direction, because of the mixed boundary condition at i=N+1, the solution procedure given in section (3.2.4) for mixed boundary condition is adopted. The mixed boundary condition at i=N+1 is transferred to a relation containing only $(T_s^*)_{N,j}$ and $(T_s^*)_{N+1,j}$ as given in eq.(3.2.15). Equation (4.1.2) can then be solved as described in section 3.2.4. Following the same procedure outlined in section 3.2.4, the first derivative g_{ij} and the second derivative G_{ij} can be determined. Again the values of F, R, and Q used in the solution procedure in section (3.2.4) are specified in eq.(4.1.2a).

Energy equation in liquid

The energy equation, equation (2.3.5), is discretized by the two step SADI procedure as follows,

Step 1, at $t^* = n+1/2$,

$$(T_\ell^*)_{ij}^{n+1/2} = (T_\ell^*)_{ij}^{n} + \frac{\Delta t^*}{2}\Big[\frac{-1}{\eta_i^{n+1}R} (\psi_y^* g)_{ij}^{n} +$$

$$\frac{1}{\eta_i^{n+1}R} (\psi_x^{*n} k^{n+1/2})_{ij} + \frac{1}{(\eta_i^{n+1})^2} G_{ij}^{n} + \frac{1}{R^2} K_{ij}^{n+1/2}\Big]$$

$$= F_{ij}^{n+1/2} + R_{ij}^{n+1/2} k_{ij}^{n+1/2} + Q_{ij}^{n+1/2} K_{ij}^{n+1/2} \qquad (4.1.4)$$

where

$$\psi_x^{\ *} = \frac{\partial \psi^*}{\partial x_\ell^{\ *}} = -\frac{\eta}{R} v^*$$

$$\psi_y^{\ *} = \frac{\partial \psi^*}{\partial y^*} = u^*$$

$$F_{ij}^{n+1/2} = (T_\ell^{\ *})_{ij}^{n} + \frac{\Delta t^*}{2}\left[\frac{-1}{\eta_i^{n+1} R} (\psi_y^{\ *} g)_{ij}^{n} + \frac{1}{(\eta_i^{n+1})^2} G_{ij}^{n}\right]$$

$$R_{ij}^{n+1/2} = \frac{\Delta t^*}{2\eta_i^{n+1} R} (\psi_x^{\ *})_{ij}^{n} \qquad (4.1.4a)$$

$$Q_{ij}^{n+1/2} = \frac{\Delta t^*}{2R^2}$$

Step 2, at $t^* = n+1$,

$$(T_\ell^{\ *})_{ij}^{n+1} = (T_\ell^{\ *})_{ij}^{n+1/2} + \frac{\Delta t^*}{2}\left[\frac{-1}{\eta_i^{n+1} R} (\psi_y^{\ *n} g^{n+1})_{ij} + \right.$$

$$\left. \frac{1}{\eta_i^{n+1} R} (\psi_x^{\ *n} k^{n+1/2})_{ij} + \frac{1}{(\eta_i^{n+1})^2} G_{ij}^{n+1} + \frac{1}{R^2} K_{ij}^{n+1/2}\right]$$

$$= F_{ij}^{n+1} + R_{ij}^{n+1} g_{ij}^{n+1} + Q_{ij}^{n+1} G_{ij}^{n+1} \qquad (4.1.5)$$

where

$$F_{ij}^{n+1} = (T_\ell^{\ *})_{ij}^{n+1/2} + \frac{\Delta t^*}{2}\left[\frac{1}{\eta_i^{n+1} R} (\psi_x^{\ *n} k^{n+1/2})_{ij} + \frac{1}{R^2} K_{ij}^{n+1/2}\right]$$

$$R_{ij}^{n+1} = \frac{-\Delta t^*}{2\eta_i^{n+1}R} (\phi_y{}^*)_{ij}^n \tag{4.1.5a}$$

$$Q_{ij}^{n+1} = \frac{\Delta t^*}{2(\eta_i^{n+1})^2}$$

and where

$$g = \frac{\partial T_\ell{}^*}{\partial x_\ell{}^*} \quad G = \frac{\partial^2 T_\ell{}^*}{\partial x_\ell{}^{*2}} \quad k = \frac{\partial T_\ell{}^*}{\partial y^*} \quad K = \frac{\partial^2 T_\ell{}^*}{\partial y^{*2}}$$

The initial and boundary conditions, for the dimensionless temperature, can be obtained from eqs.(2.3.8a)-(2.3.8d),

$$(T_\ell{}^*)_{ij}^o = \phi_h \tag{4.1.6a}$$

$$g_{1,j}^{n+1} = 0 \tag{4.1.6b}$$

$$(T_\ell{}^*)_{N+1,j}^{n+1} = 1 \tag{4.1.6c}$$

$$k_{i,1}^{n+1/2} = 0, \qquad k_{i,N+1}^{n+1/2} = 0 \tag{4.1.6d}$$

Equation (4.1.4) together with the boundary condition, eq.(4.1.6d), can be solved in a similar manner to that used to determine the energy equation in solid in y^* direction. To solve eq.(4.1.5), the second time step in x^* direction, the boundary conditions, eq.(4.1.6b) and eq.(4.1.6c) have to be used. It can be seen that the specified boundary conditions at i=1 and i=N+1 are not the same. Therefore, none of the procedures given in section 3.2.1, 3.2.2, or 3.2.3 can be used. However, the boundary condition at i=1 in eqs.(4.1.6b) and

(4.1.6c) can be considered as a special case of mixed boundary condition, case 1, given in section (3.2.4) when p and q in eq.(3.2.11) are set to zero. The mixed boundary condition at i=1 can be transferred to a relation containing $(T_\ell^*)_{1,j}$ and $(T_\ell^*)_{2,j}$ as given in eq.(3.2.13). Hence, the eq.(4.1.5) can be solved together with the transferred boundary condition and the boundary condition at i=N+1 in eq.(4.1.6c).

Vorticity equation

The discretized form of the vorticity equation, eq.(2.3.6), using the two step SADI procedure, is as follows,

Step 1, at $t^* = n+1/2$,

$$\omega_{ij}^{*n+1/2} = \omega_{ij}^{*n} + \frac{\Delta t^*}{2}\Big[\frac{-1}{\eta_i^{n+1}R}(\psi_y^{*}m)_{ij}^{n} + \frac{1}{\eta_i^{n+1}R}(\psi_x^{*n}\ell^{n+1/2})_{ij} +$$

$$Pr\Big(\frac{Ra}{Rs^3}\frac{1}{\eta_i^{n+1}}g_{ij}^{n+1} + \frac{1}{(\eta_i^{n+1})^2}M_{ij}^{n} + \frac{1}{R^2}L_{ij}^{n+1/2}\Big)\Big]$$

$$= F_{ij}^{n+1/2} + R_{ij}^{n+1/2}\ell_{ij}^{n+1/2} + Q_{ij}^{n+1/2}L_{ij}^{n+1/2} \qquad (4.1.7)$$

where

$$F_{ij}^{n+1/2} = \omega_{ij}^{*n} + \frac{\Delta t^*}{2}\Big[\frac{-1}{\eta_i^{n+1}R}(\psi_y^{*}m)_{ij}^{n} +$$

$$Pr\Big(\frac{1}{(\eta_i^{n+1})^2}M_{ij}^{n} + \frac{Ra}{Rs^3}\frac{1}{\eta_i^{n+1}}g_{ij}^{n+1}\Big)\Big]$$

$$R_{ij}^{n+1/2} = \frac{\Delta t^*}{2\eta_i^{n+1}R} (\psi_x^*)_{ij}^n \qquad (4.1.7a)$$

$$Q_{ij}^{n+1/2} = \frac{\Delta t^*}{2R^2}Pr$$

Step 2, at $t^* = n+1$,

$$\omega_{ij}^{*n+1} = \omega_{ij}^{*n+1/2} + \frac{\Delta t^*}{2}\Big[\frac{-1}{\eta_i^{n+1}R}(\psi_y^{*n} m^{n+1})_{ij} + \frac{1}{\eta_i^{n+1}R}(\psi_x^{*n} \ell^{n+1/2})_{ij}$$

$$+Pr\Big(\frac{Ra}{Rs^3}\frac{1}{\eta_i^{n+1}} g_{ij}^{n+1} + \frac{1}{(\eta_i^{n+1})^2} M_{ij}^{n+1} + \frac{1}{R^2} L_{ij}^{n+1/2}\Big)\Big]$$

$$= F_{ij}^{n+1} + R_{ij}^{n+1} m_{ij}^{n+1} + Q_{ij}^{n+1} M_{ij}^{n+1} \qquad (4.1.8)$$

where

$$F_{ij}^{n+1} = \omega_{ij}^{*n+1/2} + \frac{\Delta t^*}{2}\Big[\frac{1}{\eta_i^{n+1}R}(\omega_x^{*n} \ell^{n+1/2})_{ij} +$$

$$Pr\Big(\frac{1}{R^2} L_{ij}^{n+1/2} + \frac{Ra}{Rs^3}\frac{1}{\eta_i^{n+1}} g_{ij}^{n+1}\Big)\Big]$$

$$R_{ij}^{n+1} = \frac{-\Delta t^*}{2\eta_i^{n+1}R} (\psi_y^*)_{ij}^n \qquad (4.1.8a)$$

$$Q_{ij}^{n+1} = \frac{\Delta t^*}{2(\eta_i^{n+1})^2} Pr$$

and where the following notations are used,

$$m = \frac{\partial \omega^*}{\partial x_\ell^*} \quad M = \frac{\partial^2 \omega^*}{\partial x_\ell^{*2}} \quad \ell = \frac{\partial \omega^*}{\partial y^*} \quad L = \frac{\partial^2 \omega^*}{\partial y^{*2}} \quad g = \frac{\partial T_\ell^*}{\partial x_\ell^*}$$

The discretized forms of the initial and boundary conditions for the vorticity ω, which can be obtained from eqs.(2.3.8a)-(2.3.8d), are

$$(\omega_{ij}^*)^o = 0 \tag{4.1.9a}$$

$$(\omega_{1,j}^*)^{n+1} = \frac{-1}{R^2} (\psi_{yy}^*)^n_{1,j} \tag{4.1.9b}$$

$$(\omega_{N+1,j}^*)^{n+1} = -\left(\frac{1}{\eta_i^{n+1}}\right)^2 (\psi_{xx}^*)^n_{N+1,j} - \frac{1}{R^2} (\psi_{yy}^*)^n_{N+1,j} \tag{4.1.9c}$$

$$(\omega_{i,1}^*)^{n+1/2} = \frac{-1}{R^2} (\psi_{yy}^*)^n_{i,1},$$

$$(\omega_{i,N+1}^*)^{n+1/2} = \frac{-1}{R^2} (\psi_{yy}^*)^n_{i,N+1} \tag{4.1.9d}$$

where

$$\psi_{xx}^* = \frac{\partial^2 \psi^*}{\partial x_\ell^{*2}}$$

$$\psi_{yy}^* = \frac{\partial^2 \psi^*}{\partial y^{*2}}$$

It can be seen that, the boundary conditions in both x^* and y^* directions, are all specified in ω^* as the values of ψ_{yy}^* and ψ_{xx}^* are taken from previous time step. Hence, the solution procedure given in section (3.2.1) for prescribed boundary condition in ω^* can be directly employed. The values of F, R, and Q in the solution procedure are taken from eqs.(4.1.7a) and (4.1.8a) for y^* and x^* directions, respectively.

Stream function equation

It can be recognized that the stream function equation, eq.(2.3.7), is not explicitly a function of time. It can be considered as the steady state solution of the following equation, according to the Cauchy-Kowoleslea scheme [18].

$$\frac{\partial \psi^*}{\partial \tau} = \frac{1}{\eta^2}\frac{\partial^2 \psi^*}{\partial x_\ell^{*2}} + \frac{1}{R^2}\frac{\partial^2 \psi^*}{\partial y^{*2}} + \omega^* \qquad (4.1.10)$$

where τ expresses the dimensionless time.

The discretized forms of equation (4.1.10) by using two step SADI procedure are as follows,

Step 1, at $\tau = r+1/2$,

$$\psi_{ij}^{*r+1/2} = \psi_{ij}^{*r} + \frac{\Delta\tau}{2}\left[\frac{1}{(\eta_i^{n+1})^2} M_{ij}^r + \frac{1}{R^2} L_{ij}^{r+1/2} + \omega_{ij}^{*n}\right]$$

$$= F_{ij}^{r+1/2} + R_{ij}^{r+1/2}\ell_{ij}^{r+1/2} + Q_{ij}^{r+1/2} L_{ij}^{r+1/2} \qquad (4.1.11)$$

where

$$F_{ij}^{r+1/2} = \psi_{ij}^{*r} + \frac{\Delta\tau}{2}\left[\frac{1}{(\eta_i^{n+1})^2} M_{ij}^{r} + \omega_{ij}^{*n}\right]$$

$$R_{ij}^{r+1/2} = 0 \tag{4.1.11a}$$

$$Q_{ij}^{r+1/2} = \frac{\Delta\tau}{2R^2}$$

Step 2, at $\tau = r+1$,

$$\psi_{ij}^{*r+1} = \psi_{ij}^{*r+1/2} + \frac{\Delta\tau}{2}\left[\frac{1}{(\eta_i^{n+1})^2} M_{ij}^{r+1} + \frac{1}{R^2} L_{ij}^{r+1/2} + \omega_{ij}^{*n}\right]$$

$$= F_{ij}^{r+1} + R_{ij}^{r+1} m_{ij}^{r+1} + Q_{ij}^{r+1} M_{ij}^{r+1} \tag{4.1.12}$$

where

$$F_{ij}^{r+1} = \psi_{ij}^{*r+1/2} + \frac{\Delta\tau}{2}\left[\frac{1}{R^2} L_{ij}^{r+1/2} + \omega_{ij}^{*n}\right]$$

$$R_{ij}^{r+1} = 0 \tag{4.1.12a}$$

$$Q_{ij}^{r+1} = \frac{\Delta\tau}{2(\eta_i^{n+1})^2}$$

and where

$$m = \frac{\partial\psi^*}{\partial x_\ell^*} \quad M = \frac{\partial^2\psi^*}{\partial x_\ell^{*2}} \quad \ell = \frac{\partial\psi^*}{\partial y^*} \quad L = \frac{\partial^2\psi^*}{\partial y^{*2}}$$

The initial and boundary conditions for the stream function ψ^*, which can be obtained from eqs.(2.3.8a)-(2.3.8d) used to solve equations (4.1.11) and (4.1.12), are discretized as follows,

$$(\psi^*)^o_{ij} = 0 \tag{4.1.13a}$$

$$M^{r+1}_{1,j} = 0 \tag{4.1.13b}$$

$$m^{r+1}_{N+1,j} = 0 \tag{4.1.13c}$$

$$\ell^{r+1/2}_{i,1} = \ell^{r+1/2}_{i,N+1} = 0, \tag{4.1.13b}$$

The steady state solution of eq.(4.1.10) can be obtained by alternatively iterating eqs.(4.1.11) and (4.1.12) until convergence. Attention must be given to the difference between the superscripts r and n. n denotes the time used in the numerical solution procedure of the fusion-welding problem, while r expresses the time used in solving the stream function equation (4.1.10) only. Therefore, the time interval Δr for the calculation of the stream function may not be necessarily the same as the one used in solving energy and vorticity, equations.

Actually, at any given time n, an iteration of eqs.(4.1.11) and (4.1.12) will be required. Hence the initial condition for a given time n for solving eq.(4.1.10) can be stated as follows,

$$[(\psi_{ij}{}^*)^r]_{r=o} = (\psi_{ij}{}^*)^n \tag{4.1.13d}$$

Equation (4.1.11) can be solved in the manner previously used to solve the energy equation, eq.(4.1.1), in the y^* direction. To solve eq.(4.1.12), the second time step in the x^* direction, the mixed boundary conditions, eqs.(4.1.13b) and (4.1.13c)), are used. The boundary condition at i=1 can be transferred to a relation containing ψ_1 and ψ_2 as given in eq.(3.2.18), and the boundary condition at i=N+1 can be transferred to a relation containing ψ_N and ψ_{N+1} as given in eq.(3.2.15). The transferred boundary conditions together with eq.(4.1.12) can then be solved as described in section (3.2.4).

Energy equation at moving interface

Equation (2.3.9) can be written in the following form to avoid the singularity at $\eta=0$,

$$\frac{\partial \eta^2}{\partial t^*} = \frac{2}{Ste}\left(k_r \frac{\eta}{1-\eta} \frac{\partial T_s^*}{\partial x_s^*} - \frac{\partial T_\ell^*}{\partial x_\ell^*}\right) \tag{4.1.14}$$

or in the discretized form

$$\eta_i^{n+1} = \sqrt{\frac{2\Delta t^*}{Ste}\left(k_r \frac{\eta_i^{n+1}}{1-\eta_i^{n+1}} \left(\frac{\partial T_s^*}{\partial x_s^*}\right)_{1,j}^n - \left(\frac{\partial T_\ell^*}{\partial x_\ell^*}\right)_{N+1,j}^n\right) + (\eta_i^n)^2} \tag{4.1.15}$$

This equation can be solved by using the iteration method, the values of $\partial T_s^*/\partial x_s^*$ and $\partial T_\ell^*/\partial x_\ell^*$ being taken from the previous time step.

4.2. Numerical Solution Methodology

Sparrow et al. [4] introduced a scheme called Quasi-Steady assumption to solve phase-change problems involving natural convection. In this scheme, it is assumed that at an instant of time t, the dependent variables are known. By considering the interface as fixed for a small time interval Δt, the dependent variables can be evaluated for time $t+\Delta t$. The moving interface can then be determined by making use of the currently available values of the temperature distribution. But this scheme needs the adjustments of the computational spatial grid at each time step after the moving interface is determined and in turn the interpolations of the dependent variables. Instead of the calculation of the moving phase position at the end of each time step followed by adjustment of the dependent variables, Ramachandran et al. [5] suggested another scheme by which the position of moving interface is determined at the beginning of each time step, and without adjustments to the computational grid and the interpolations of the dependent variables.

In both Sparrow and Ramachandran's schemes, potential computational difficulties at $t=0$ exist, as the presence of the singularity of $\eta=0$. Sparrow assumed the existence of a very thin melt region for the first time step. The corresponding time interval was determined from the Neumann's solution of the Stefan problem. In Ramachandran's scheme, it is assumed that at $t=0$, there exists a very small thickness of the solid in a solidification process, with a linear temperature profile. The starting thickness of the melt region in [4], or solidification region in [5], was varied to ensure that the assumed layer thickness did not affect the subsequent results.

In this section, the methodology to solve a fusion-welding problem using cubic spline approximation procedure is introduced. To avoid the interpolation of the dependent variables used in [4], a procedure similar to that described in [5] is used. At each time step, the position of the moving interface is computed first, followed by evaluations of the temperature distributions in both liquid and solid regions, the solution of the vorticity equation, and finally, the computation of the stream function. This procedure is carried out repeatedly until the end of the time period of interest (defined as when any point along the moving interface reaches the center of liquid region).

Unlike [4] and [5], we do not assume a very small part of the melt layer or the solidification layer. Instead, prior to advancing to the second time step, $t=2\Delta t$, iterative evaluations of the dependent variables in the sequence of the moving interface, the temperature ditributions in the liquid and solid regions, the vorticity, and the steam function, are made until the following condition are satisfied.

$$\max\left|(\eta_i^1)^{r+1} - (\eta_i^1)^r\right| < \epsilon \qquad \text{for all } i$$

where r represents the time of iteration.

and $$\max\left|\eta_i^1 - \eta_i^0\right| < \delta \qquad \text{for all } i$$

The first condition states for the convergence of the iteration. The second one controls the movement of the liquid-solid interface. If the second condition is not satisfied while the first one does, the time interval of computation has to be reduced. The iteration of the dependent variable in the aforementioned sequence is made again in order to satisfy both conditions. The values of ϵ and δ are determined by trial and error.

More precisely, when the numerical calculation computations at time t^* is completed, the numerical values of η, T_ℓ^*, T_s^*, ω^*, ψ^* and their corresponding first and second derivatives in both x^* and y^* directions are available. At time $t^*+\Delta t^*$, the variables η, T_ℓ^*, T_s^*, ω^* and ψ^* are evaluated in the following sequence,

1. Taking the values of η, $\dfrac{\partial T_\ell^*}{\partial x_\ell^*}$, and $\dfrac{\partial T_s^*}{\partial x_s^*}$ from previous time step, locate the position of the liquid-solid interface by iterating eq.(4.1.15).

2. Using the currently available value of η, calculate temperature distributions in solid (T_s^*) by evaluating equations (4.1.1) and (4.1.2), and determine its corresponding first and second derivatives by employing the cubic spline procedure as described in section 4.1.

3. Using the currently available value of η, and the values of ψ_x^*, ψ_y^* available from previous time step, calculate temperature distributions in liquid (T_ℓ^*) by evaluating equations (4.1.4) and (4.1.5), and determine its corresponding first and second derivatives by employing the cubic spline procedure described in section 4.1.

4. Using the currently available values of η and $\frac{\partial T_\ell^*}{\partial x_\ell^*}$ and the values of ψ_x^*, ψ_y^* available from the previous time step, compute the values of vorticity by evaluating equations (4.1.7) and (4.1.8), and determine its first and second derivatives, as described in section 4.1.

5. Using the currently available ω^* and η, evaluate equations (4.1.11) and (4.1.12) iteratively for the values of ψ^*, and its first and second derivatives until a steady state solution is obtained.

6. Return to step 1, and repeat until the end of the time period of interest.

4.3. Stability Consideration

By using the methodology stated in the last section, the coupled system of equations of the fusion-welding problem can be decoupled. To analyze the stability of such a decoupled system discretized by using the two step SADI method, there are four equations needed to be examined. These are the vorticity equation, the stream function equation, the energy equation for liquid region, and the energy equation for solid region. Under direct observation on the structure of those four equations, it can be found that, the stream function equation and the energy equations for liquid and solid regions are the special cases of the vorticity equation. Therefore, in the following analysis, only the vorticity equation is taken into the consideration of the stability of SADI procedure. The vorticity equation (2.3.6) is rewritten as follows, (for convenience, the superscript "*" for dimensionless variables is neglected in this section.)

$$\frac{\partial \omega}{\partial t} + \frac{u}{R\eta}\frac{\partial \omega}{\partial x} + \frac{v}{R^2}\frac{\partial \omega}{\partial y} = \mathrm{Pr}\left(\frac{1}{\eta^2}\frac{\partial^2 \omega}{\partial x^2} + \frac{1}{R^2}\frac{\partial^2 \omega}{\partial y^2} \right) + \frac{\mathrm{RaPr}}{\mathrm{Rs}^3}\,\frac{1}{\eta}\,\frac{\partial T}{\partial x} \tag{4.3.1}$$

If the SADI procedure is adopted, the two time steps of equations can be rewritten as below.

$$\omega_{ij}^{n+1/2} = \omega_{ij}^{n} + \frac{\Delta t}{2}\Big[\frac{-1}{\eta_i^{n+1} R}\,(u^n m^n)_{ij} + \frac{-1}{R^2}\,(v^n \ell^{n+1/2})_{ij} +$$

$$\Pr\left(\frac{1}{(\eta_i^{n+1})^2} M_{ij}^{n} + \frac{1}{R^2} L_{ij}^{n+1/2} + \frac{Ra}{Rs^3} \frac{1}{\eta_i^{n+1}} g_{ij}^{n+1} \right)] \qquad (4.3.2)$$

$$\omega_{ij}^{n+1} = \omega_{ij}^{n+1/2} + \frac{\Delta t}{2}[\frac{-1}{\eta_i^{n+1} R} (u^n m^{n+1})_{ij} + \frac{-1}{R^2} (v^n \ell^{n+1/2})_{ij} +$$

$$\Pr\left(\frac{1}{(\eta_i^{n+1})^2} M_{ij}^{n+1} + \frac{1}{R^2} L_{ij}^{n+1/2} + \frac{Ra}{Rs^3} \frac{1}{\eta_i^{n+1}} g_{ij}^{n+1} \right)] \qquad (4.3.3)$$

The values of u and v are taken from the previous time step. The values of η and $g(=\partial T_\ell/\partial x)$ are currently available as stated in section (4.1).

If it is assumed that u, v, η, and g are pseudo constants, the nonlinear equations, eqs.(4.3.2) and (4.3.3), become the linearized ones.

With the basic cubic spline relations, equations (3.1.2) and (3.1.3), in both x and y directions, and with a uniform mesh ($h_{ij}=h$), a system of 5(N-1) equations of 5(N+1) unknowns for equation (4.3.2) is obtained, the system being written as,

$$A_{ij} V_{i,j-1}^{n+1/2} + B_{ij} V_{ij}^{n+1/2} + C_{ij} V_{i,j+1}^{n+1/2} = D_{ij} V_{ij}^{n} + E_{ij} \qquad (4.3.4a)$$

where

$$V_{ij} = [\omega_{ij}, m_{ij}, M_{ij}, \ell_{ij}, L_{ij}]^T \qquad (4.3.4b)$$

$$A_{ij} = \begin{bmatrix} 0, & 0, & 0, & 0, & 0 \\ \frac{-1}{h}, & 0, & 0, & 0, & \frac{h}{6} \\ \frac{3}{h^2}, & 0, & 0, & \frac{1}{h}, & 0 \\ \frac{-1}{h}, & 0, & \frac{h}{6}, & 0, & 0 \\ \frac{3}{h^2}, & \frac{1}{h}, & 0, & 0, & 0 \end{bmatrix} \qquad (4.3.4c)$$

$$B_{ij} = \begin{bmatrix} 1, & 0, & 0, & \frac{\Delta t}{2R^2} v^n, & \frac{-\Delta t}{2R^2} Pr \\ \frac{2}{h}, & 0, & 0, & 0, & \frac{2h}{3} \\ 0, & 0, & 0, & \frac{4}{h}, & 0 \\ \frac{2}{h}, & 0, & \frac{2h}{3}, & 0, & 0 \\ 0, & \frac{4}{h}, & 0, & 0, & 0 \end{bmatrix} \qquad (4.3.4d)$$

$$C_{ij} = \begin{bmatrix} 0, & 0, & 0, & 0, & 0 \\ \frac{-1}{h}, & 0, & 0, & 0, & \frac{h}{6} \\ \frac{-3}{h^2}, & 0, & 0, & \frac{1}{h}, & 0 \\ \frac{-1}{h}, & 0, & \frac{h}{6}, & 0, & 0 \\ \frac{-3}{h^2}, & \frac{1}{h}, & 0, & 0, & 0 \end{bmatrix} \qquad (4.3.4e)$$

and where

$$
D_{ij} = \begin{bmatrix} 1, & \dfrac{-\Delta t}{2\eta_i^{n+1} R} u^n, & \dfrac{\Delta t}{2(\eta_i^{n+1})^2} Pr, & 0, & 0 \\ & & & & \\ & & \mathbf{O} & & \end{bmatrix} \qquad (4.3.4f)
$$

$$
E_{ij} = \begin{bmatrix} Pr \dfrac{Ra\Delta t}{2Rs^3 \eta_i^{n+1}} g_{ij}^{n+1} \\ \\ \mathbf{O} \end{bmatrix} \qquad (4.3.4g)
$$

And where A, B, C, and D, are 5 by 5 matrices. E is a vector of five elements.

Considering the stability of the interior points with the Von-Neumann Fourier decomposition [10], let

$$
V_{i,j+\delta}^{n} = V_{ij}^{n} e^{I\Omega(j+\delta)h} \qquad (4.3.5)
$$

where $\delta = -1$, o, or $+1$ and $I = \sqrt{-1}$. After substituting eq.(4.3.5) into (4.3.4a), and considering that the vector E_{ij} will not effect the stability of the system, equation (4.3.4a) becomes

$$
T_{ij} V_{ij}^{n+1/2} = D_{ij} V_{ij}^{n} \qquad (4.3.6a)
$$

where

$$T_{ij} = \begin{bmatrix} 1, & 0, & 0, & \frac{\Delta t}{2R^2}v^n, & \frac{-\Delta t}{2R^2}Pr \\ t_{21}, & 0, & 0, & 0, & t_{25} \\ t_{31}, & 0, & 0, & t_{34}, & 0 \\ t_{41}, & 0, & t_{43}, & 0, & 0 \\ t_{51}, & t_{52}, & 0, & 0, & 0 \end{bmatrix} \qquad (4.3.6b)$$

And the matrix D_{ij} is defined as the same as in eq.(4.3.4f). Also

$$t_{21} = t_{41} = \frac{1}{h}(2-e^{-I\phi}-e^{I\phi}) = \frac{2}{h}(1-\cos\phi) \qquad (4.3.6c)$$

$$t_{25} = t_{43} = \frac{h}{6}(4+e^{-I\phi}+e^{I\phi}) = \frac{h}{3}(2+\cos\phi) \qquad (4.3.6d)$$

$$t_{31} = t_{51} = \frac{3}{h^2}(e^{-I\phi}-e^{I\phi}) = \frac{-6}{h^2} I\sin\phi \qquad (4.3.6e)$$

$$t_{34} = t_{52} = \frac{1}{h}(4+e^{-I\phi}+e^{I\phi}) = \frac{2}{h}(2+\cos\phi) \qquad (4.3.6f)$$

where $\phi = \Omega h$. Therefore,

$$V_{ij}^{n+1/2} = G_{ij}V_{ij}^{n} \qquad (4.3.7)$$

where $G_{ij} = T_{ij}^{-1}D_{ij}$ is the amplification matrix.

The eigenvalues of G are found from the following characteristic equation

$$\left| T_{ij}^{-1} D_{ij} - \lambda_i I \right| = 0$$

where I is the identity matrix.

The only one nonzero eigenvalue of G found is,

$$\lambda_1 = \frac{1-\beta_1 a-\Phi_1 b}{1+\beta_2 a+\Phi_2 b} \tag{4.3.8}$$

where

$$\beta_1 = \frac{Pr\Delta t}{h^2(\eta_i^{n+1})^2} \qquad \beta_2 = \frac{Pr\Delta t}{h^2R^2}$$

$$\Phi_1 = \frac{u^n\Delta t}{2\eta_i^{n+1}Rh} \qquad \Phi_2 = \frac{v^n\Delta t}{2hR^2} \tag{4.3.8a}$$

$$a = \frac{3(1-\cos\phi)}{(2+\cos\phi)} \qquad b = \frac{3I\sin\phi}{(2+\cos\phi)}$$

Following the same procedure in obtaining equation (4.3.4a), equation (4.3.3) can be transferred as follows,

$$A_{ij}V_{i-1,j}^{n+1} + B_{ij}V_{i,j}^{n+1} + C_{ij}V_{i+1,j}^{n+1} = D_{ij}V_{i,j}^{n+1/2} + E_{ij} \tag{4.3.9a}$$

where V_{ij}, A_{ij}, C_{ij} and E_{ij} have the same form as defined in equations (4.3.4b), (4.3.4c), (4.3.4e) and (4.3.4g). Matrices B_{ij} and D_{ij} in eq.(4.3.9a) can be expressed by

$$B_{ij} = \begin{bmatrix} 1, & \frac{\Delta t u^n}{2R\eta_i^{n+1}}, & \frac{-\Delta t}{2(\eta_i^{n+1})^2}Pr, & 0, & 0 \\ \frac{2}{h}, & 0, & 0, & 0, & \frac{2h}{3} \\ 0, & 0, & 0, & \frac{4}{h}, & 0 \\ \frac{2}{h}, & 0, & \frac{2h}{3}, & 0, & 0 \\ 0, & \frac{4}{h}, & 0, & 0, & 0 \end{bmatrix} \tag{4.3.9b}$$

$$D_{ij} = \begin{bmatrix} 1, & 0, & 0, & \frac{-\Delta t}{2R^2}v^n, & \frac{\Delta t}{2R^2}Pr \\ & & & & \\ & \mathbf{O} & & & \end{bmatrix} \tag{4.3.9c}$$

Similarly as arrived at eq.(4.3.6a), eq.(4.3.9a) can be derived as follows,

$$T_{ij}V_{ij}^{n+1} = D_{ij}V_{ij}^{n+1/2} \tag{4.3.10}$$

where

$$T_{ij} = \begin{bmatrix} 1, & \frac{\Delta t}{2\eta_i^{n+1}R}u^n, & \frac{-\Delta t}{2(\eta_i^{n+1})^2}Pr, & 0, & 0 \\ t_{21}, & 0, & 0, & 0, & t_{25} \\ t_{31}, & 0, & 0, & t_{34}, & 0 \\ t_{41}, & 0, & t_{43}, & 0, & 0 \\ t_{51}, & t_{52}, & 0, & 0, & 0 \end{bmatrix} \tag{4.3.10a}$$

where the coefficients are defined in the same way as in eqs.(4.3.6c)-(4.3.6f).

Further we may write equation (4.3.10) as,

$$V_{ij}^{n+1} = G_{ij}\ V_{ij}^{n+1/2} \tag{4.3.11}$$

where $G_{ij} = T_{ij}^{-1} D_{ij}$, is once again the amplification matrix. Only one non-zero eigenvalue is found as,

$$\lambda_2 = \frac{1-\beta_2 a-\Phi_2 b}{1+\beta_1 a+\Phi_1 b} \tag{4.3.12}$$

where β_1, β_2, Φ_1, Φ_2, a and b are defined as the same as in equation (4.3.8a).

The Von-Neumann's stability consideration for two-dimensional problem for the interior points requires that [10],

$$|\ \lambda_i\ \lambda_j\ | \leq 1$$

where λ_i is for the eigenvalues of the amplification matrix of the first step, as given in equation (4.3.8), and λ_j is for the eigenvalues of the amplification matrix of the second step as given in equation (4.3.12). It is not difficult to see that after substituting eqs.(4.3.8) and (4.3.12) into Von-Neumann's condition, the condition

$$|\ \lambda_1\ \lambda_2\ | \leq 1 \tag{4.3.13}$$

is always satisfied. Therefore the SADI procedure for the decoupled vorticity equation is unconditionally stable. The same results for the stream function equation, the energy equations in liquid and solid can be obtained by using the same procedure as arrived at equation (4.3.13). There are several points which need to be emphasized,

1. The Von-Neumann condition is only a necessary one for present problem, as mentioned in [10].

2. The effects of boundary conditions for the stability are not considered.

For the study of nonlinear equations, Hicks [19] suggests skipping over the problem of stability criteria and going directly to the heart of the matter, i.e. convergence, and the stability is of the second interest.

4.4. Truncation Error

A complete analysis of truncation error in the SADI procedure for the solution of nonlinear coupled system of equations is very difficult. If the effects of decoupling are not taken into account, it can be easily concluded that as discussed in section 3.5, an overall second order accuracy for the time interval will result from using the two step SADI procedure, regardless of the uniformity of the spatial interval.

To ensure the validity of the results obtained in this thesis, a result obtained from a simplified fusion-welding problem using a high order accuracy cubic spline numerical approximation [2] can be compared with the one obtained in this thesis. The mathematical model used in [2] is similar to the one used in this thesis except that the effects of natural convection are not taken into consideration. A detailed discussions concerning these comparisions will be presented in the next chapter.

CHAPTER FIVE

NUMERICAL SOLUTIONS AND DISCUSSIONS

5.1 Parameter and Grid Selections

Examination of the governing equations and the corresponding initial and boundary conditions, reveals that there are ten dimensionless parameters whose values have to be specified prior to the computation of the numerical solutions. These include the Rayleigh number Ra, the Prandtl number Pr, the Stefan number Ste, the Biot number Bi, the ratio of the initial liquid width to the total width Rs, the ratio of thermal diffusivity of solid to liquid α_r, the ratio of thermal conductivity of solid to liquid k_r, the superheating coefficient ϕ_h, the subcooling coefficient ϕ_c, and the aspect ratio R.

In selecting values for these parameters, guide-lines were derived from metal fusion-welding process. The properties for some of the metal materials are listed in Table 2a [20,21] and the derived dimensionless parameters are given in Table 2b which are calculated according to equations in section 2.3.

Following the determination of some dimensionless parameter values, the values of ϕ_h and ϕ_c were taken as equal to 2.6 and 0.46 respectively, so as to observe continuously both the melting and solidification processes presented in the numerical results. The values of Rs and R were chosen both equal to 0.23, so as to get an approximate square initial liquid region.

For the remainder of this chapter, except where stated, the above-described values of the dimensionless parameters are used as the essential data in the solution of the two-dimensional fusion-welding problem.

In order to ensure the validity of the 2-dimensional model and the simulation results, two sets of results for aluminium fusion welding process, one obtained from one-dimensional model by Wang et al. [2] and the other for average moving front by the two-dimensional model in this thesis, are presented in figure 2. The results for the two-dimensional model were obtained using the time interval $\Delta t^*=0.0005$ and a 15×15 uniform grid over each liquid and solid region. Wang's one-dimensional model incorporated a uniform grid of size 21 over each liquid and solid region. Even there is no way to compare directly these two sets of results because of the complexity involved in the two-dimensional model, it still can be seen in fig.2 that the average value of moving interface obtained by the two-dimensional model is similar to that obtained by Wang et al. except it has a large value in moving front, which is physically coincidental with the prediction because of the involving of the convective heat transfer.

The computation was carried out on computer CYBER 170/835. The elapsed time used to accomplish the "computation of interest"* is

(*) the "computation of interest" is defined as the time period before any discretized point along liquid-solid interface reaches the center of liquid region in which case the 2-dimensional model will fail.

approximately 500 computer seconds for 15 by 15 grids and over 2000 seconds for 30 by 30 grids. To reduce the cost in computation time, a non-uniform mesh with a larger spatial interval could be used. Figure 3 shows that, the tendency of values obtained from the non-uniform 6×6 mesh with a "space ratio"** equal to 1.08 is coincide with the results obtained from the 15×15 and 20×20 uniform grids. While the total time required to complete the computation of interest was reduced to approximately 50 computer seconds. And the difference between the results obtained from 15×15 grid and 20×20 grid is acceptable. To accommodate between the accuracy and the cost of computation time, a 15×15 non-uniform grid with spatial ratio of 1.08 was used throughout the following discussions. The time intervals used were $\Delta t^*=0.0005$ for aluminium ($Ra\leq10^4$) and $\Delta t^*=0.0002$ for lead ($Ra\geq10^4$).

(**) the "space ratio" is defined in two cases as follows,

case 1. space ratio $= h_{i+1}/h_i$, for $0\leq y^*\leq1/2$ in the calculation of y^*-direction, or $0\leq(x_\ell^*,x_s^*)\leq1/2$ in the calculation of x^*-direction.

case 2. space ratio $= h_i/h_{i+1}$, for $1/2\leq y^*\leq1$ in the calculation of y^*-direction, or $1/2\leq(x_\ell^*,x_s^*)\leq1$ in the calculator of x^*-direction.

Table 2a Thermal properties of some metal materials.

Element	Melting Point (oC)	Latent Heat of Fusion (KJ/Kg)	Density (Kg/m3)	Specfic Heat (KJ/Kg/oC)	Thermal Conductivity (W/m/oC) Liquid	Thermal Conductivity (W/m/oC) Solid	Thermal Diffusivity (m2/s) Liquid	Thermal Diffusivity (m2/s) Solid	Viscosity (Kg/m/s)	Expansion Coefficient (x10E+6)
Aluminium (Al)	660	387	2370	1.084	92.0	238.6	3.58E-5	8.24E-5	4.50E-3	23.5
Copper (Cu)	1083	203	8240	0.494	131.4	341.0	3.22E+5	9.69E-5	4.50E-3	17.0
Lead (Pb)	327	24	10600	0.152	16.3	32.2	1.01E-5	2.27E-5	2.60E-3	29.0
Zinc (Zn)	420	111	6600	0.481	60.3	105.0	1.90E-5	3.84E-5	3.93E-3	31.0

Table 2b Calculated dimensionless parameters for some metal materials.

Element	Pr	Ra	Ste	Bi	kr	αr
Aluminium (Al)	0.053	7199	0.56	0.7	2.59	2.30
Copper (Cu)	0.017	33676	0.39	0.49	2.60	3.01
Lead (Pb)	0.0242	115124	0.53	3.99	1.98	2.25
Zinc (Zn)	0.0313	35326	0.59	1.08	1.74	2.02

Note: In the determination of values of Ra and Bi, the values of dl and h were chosen equal to 0.015 m and 9.6 W/m^2oC, respectively.

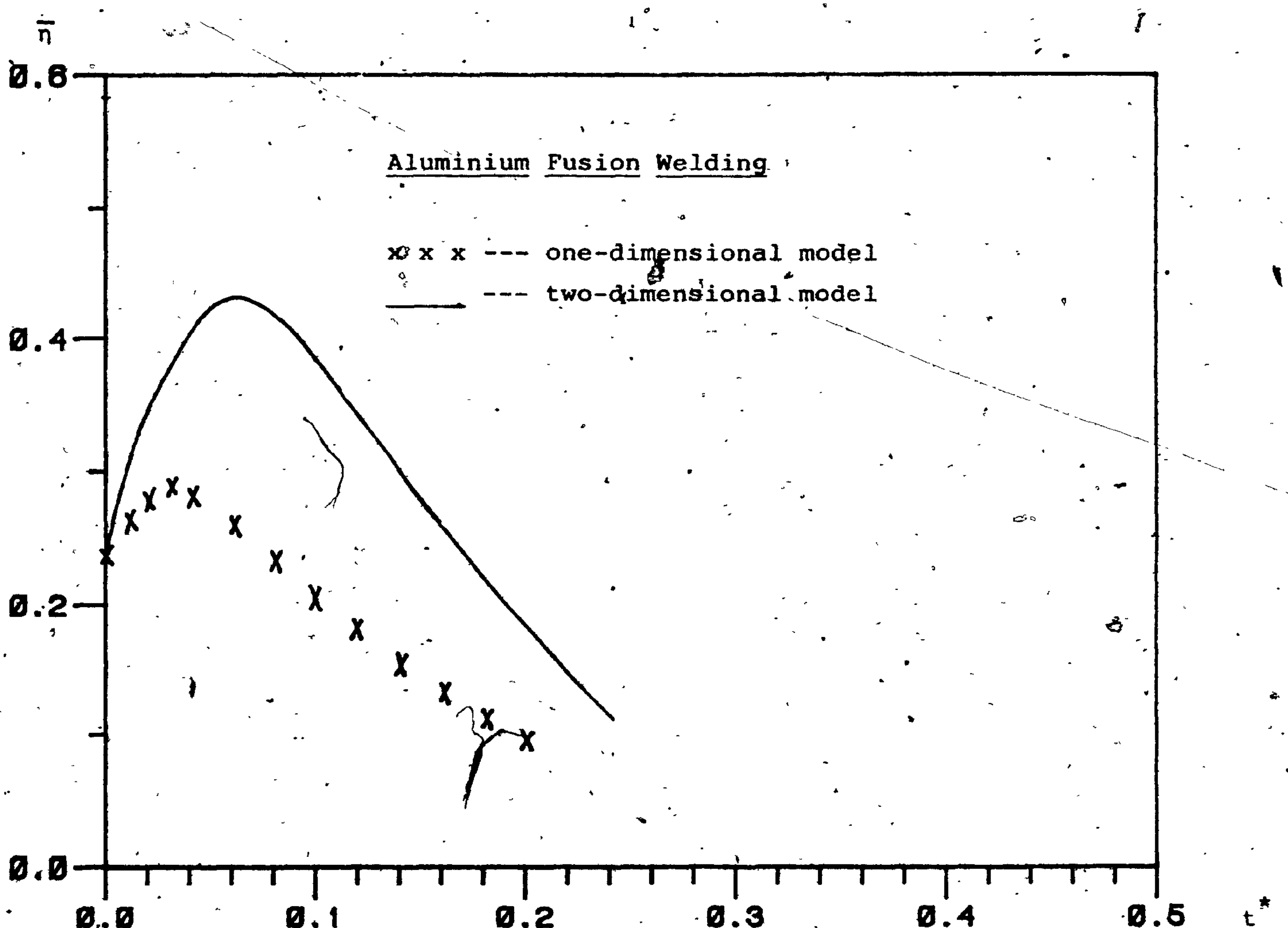

Figure 2. Comparison of the results obtained from one and two-dimensional models.

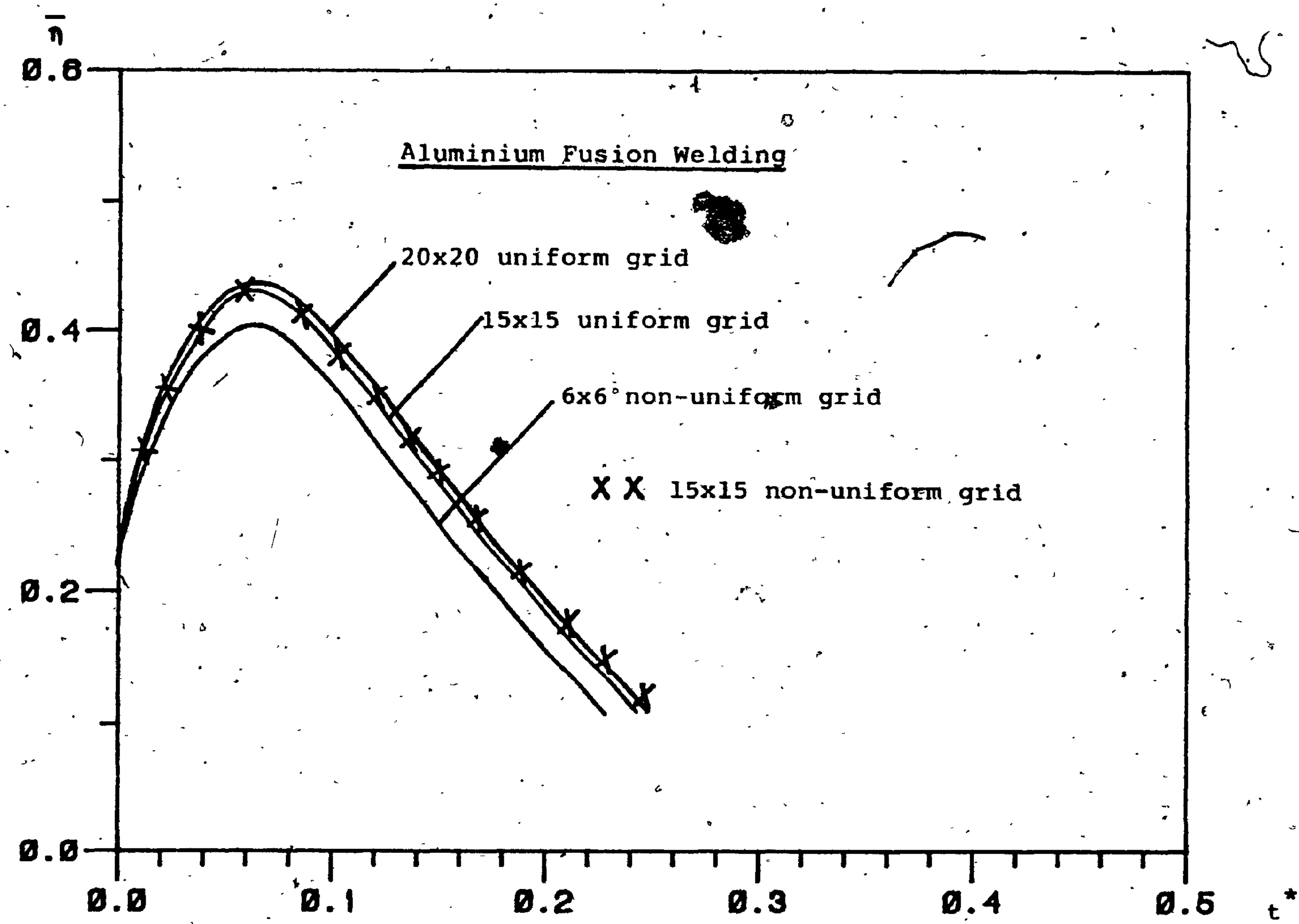

Figure 3. Comparison of the results obtained for different grid systems in 2-dimensional model.

5.2 Effect of Ra Numbers

In this section the effect of Ra number on the fusion welding process is studied. The numerical results calculated for the aluminium and lead fusion welding processes for the average value of the moving front, the pattern of the moving front, the isothermals, the temperature distributions, the stream lines, the average Nu number on the moving front, and the local Nu number on the moving front, are presented in fig.4 to fig.11 respectively.

As given in Table 2b, the Ra numbers for aluminium and lead fusion welding processes are about 7,000 and 115,000 respectively. The rest of dimensionless parameters calculated for these two processes are almost in the same magnitudes. Therefore the variation of values of Ra number will be considered as the main source effecting the numerical simulations.

The Movement of the Liquid-Solid Interface

In figure 4, the average value of the location of the moving liquid-solid interface defined as $\bar{\eta}=\sum_i(\eta_i/N)$ with time is presented for both the aluminium and lead fusion welding processes. In this figure, the slope of the $\bar{\eta}$-t^* curves represents the rate of propogation of the moving interface. The positive and negative values of $d\bar{\eta}/dt^*$ indicate the melting and solidification processes, respectively. The moving interface reaches its maximum value when the melting process stops. The solidification process starts following $d\bar{\eta}/dt^*=0$. As a higher value of Ra presents in the lead fusion welding process; a faster melting rate will result (as indicated in fig.4) due to the presence of a stronger natural convection. It is found that an almost the same cooling rate will appear in both processes shortly after the moving front reaches its maximum position. This can be considered to be the result of a flat temperature distribution in the liquid region in the solidification stage and a smaller temperature difference between the liquid and solid regions, as discussed late. A longer time will be needed for the process having a higher value of Ra to cool down the entire liquid region because of the larger molten region.

The Moving Interface Patterns

Disregarding the rate of movement of the liquid-solid interface, a study on the shape of the moving interface was carried out. The results are presented in figs.5 and 6 for both the aluminium and lead fusion welding processes respectively.

Examination of figs.5 and 6 reveals that, changing the values of Ra will result in the change of the shape of the liquid-solid interface. Increasing the value of Ra, will strengthen the non-linearity of the liquid-solid interface and will have a pronounced effect on the pattern of the liquid-solid interface.

The Isothermals

The isothermals for the aluminium fusion welding process are presented in figs.7a, 7b, and 7c for $t^*=0.01$, 0.03, and 0.05, respectively. The isothermal of $T^*=1.0$ $(=(T-T_a)/(T_m-T_a))$, represents the position of moving interface. It has been found that the isothermals are almost parallel and linear-vertical in the starting period as shown in fig.7a. Since there is almost no temperature difference in the y^*-direction, the effect of convection is minimal. Hence, in this case, conduction is the dominant part of heat transfer. The parallelism of the isothermals near the moving interface implies that a uniform heat transfer rate can be expected along the moving interface. Therefore a linear-vertical interface can be found as shown by $T^*=1.0$. While shortly after the starting period, a non-parallel and nonlinear-vertical isothermals are presented as shown in Figs. 7b and 7c.

By contrast in the lead fusion welding process, the isothermals for $t^*=0.01$, 0.03, and 0.05 appear as shown in figures 8a, 8b, and 8c, respectively. It can be observed that even in the early time step ($t^*=0.01$), the isothermals are no longer parallel and linear-vertical. As shown in Figs. 7b, 7c and Figs. 8a to 8c, a large vertical temperature difference is particularly evident in the liquid region. This would theoretically give rise to a strong convective circulation. A non-parallel isothermal in the liquid region will result in a non-uniform heat transfer rate along the vertical direction, and consequently a non-linear moving interface forms (as shown by the isothermal $T^*=1.0$).

Also it is noted in figs.7 and 8 that, the spacing of the isothermals is closer near the liquid-solid interface but wider near center of the liquid region. The gradient of the isothermals, when they are considered as functions of x_ℓ^*, have their maximum values near the top of the enclosure and close to the liquid-solid interface.

This characteristic can be explained by the flow pattern as shown later in figs.12 and 13. The maximum value of the gradient of isothermals is caused by the downward flow of the lower temperature liquid which has been cooled by the liquid-solid interface.

The Temperature Distributions

The dimensionless temperature distributions along center line ($y^*=1/2$), for both the liquid and solid regions, are presented for the aluminium and lead fusion welding processes in figures 9 and 10, respectively.

Comparing fig.9 with fig.10, it can be seen that, the temperatures near the centre of the liquid region ($y^*=1/2$), at $t^*=0.01$, are very similar. As the time progresses, the temperature drop near the centre of the liquid region for lead is faster than that for aluminium (see figs.9 and 10 at $t^*=0.03$ and 0.05). The reasons behind this phenomena are outlined below.

As the initial temperature is uniform in the liquid region, at the beginning of the fusion-welding process, the heat transfer process from the liquid to the solid phase is primarily due to conduction. Since the relevant material properties are very close for both the processes, the conduction rates should be similar. Hence the temperature reduction near the centre of the liquid region at the initial stage, for aluminium and lead, are very close.

With the development of fusion welding, the isothermals are no longer linear-vertical for the process having high values of Ra. There is a large temperature difference formed in the vertical direction.

Therefore a strong convective circulation appears in the liquid region. Hence more heat is taken away from the liquid region. This gives a faster drop in temperature near the centre of the liquid region for the process having high values of Ra. Because much heat is taken away from the liquid region, the temperature distribution in the liquid region along x^*-direction becomes flat as shown in fig.10 at $t^*=0.03$ and 0.05. The temperature difference between the solid and liquid regions is then small. This inversly slows down the heat transfer process as a small rate of conduction presences in this case.

A 3-dimensional plotting for the lead fusion welding process at different times is shown in fig.11. This gives another view of the temperature distributions in the whole field.

The Streamline Patterns

The results of the study of the streamline patterns with respect to the change of the values of Ra are presented in figures 12(a,b,c) and 13(a,b,c). Figs.12a and 13a, 12b and 13b, and 12c and 13c, are presented for different dimensionless values of time, $t^*=0.01$, 0.03, and 0.05, respectively. It can be observed that the general characteristic of the flow patterns is an upflow near the centre of liquid region, at $x_\ell^*=0$, where the molten metal is hotter, with a downflow near the liquid-solid interface, where the molten metal is cooler. It is found from the concentration of the stream lines that the velocities along the liquid-solid interface are higher than the velocities along both the horizontal walls and the center of the liquid region.

As indicated in fig.12b, the maximum value of ψ^* for the aluminium fusion welding process which has a smaller Ra value, is about -2.23. The maximum value of ψ^* for the lead fusion welding process which has a larger Ra value, is found to be equal to -19.5, as indicated in fig.13b. Hence, it can be estimated that the fluid flow for lead is almost 10 times stronger than that for aluminium . This supports the indication in the previous discussion, that when the value of Ra is large, a strong natural convective circulation will be presented.

A rather interesting situation appears in the lead fusion welding process as shown in figs.13b and 13c. A secondary flow near the bottom of the center is developed shortly after the starting period, at $t^*=0.03$. The secondary flow develops rapidly and occupies nearly the half space of the liquid region at $t^*=0.05$.

Both the stream lines and isothermals indicate that the thichness of the liquid region is greatest at the top and least at the bottom of the enclosure. It is interesting to note that the streamlines of higher values are restricted to the top portion of the liquid region and near the liquid-solid interface, where the temperature gradient is higher and hence the flow is maximum.

Nu Numbers Along the Liquid-Solid Interface

The local Nusselt numbers on the liquid-solid interface at different times for the cases of the aluminium and lead fusion welding processes are shown in figs.14 and 15, respectively. Where the local Nusselt number was defined based on the temperature gradient as follows,

$$Nu_y = - \frac{\partial T_\ell^*}{\partial x_\ell^*} \frac{y^*R}{\eta}\Big|_{x_\ell^*=1}$$

It is found from figs.14 and 15 that the local Nusselt number on the liquid-solid interface decreases considerablely with time.

The variation of the average Nusselt numbers on the liquid-solid interface with dimensionless time t^* for the cases of the aluminium and lead fusion welding processes are shown in figs.16 and 17, respectively. The average Nusselt number on the liquid-solid interface was defined as follows,

$$\overline{Nu}_y = \int_0^1 Nu_y \, dy^* = \sum_{i=1}^{N} Nu_{y_i} \, \Delta y_i^*$$

where N is the number of the grids in y^* direction.

The examination of these figures reveals that the natural convection in the liquid region dominates the heat transfer process in the early melting stage (except the very beginning). The natural convection will slow down in the transition from the melting process to the solidification process and then keep minimum afterwards during the rest of the solidification process. This phenomenon suggests that a pseudo one-dimensional model could be applied when the values of Nu number reaches its minimum during the solidification process. This means that in such situation there is no need in the calculation of the fluid flow and the temperature distribution in the liquid region as the temperature is at the melting point and uniformly distributed in the liquid region. This will subsequently save almost one third of the computation time. But the temperature gradient in y^* direction in the solid region still exist and should be determined from time to time.

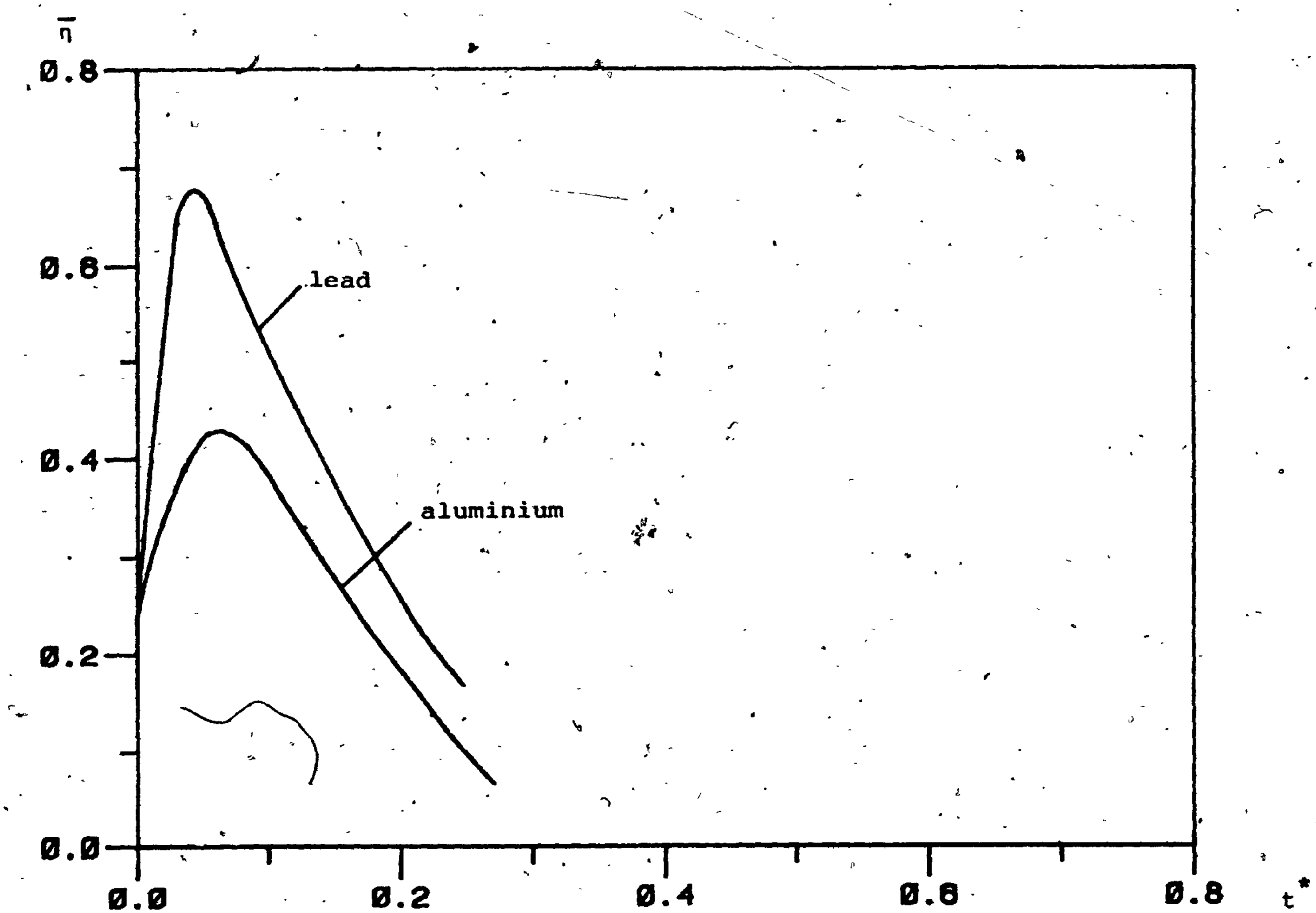

Figure 4. Average value of the location of the liquid-solid interface as a function of the dimensionless time for aluminium and lead fusion welding.

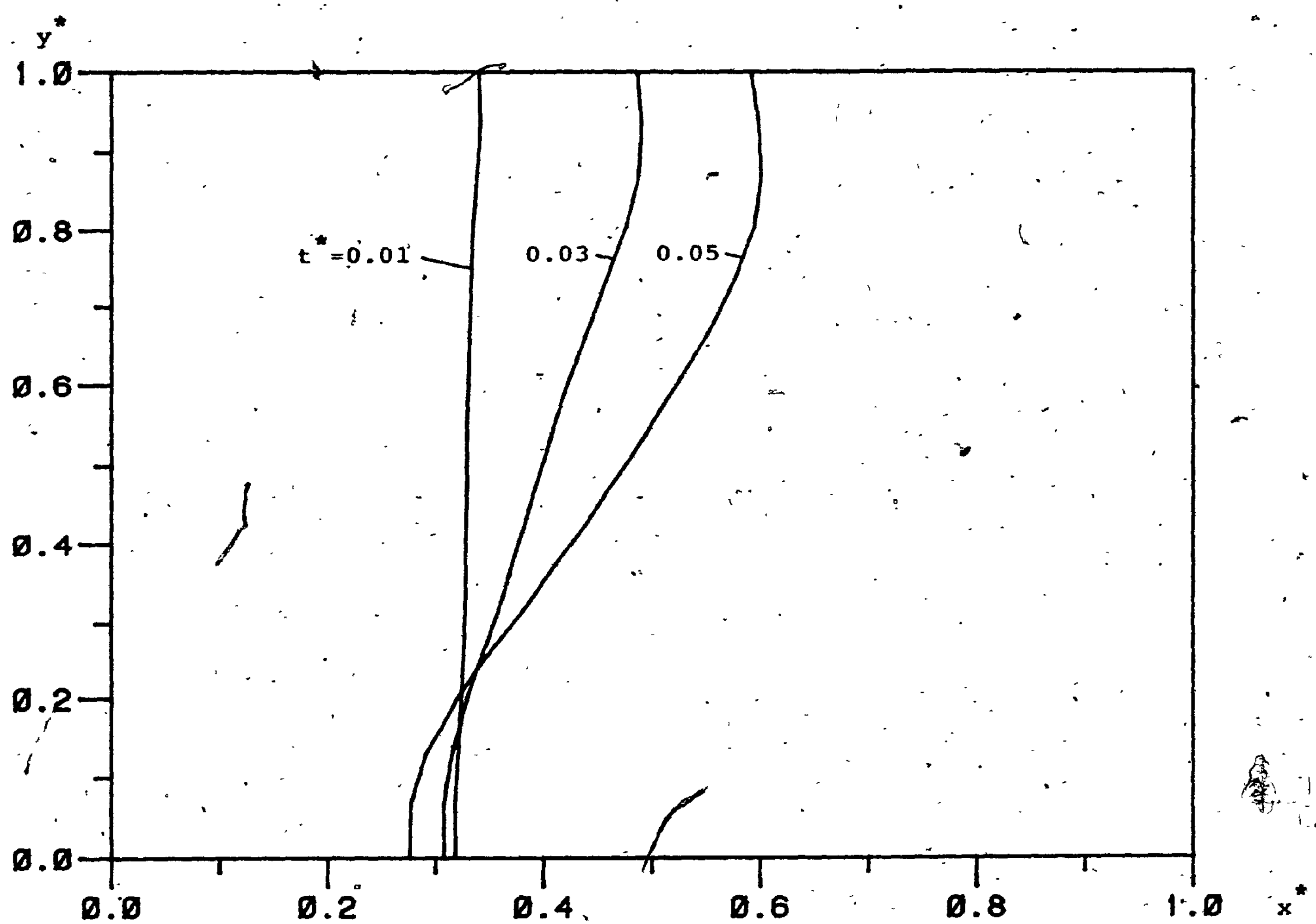

Figure 5. Moving interface patterns for aluminium fusion weddıng with the time as a parameter.

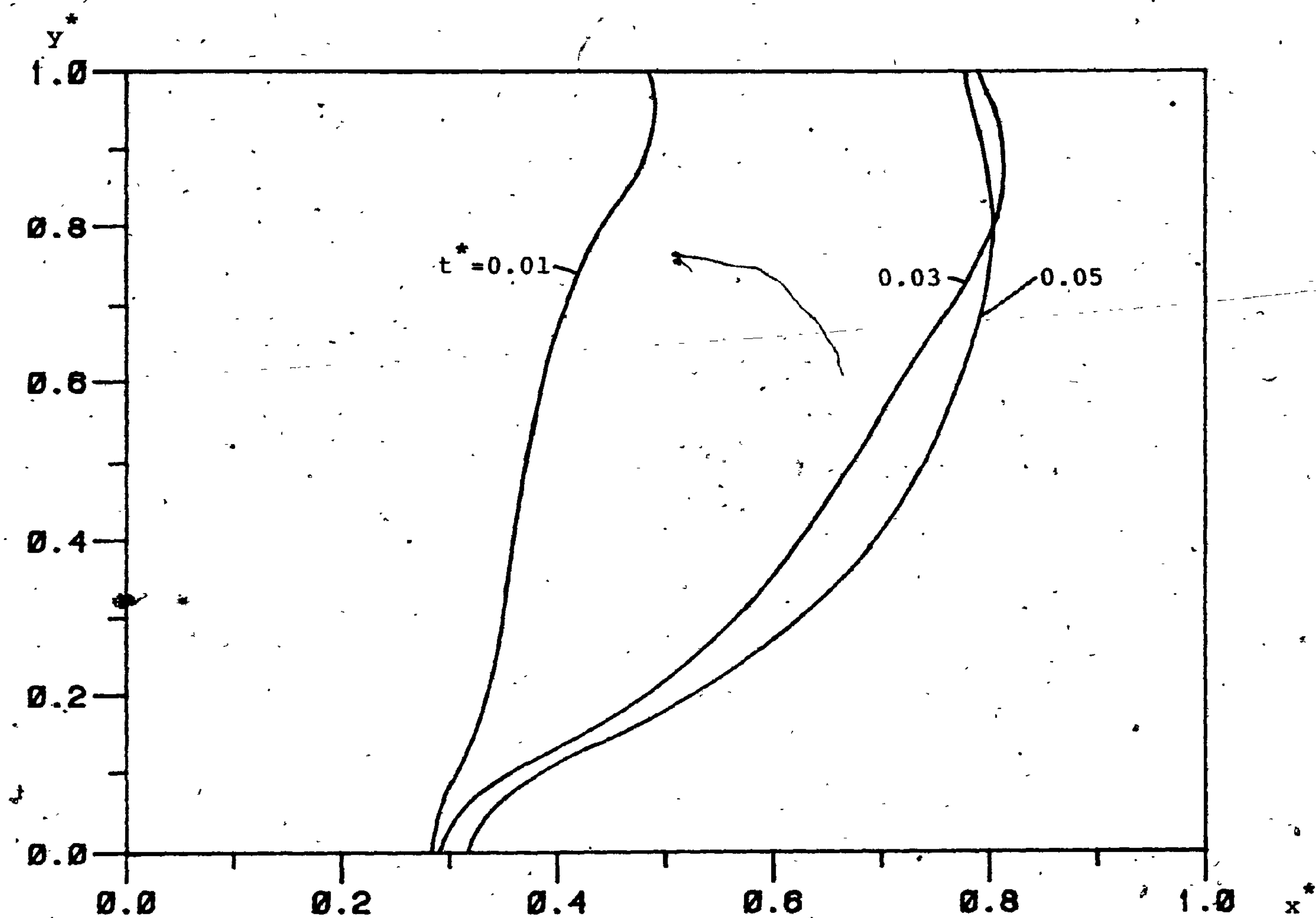

Figure 6. Moving interface patterns for lead fusion welding with the time as a parameter.

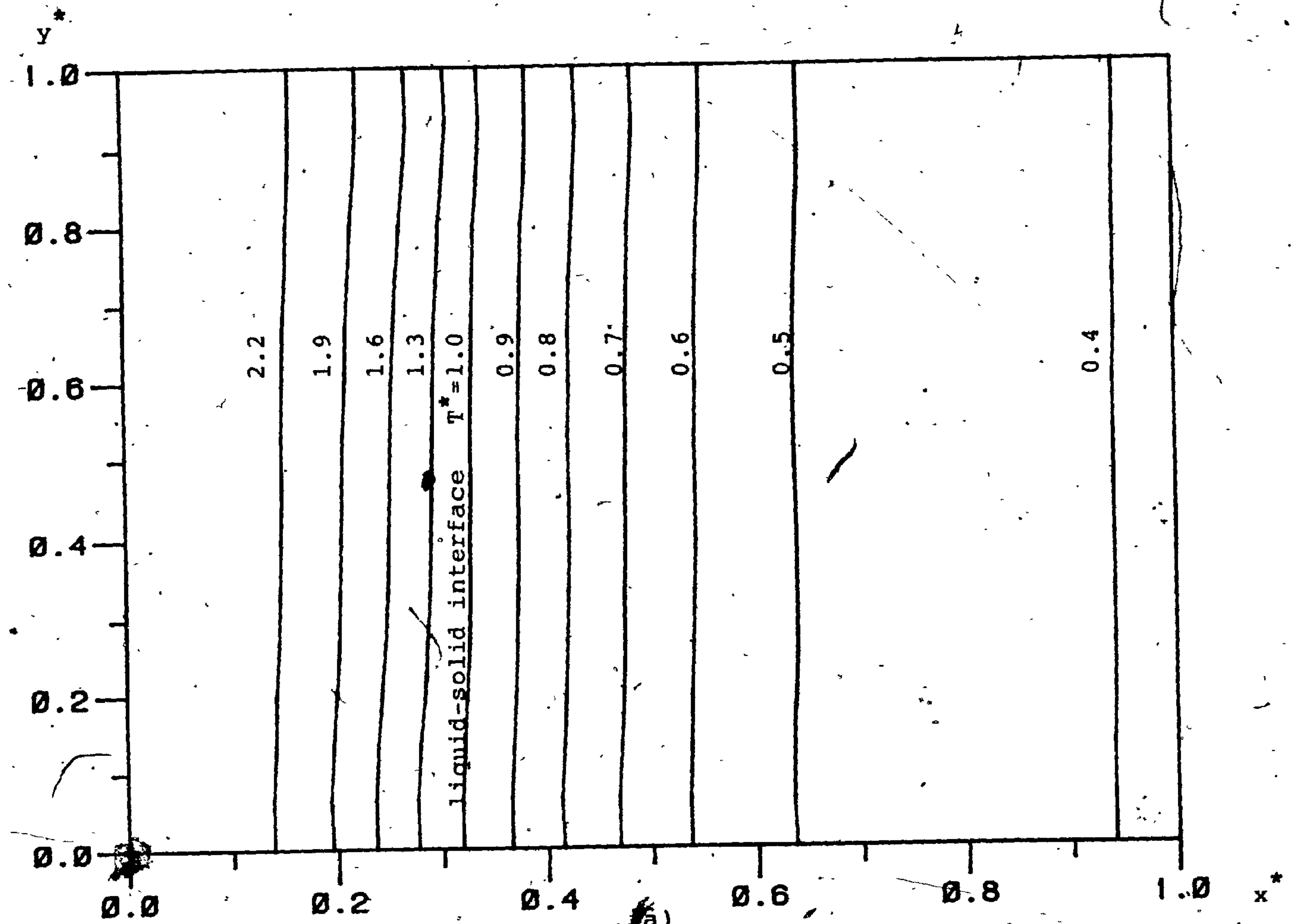

Figure 7. Isothermals for aluminium fusion welding for (a) $t^* = 0.01$ (b) $t^* = 0.03$ (c) $t^* = 0.05$.

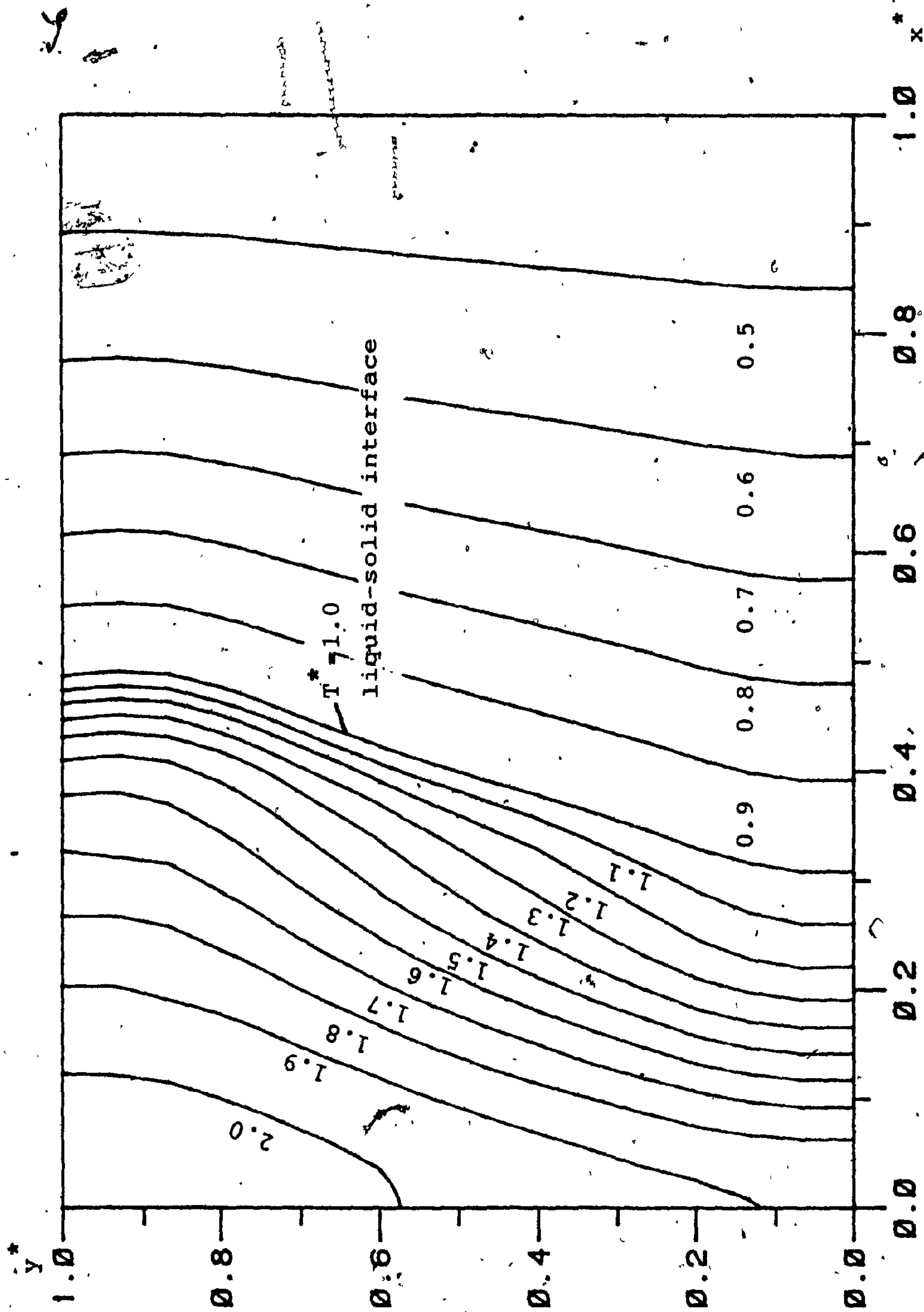
x*
y*
0.0
0.2
0.4
0.6
0.8
1.0
liquid-solid interface
T* = 1.0
0.5
0.6
0.7
0.8
0.9
1.1
1.2
1.3
1.4
1.5
1.6
1.7
1.8
1.9
2.0

(b)

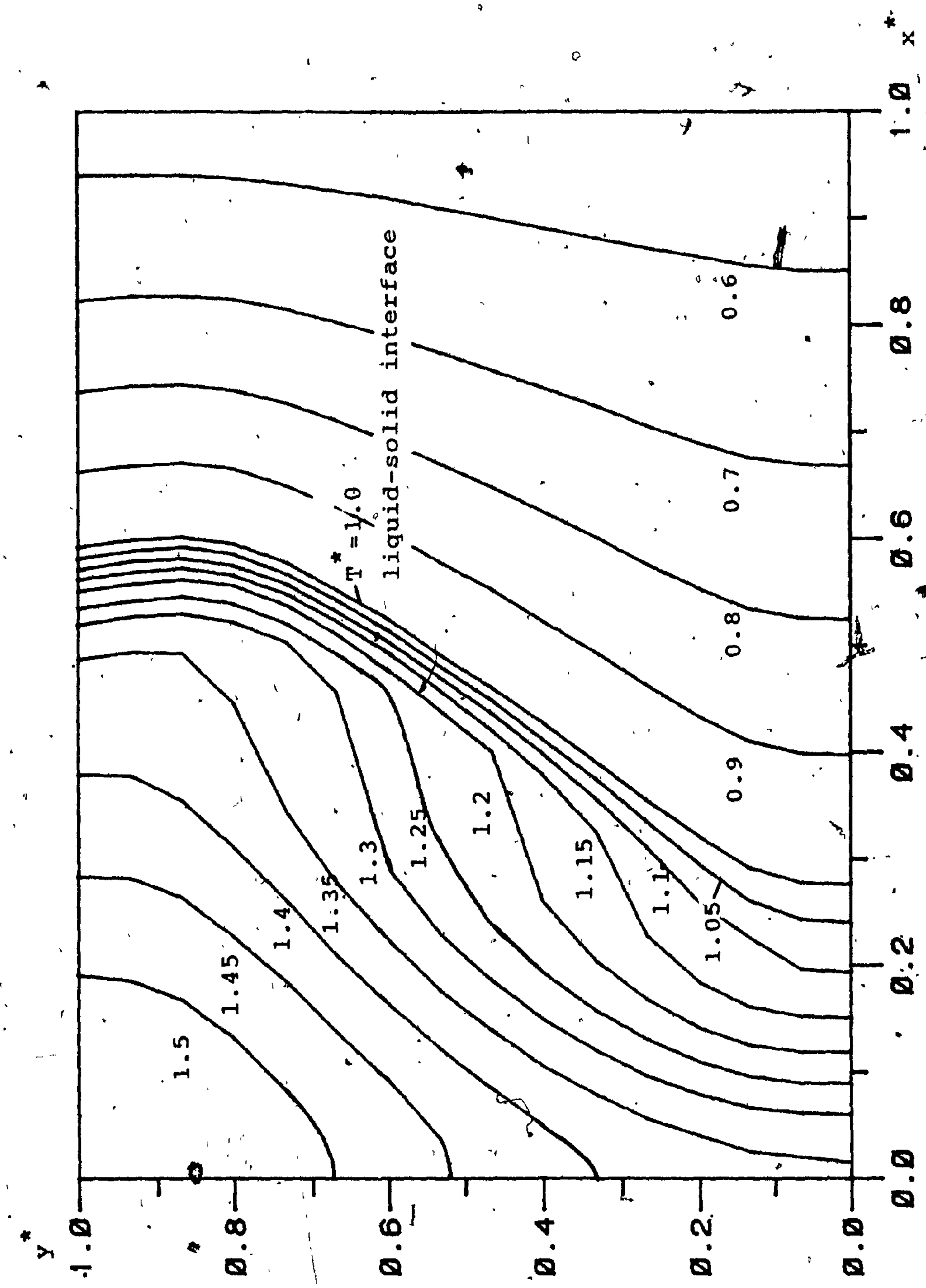

liquid-solid interface
T* = 1.0
0.6
0.7
0.8
0.9
1.05
1.1
1.15
1.2
1.25
1.3
1.35
1.4
1.45
1.5
x*
y*
0.0
0.2
0.4
0.6
0.8
1.0

(c)

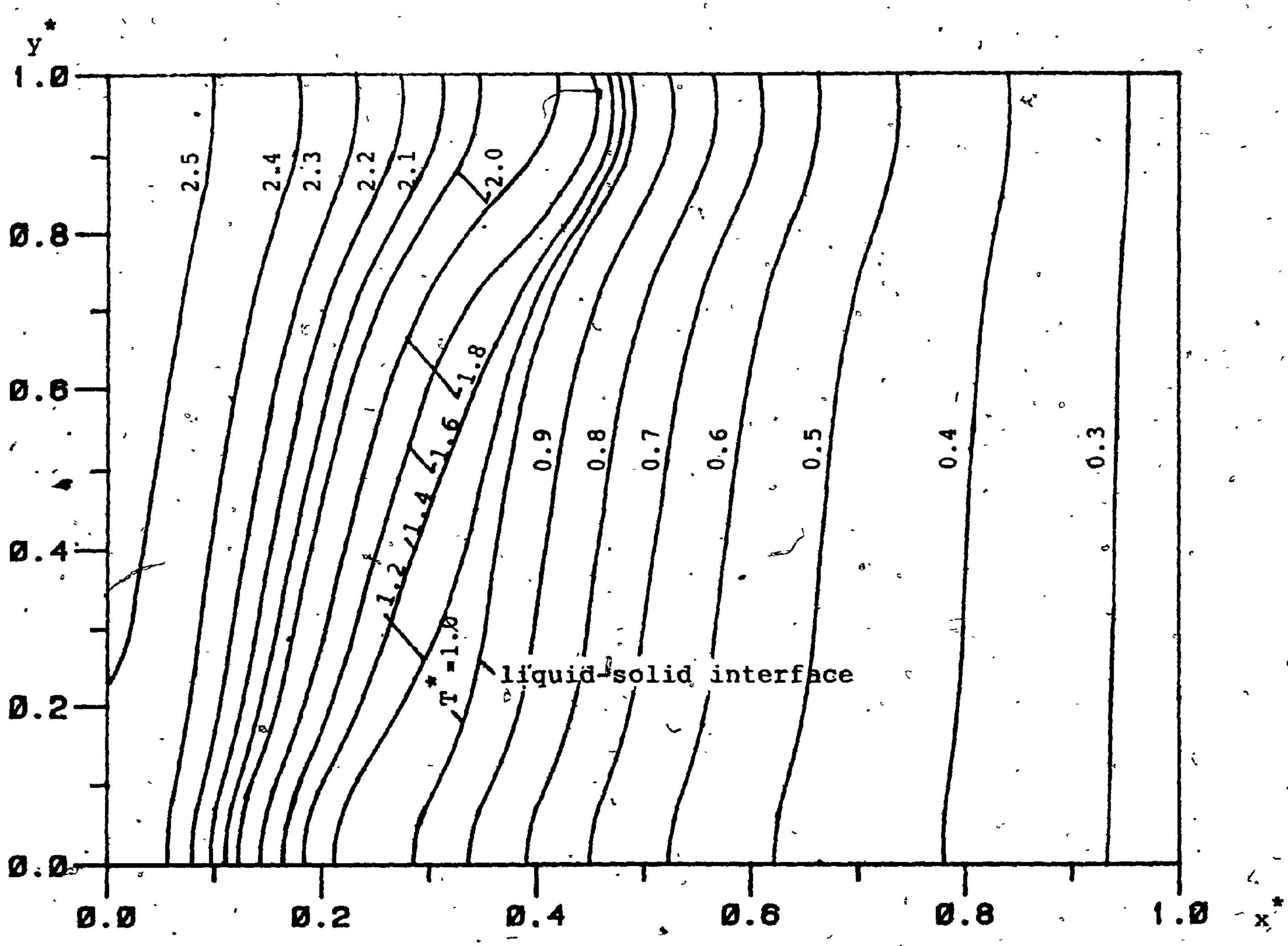

(a)

Figure 8. Isothermals for lead fusion welding for (a) $t^*=0.01$ (b) $t^*=0.03$ (c) $t^*=0.05$.

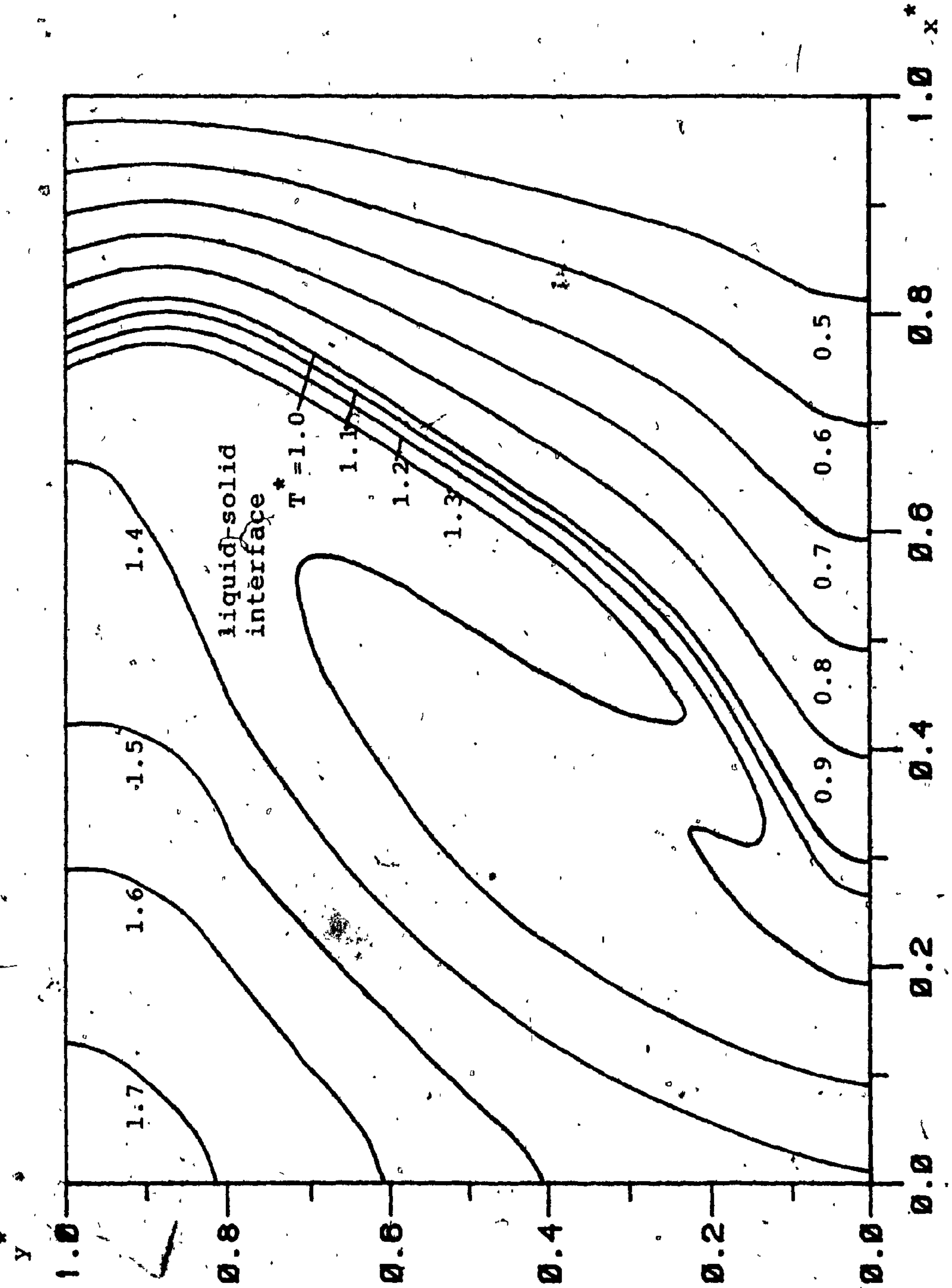

y^*
1.0
0.8
0.6
0.4
0.2
0.0
x^*
liquid-solid interface
T^* =1.0
1.1
1.2
1.3
1.4
1.5
1.6
1.7
0.5
0.6
0.7
0.8
0.9

(b)

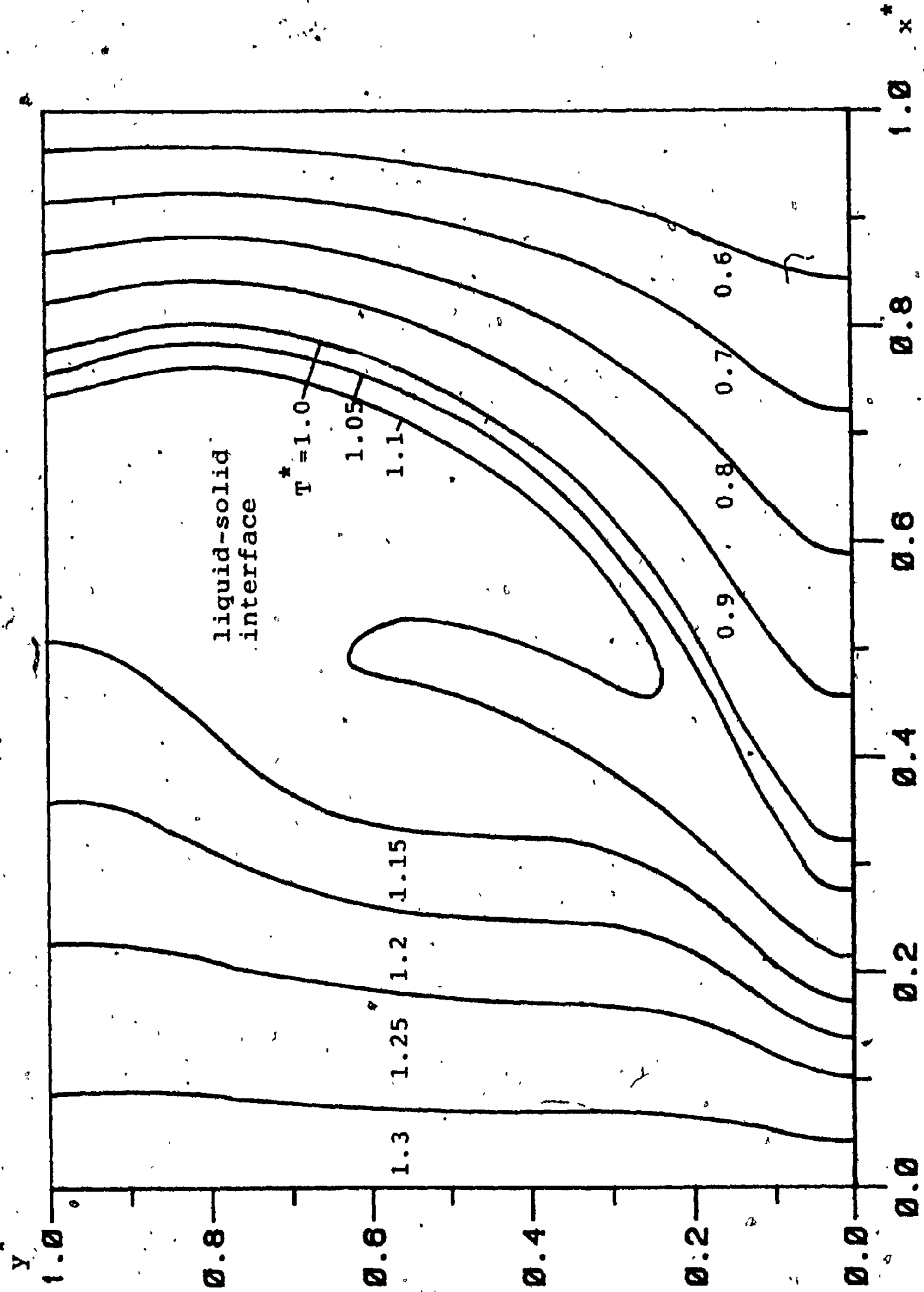

liquid-solid
interface
T^*=1.0
1.05
1.1
0.6
0.7
0.8
0.9
1.15
1.2
1.25
1.3
x^*
0.0
0.2
0.4
0.6
0.8
1.0
y^*
0.0
0.2
0.4
0.6
0.8
1.0

(c)

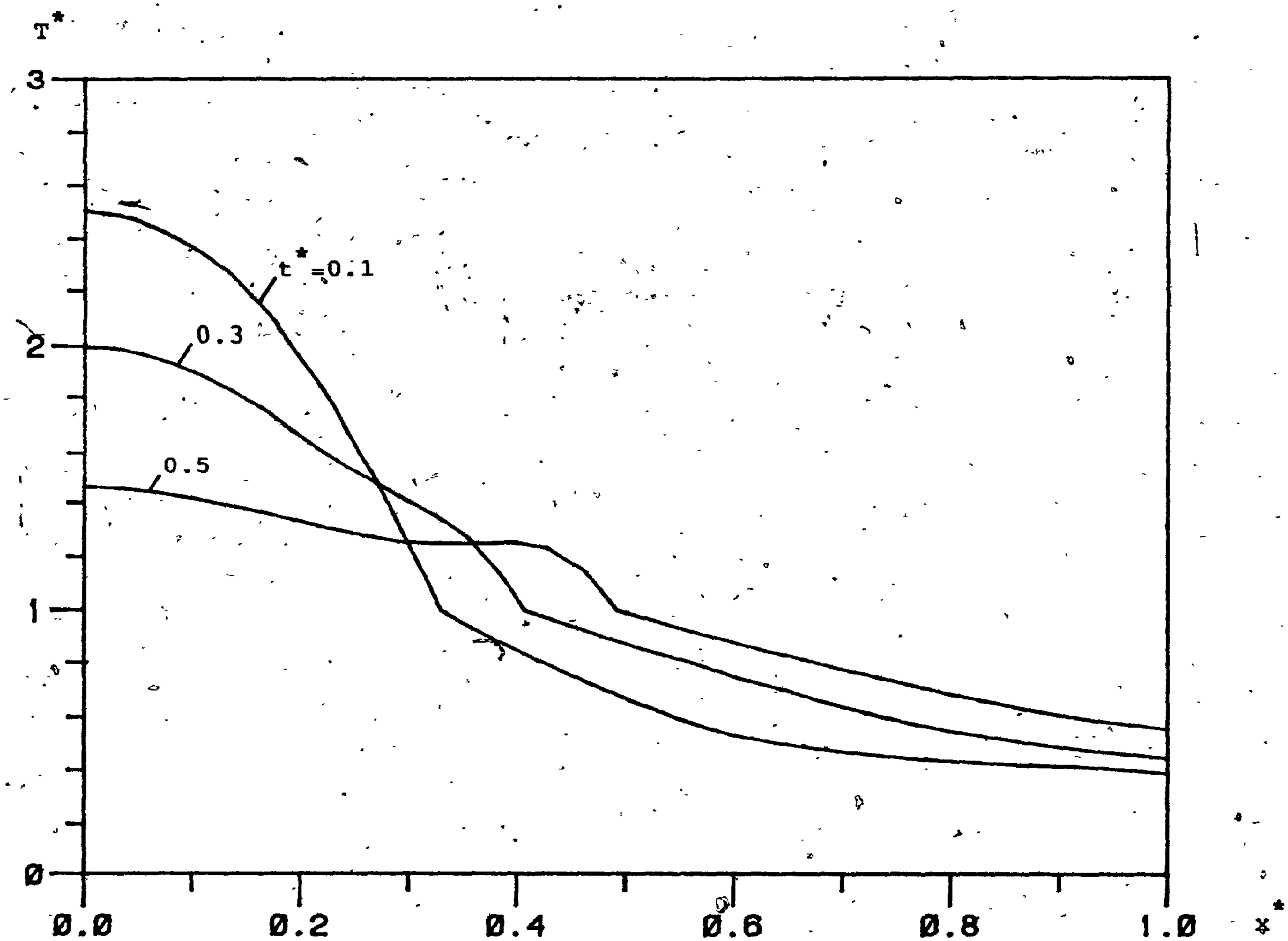

Figure 9. Temperature distribution along center line ($y^*=\frac{1}{2}$) for aluminium fusion welding.

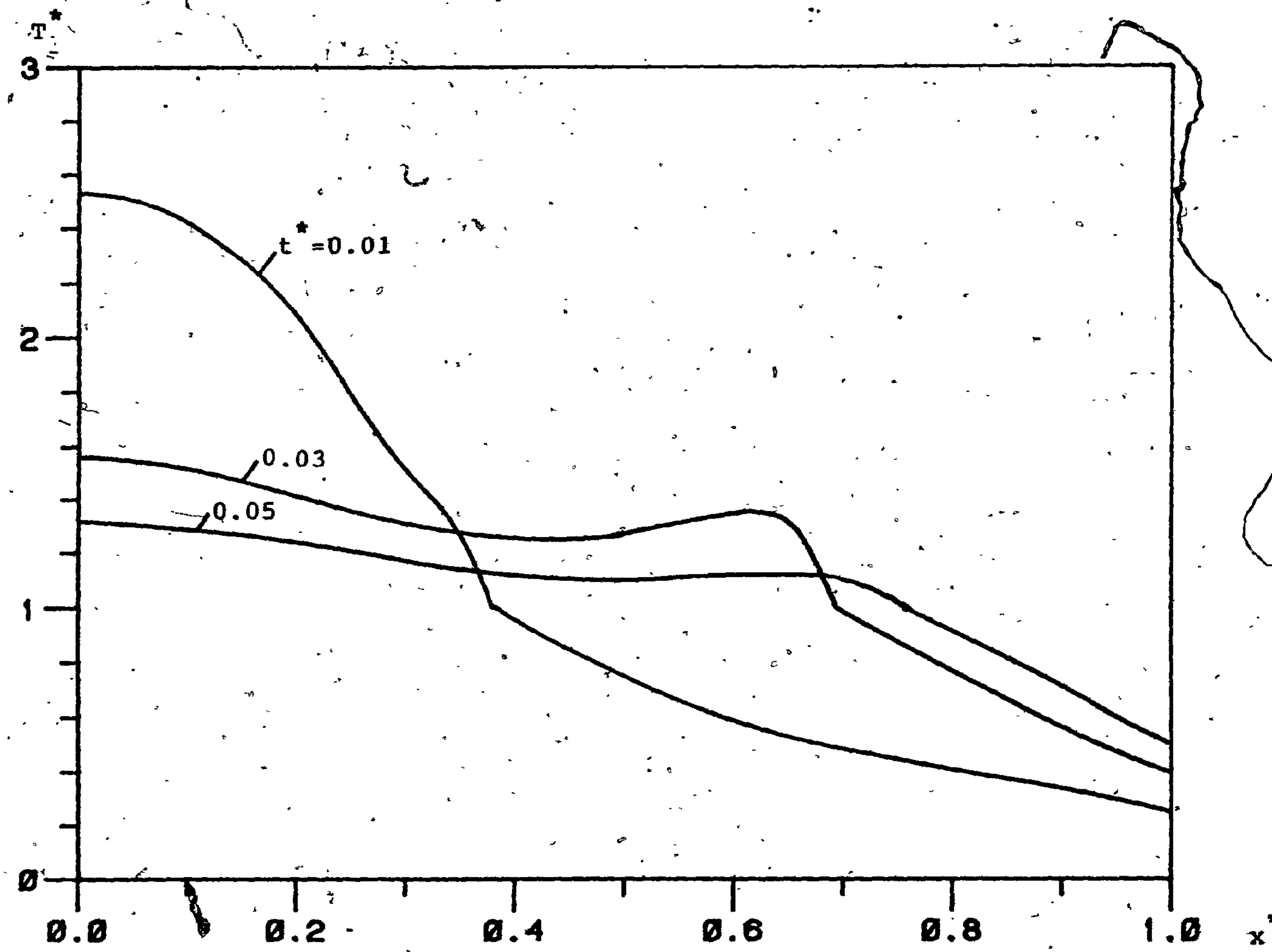

Figure 10. Temperature distribution along center line ($y^* = \frac{1}{2}$) for lead fusion welding.

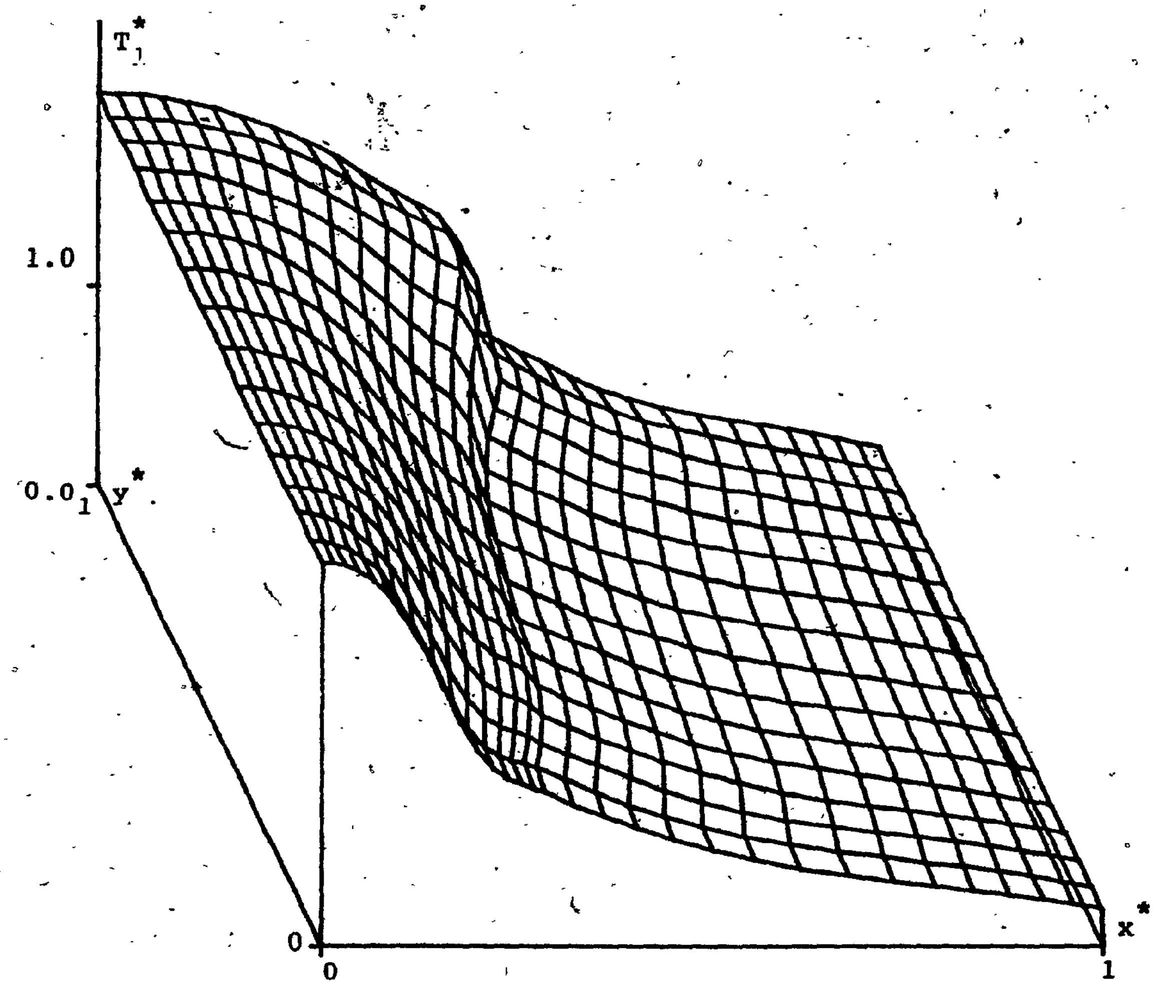

(a)

Figure 11. A 3-D temperature distribution for lead fusion welding for (a) $t^*=0.01$ (b) $t^*=0.03$ (c) $t^*=0.05$.

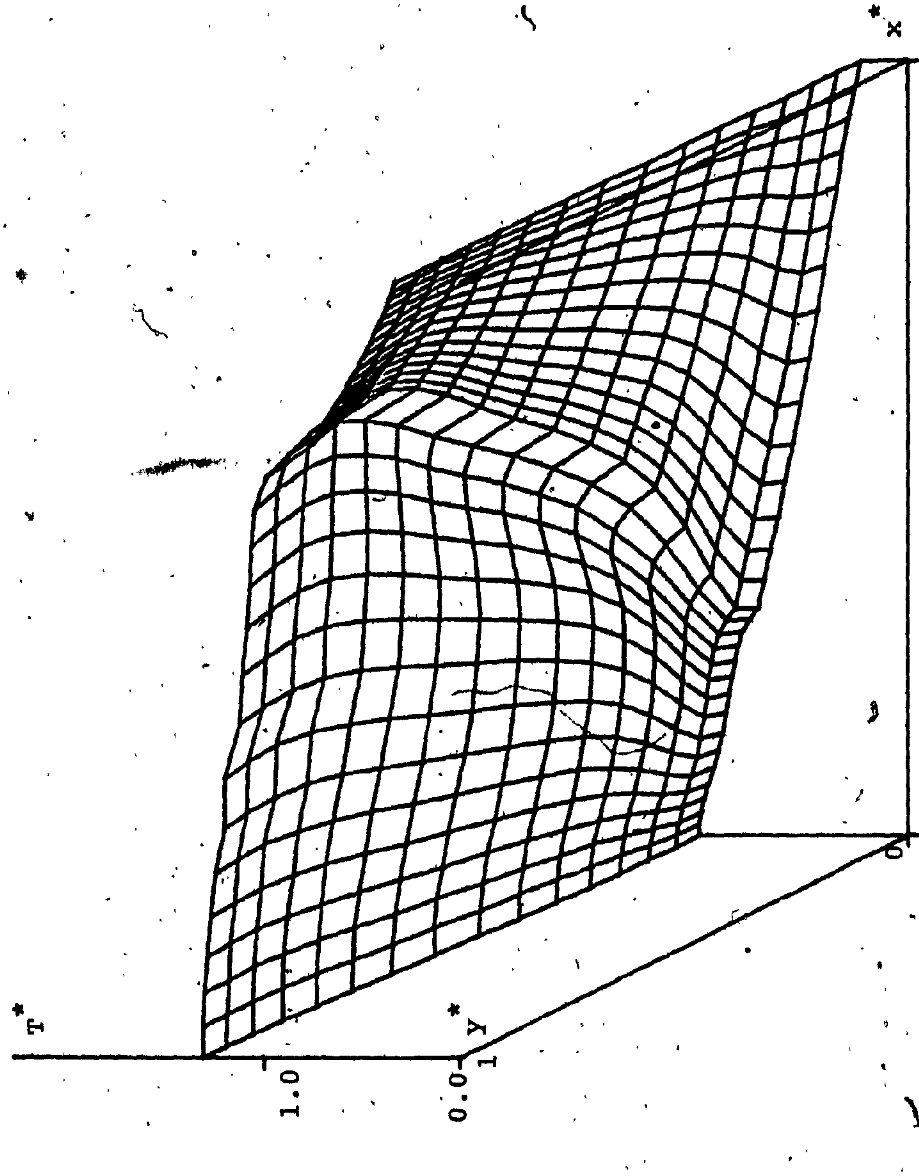

(b)

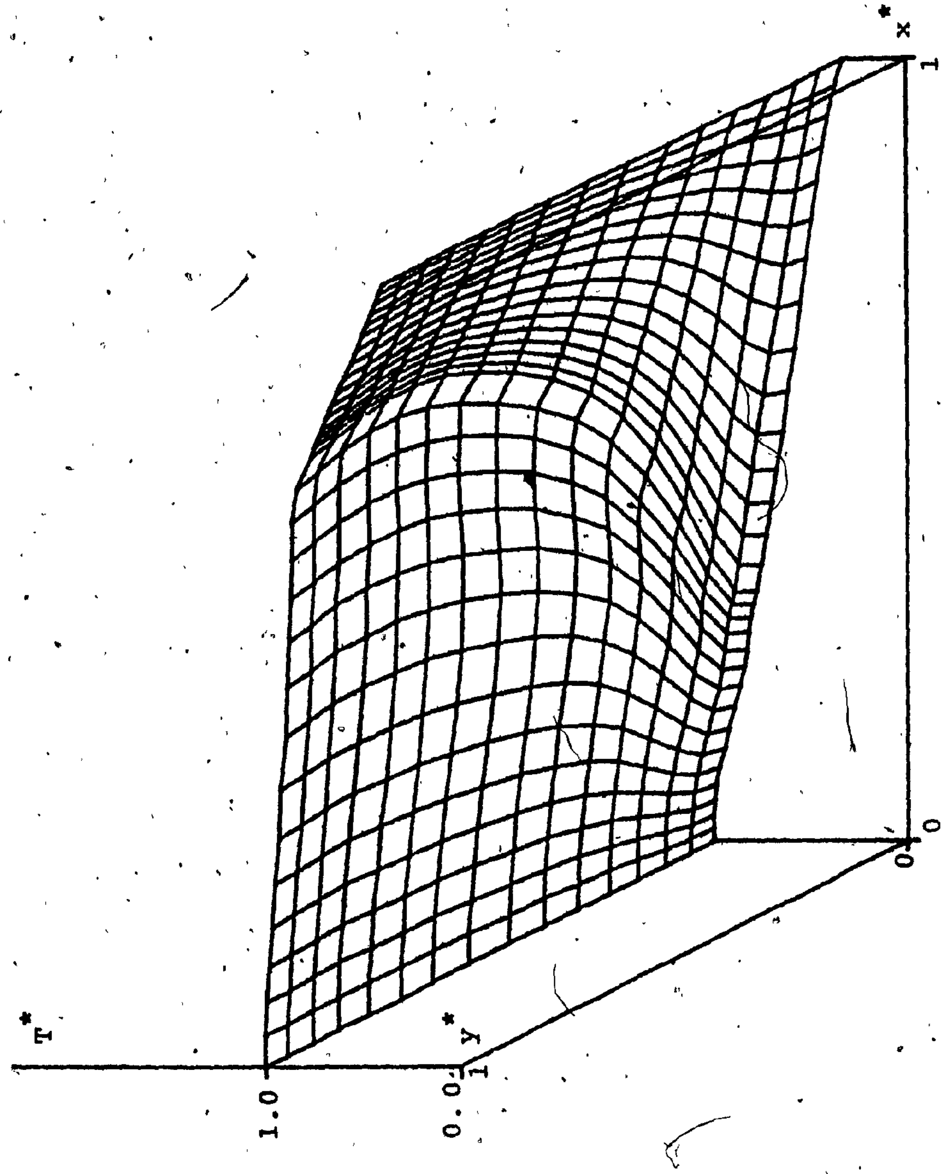

(c)

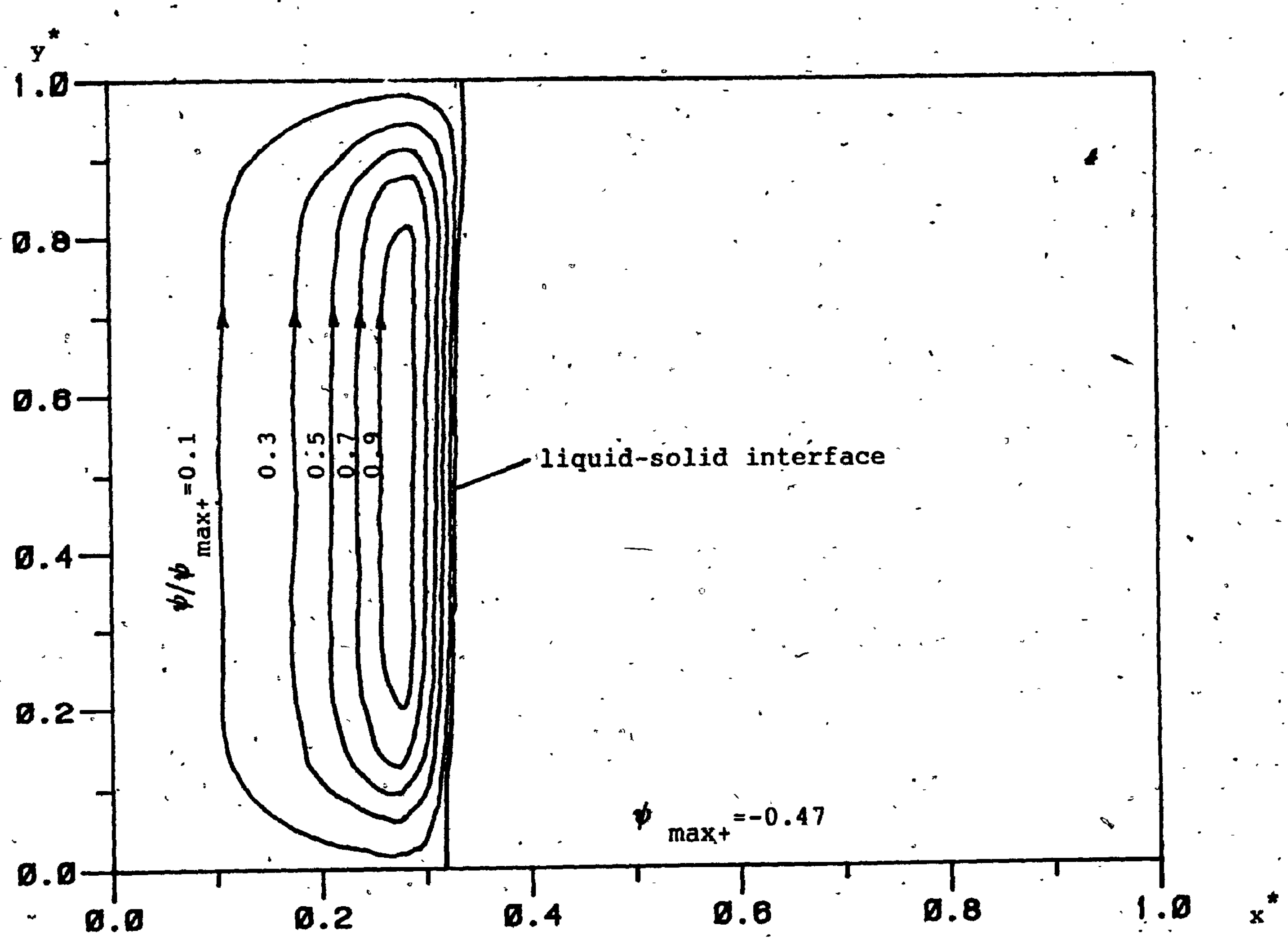

(a)

Figure 12. Stream line contours for aluminium fusion welding for (a) $t^*=0.01$ (b) $t^*=0.03$ (c) $t^*=0.05$.

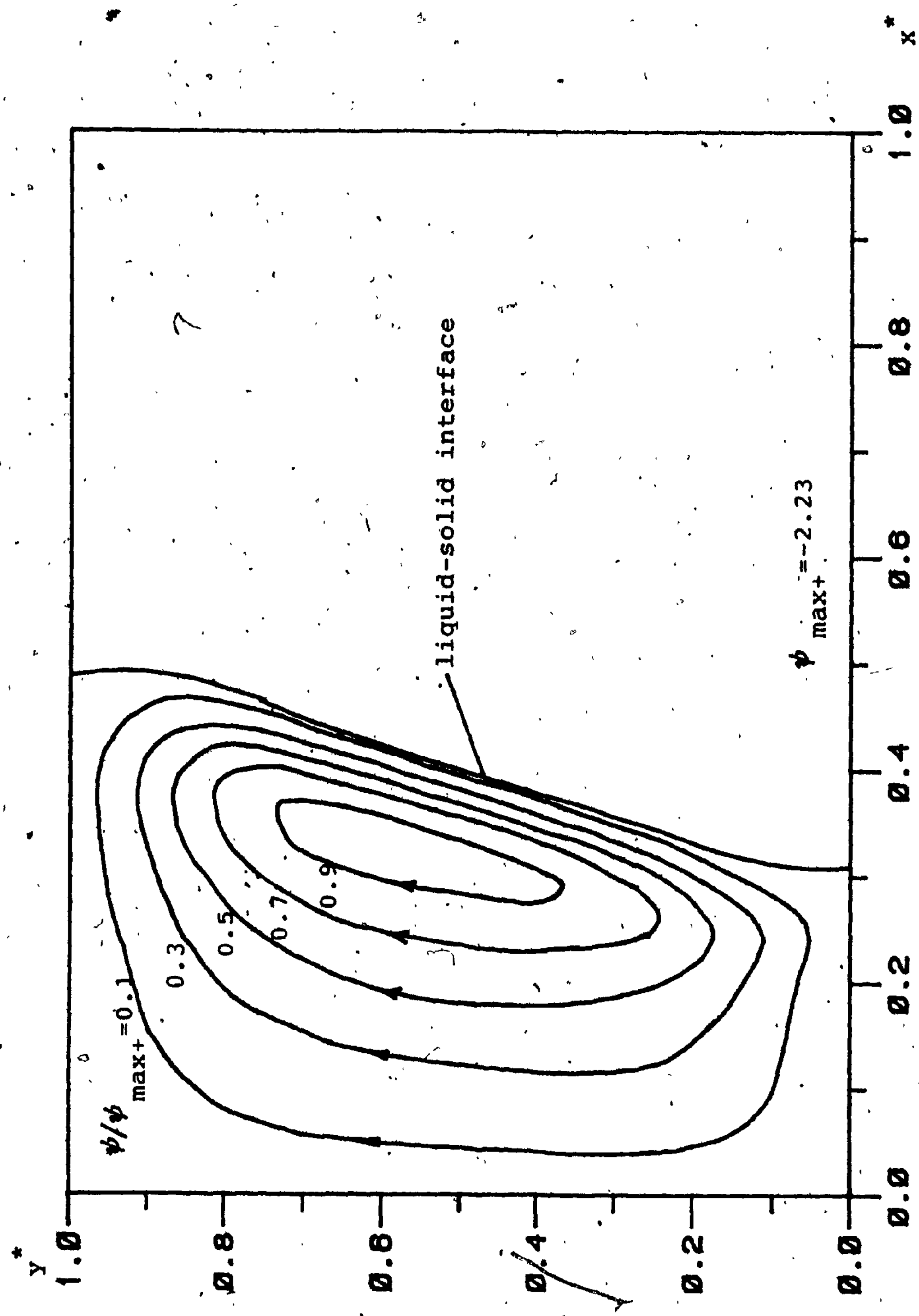

y*
1.0
0.8
0.6
0.4
0.2
0.0
x*
0.0
0.2
0.4
0.6
0.8
1.0
liquid-solid interface
ψ/ψ max+ =0.1
0.3
0.5
0.7
0.9
ψ max+ =-2.23

(b)

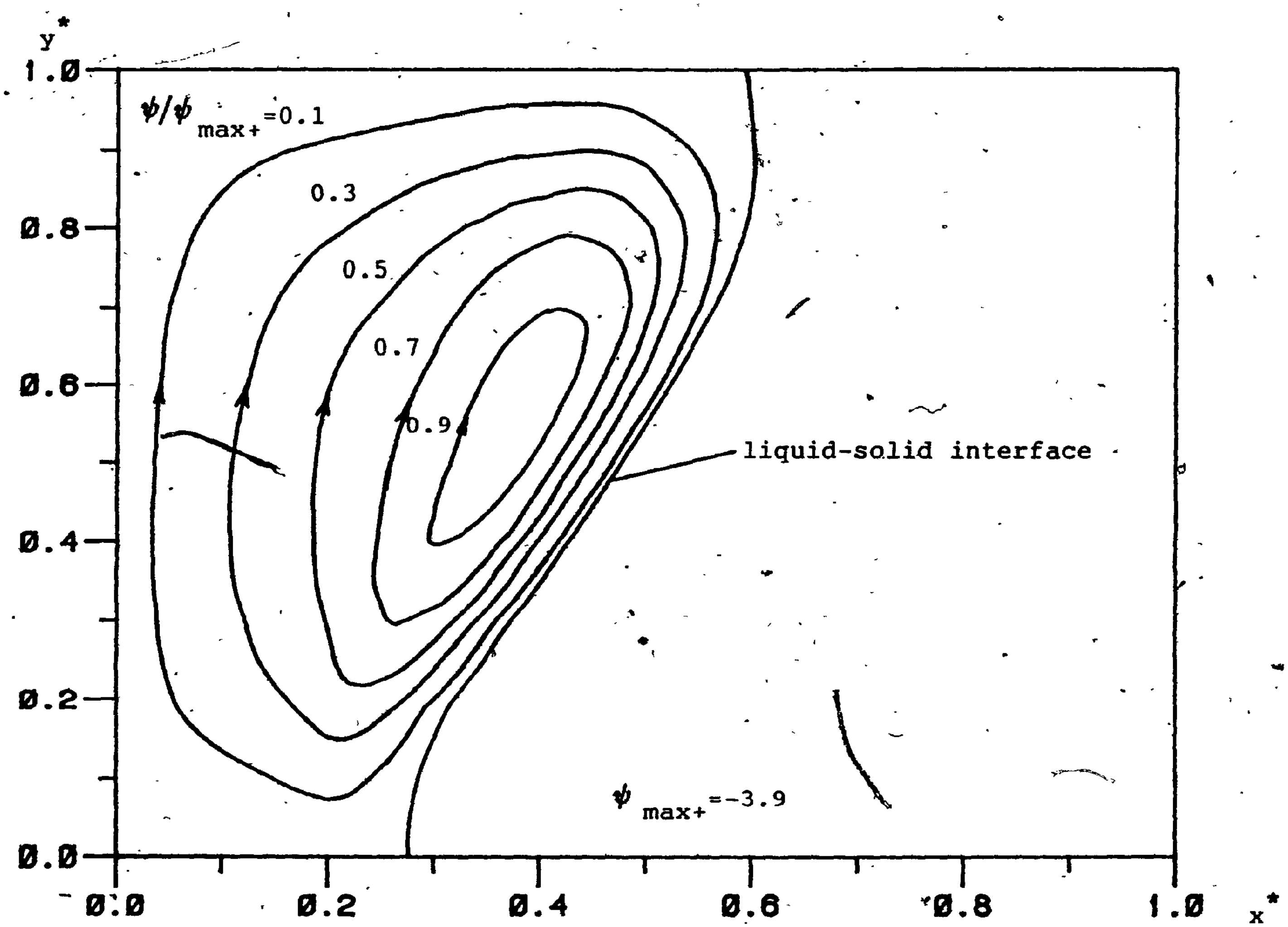
y*
1.0
0.8
0.6
0.4
0.2
0.0
0.0
0.2
0.4
0.6
0.8
1.0
x*
ψ/ψ max+=0.1
0.3
0.5
0.7
0.9
liquid-solid interface
ψ max+=-3.9

(c)

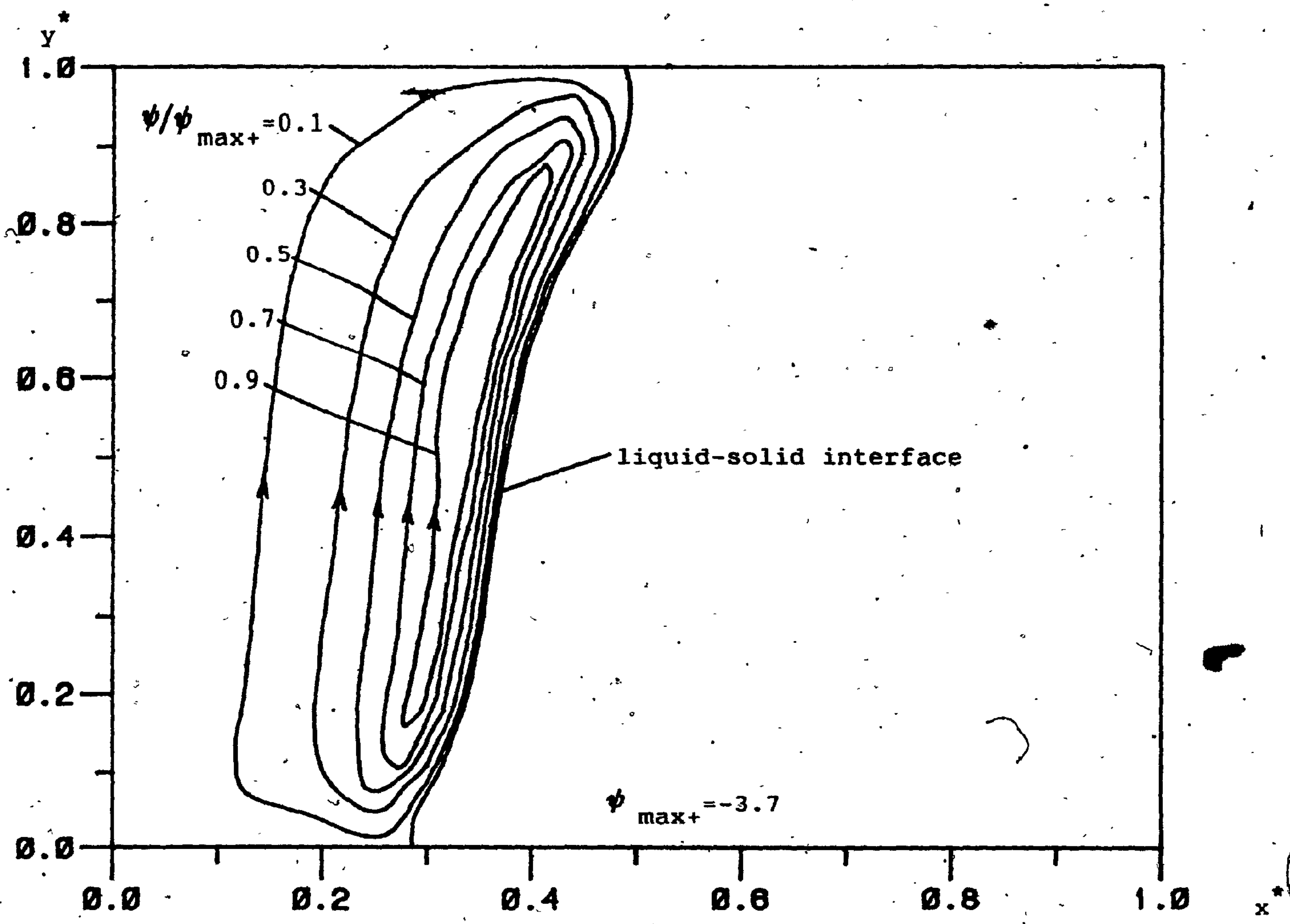

(a)

Figure 13. Stream line contours for lead fusion welding for (a) $t^*=0.01$ (b) $t^*=0.03$ (c) $t^*=0.05$.

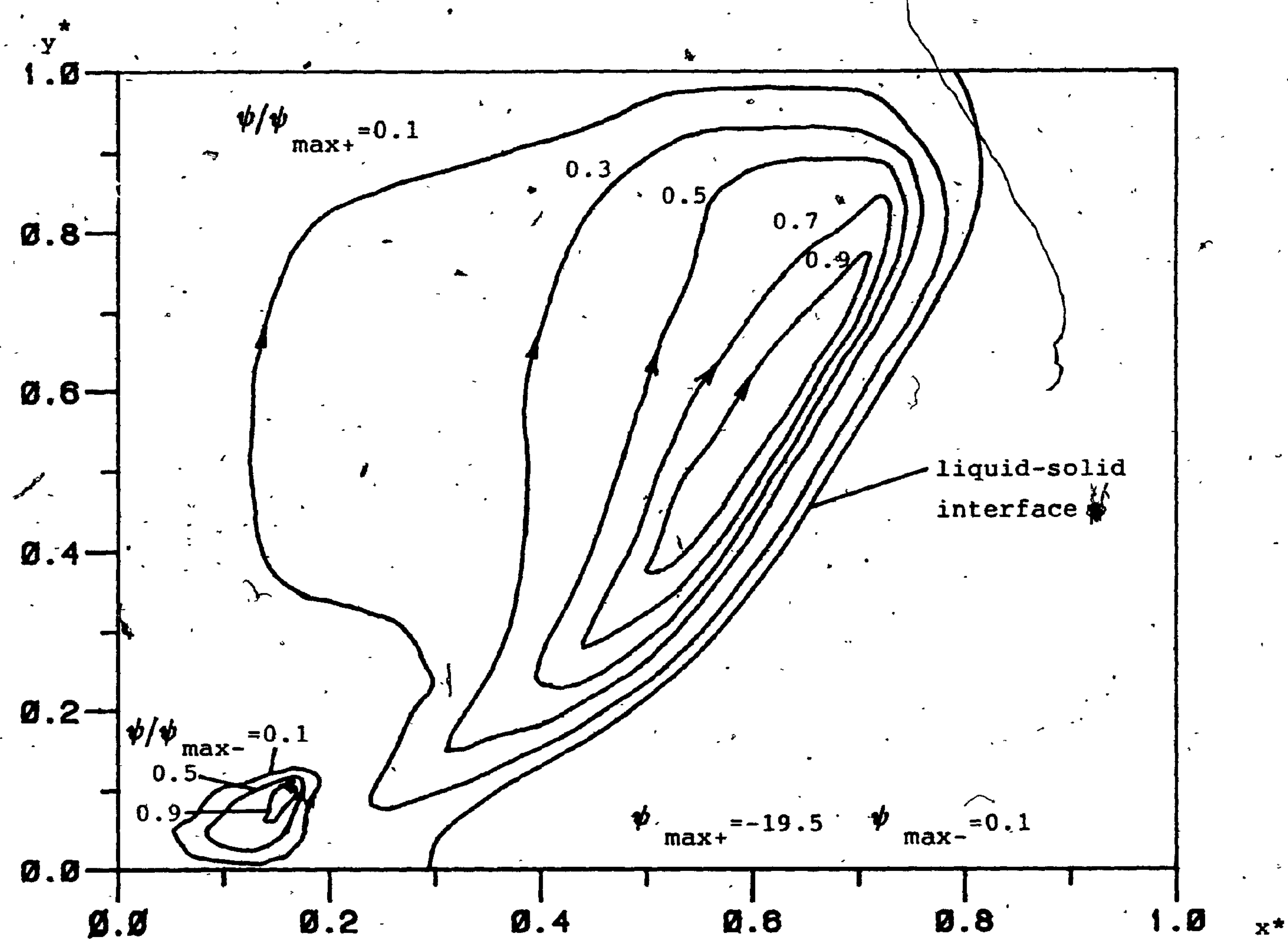
y*
1.0
0.8
0.6
0.4
0.2
0.0
0.0
0.2
0.4
0.6
0.8
1.0
x*
ψ/ψ max+ =0.1
0.3
0.5
0.7
0.9
liquid-solid
interface
ψ/ψ max- =0.1
0.5
0.9
ψ max+ =-19.5 ψ max- =0.1

(b)

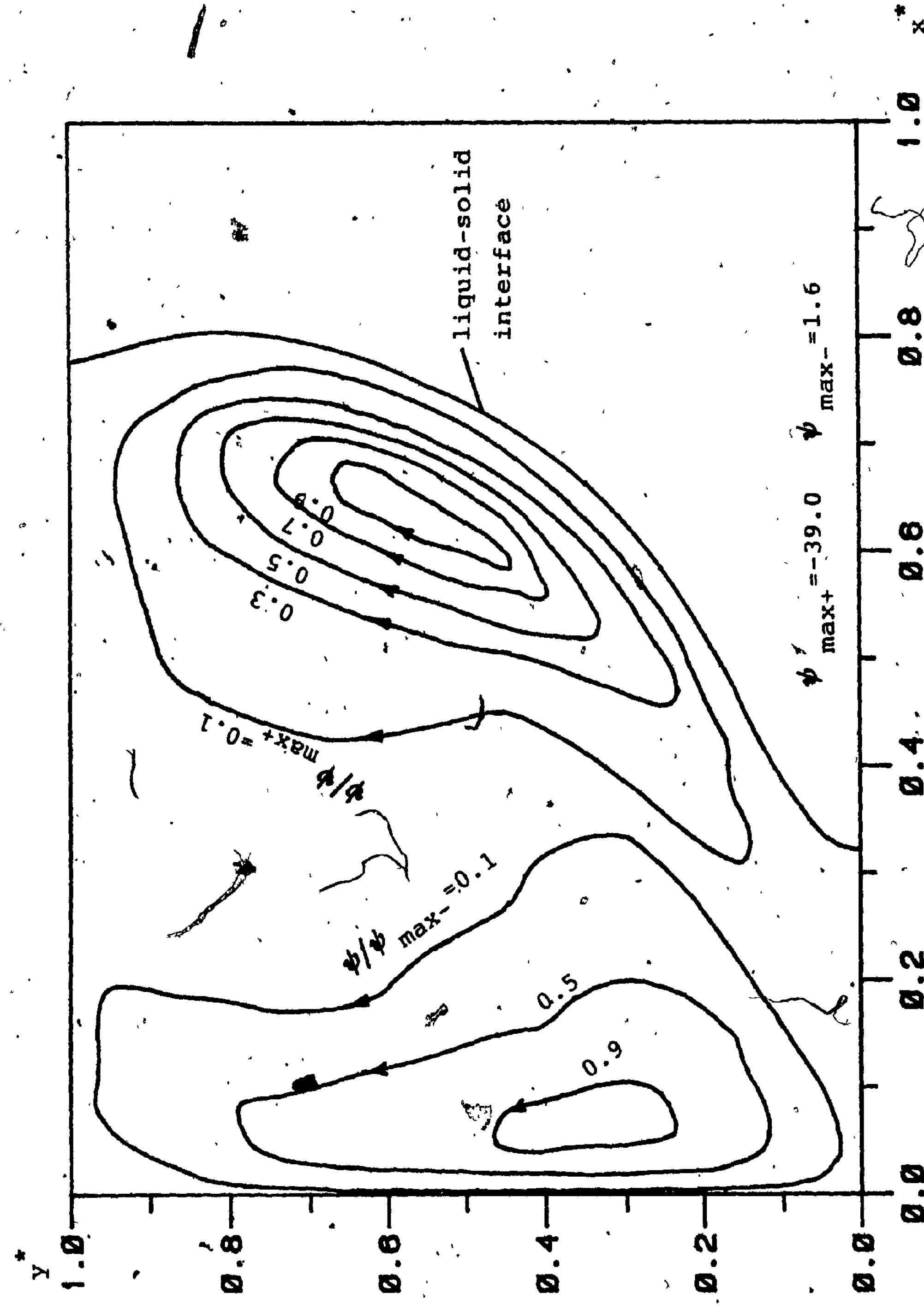
liquid-solid interface
ψ/ψ max+ =0.1
0.3
0.5
0.7
0.9
ψ/ψ max- =0.1
0.5
0.9
ψ max+ =-39.0 ψ max- =1.6
x*
y*
0.0
0.2
0.4
0.6
0.8
1.0

(c)

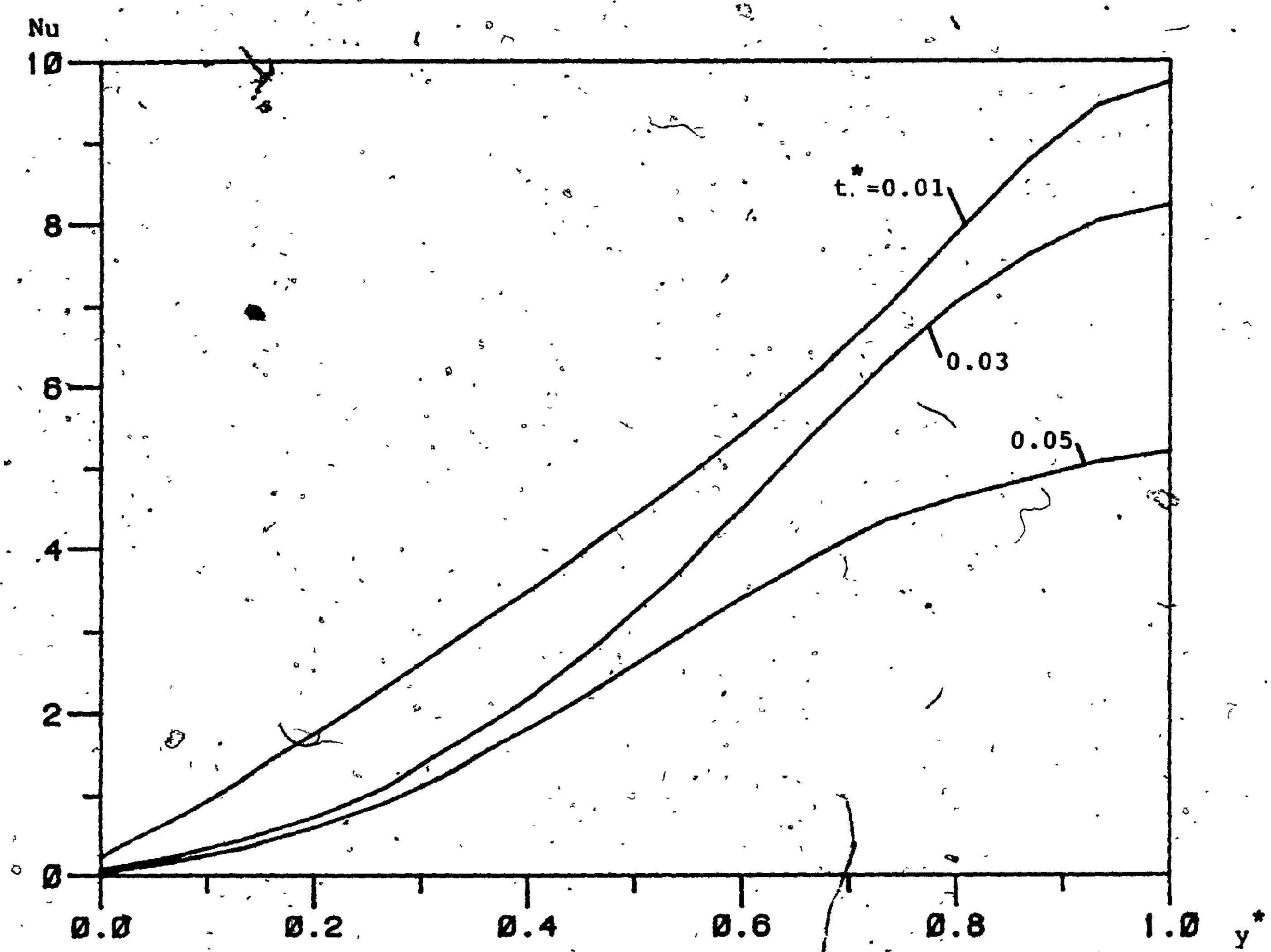

Figure 14. Calculated local Nusselt numbers along the liquid-solid interface for aluminium fusion welding with time as parameter.

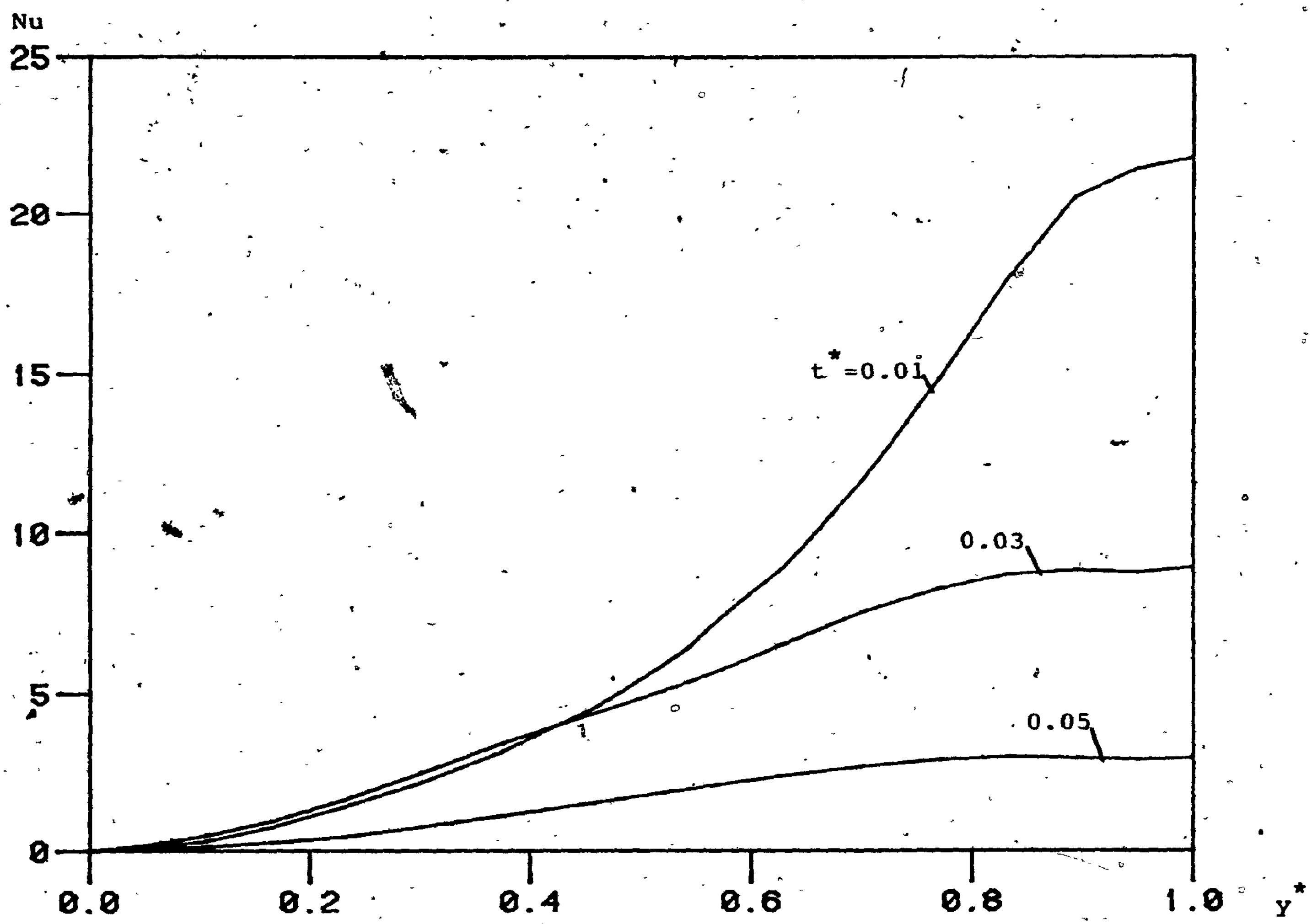

Figure 15. Calculated local Nusselt numbers along the liquid-solid interface for lead fusion welding with time as parameter.

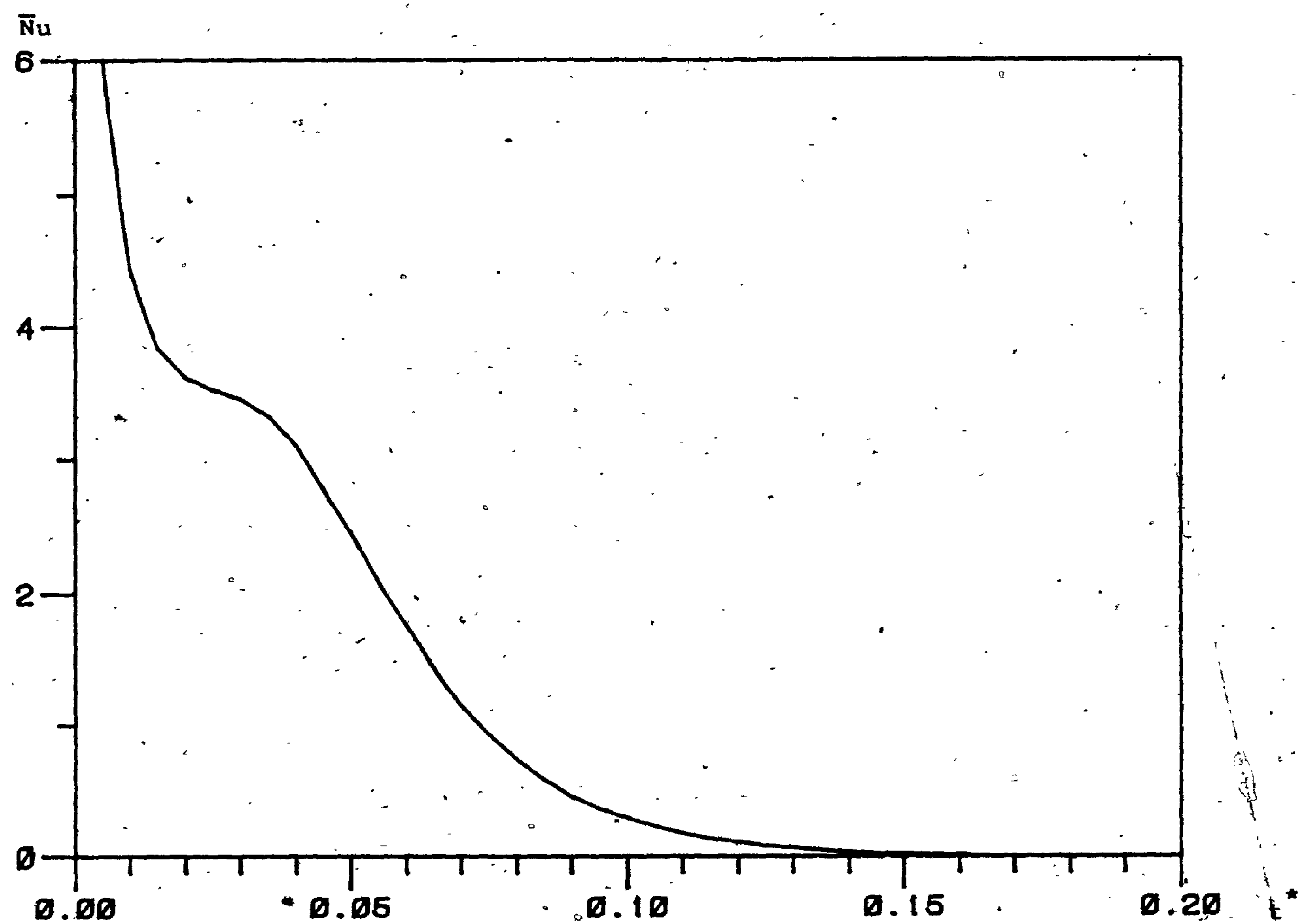

Figure 16. Variation of the average Nusselt number on the liquid-solid interface for the aluminium fusion welding with time.

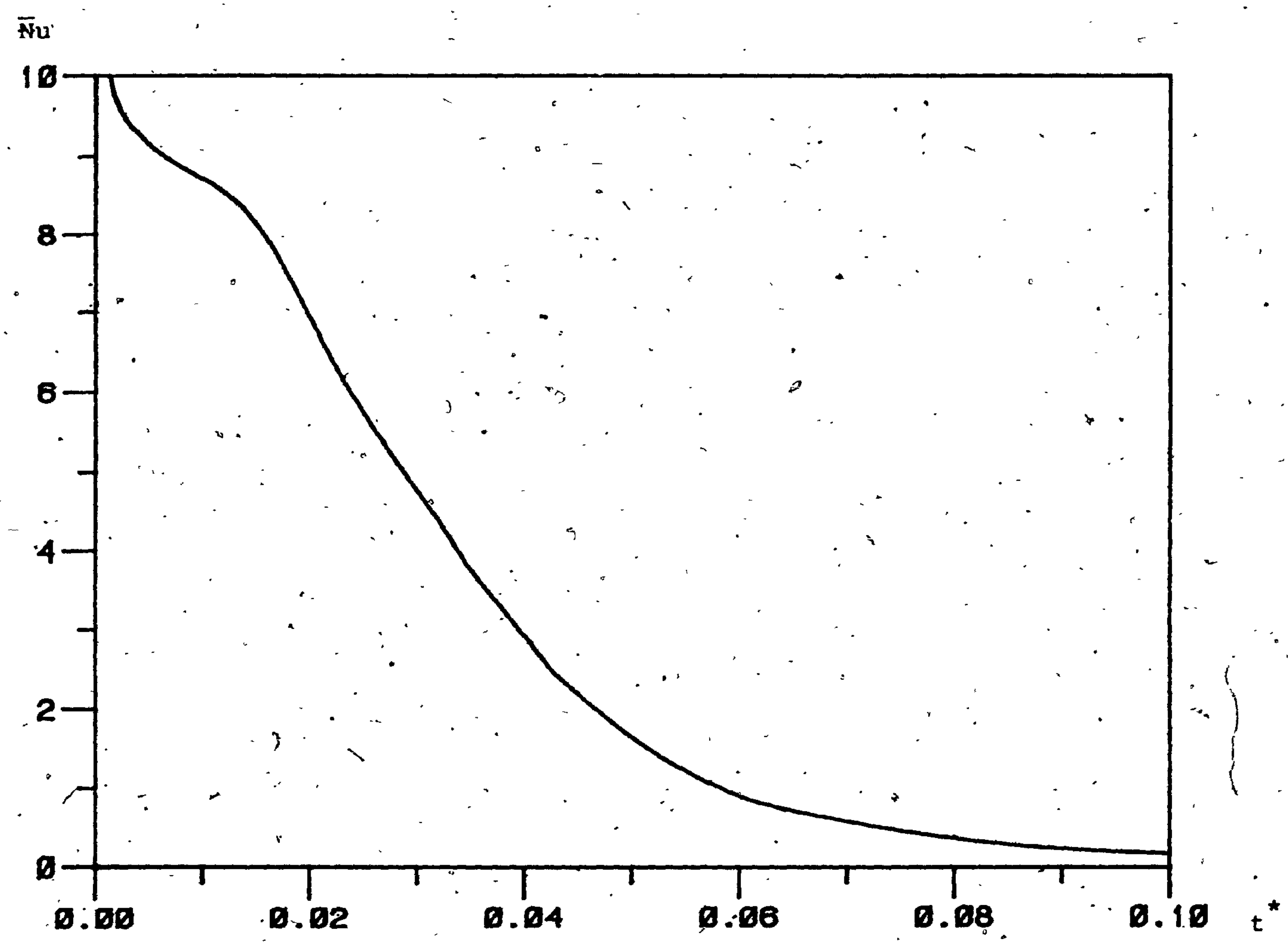

Figure 17. Variation of the average Nusselt number on the liquid-solid interface for the lead fusion welding with time.

5.3 Effect of Bi Numbers

A change in the value of Bi was made to study its effect on the average value of the movement of the liquid-solid interface. The result presented in fig.18 shows that the total time required to cool the entire liquid region can be reduced by increasing the value of Bi. However, the melting rate and the maximum movement of the liquid-solid interface are not significantly affected by changing the value of Bi. This can be understand in the following way. For a larger value of Bi ($=hD/k_s$), a larger convection will be presented to the outer surface of the solid metal. Consequently, more heat will be transferred to the ambient. Thus, only a shorter time will be required to cool the entire liquid region. On the other hand, the convection at the outer surface of the solid metal acts indirectly upon the liquid-solid interface, through the solid region. This results in a minimal effect on the melting rate and on the maximum movement of the liquid-solid interface as a result of changing Bi.

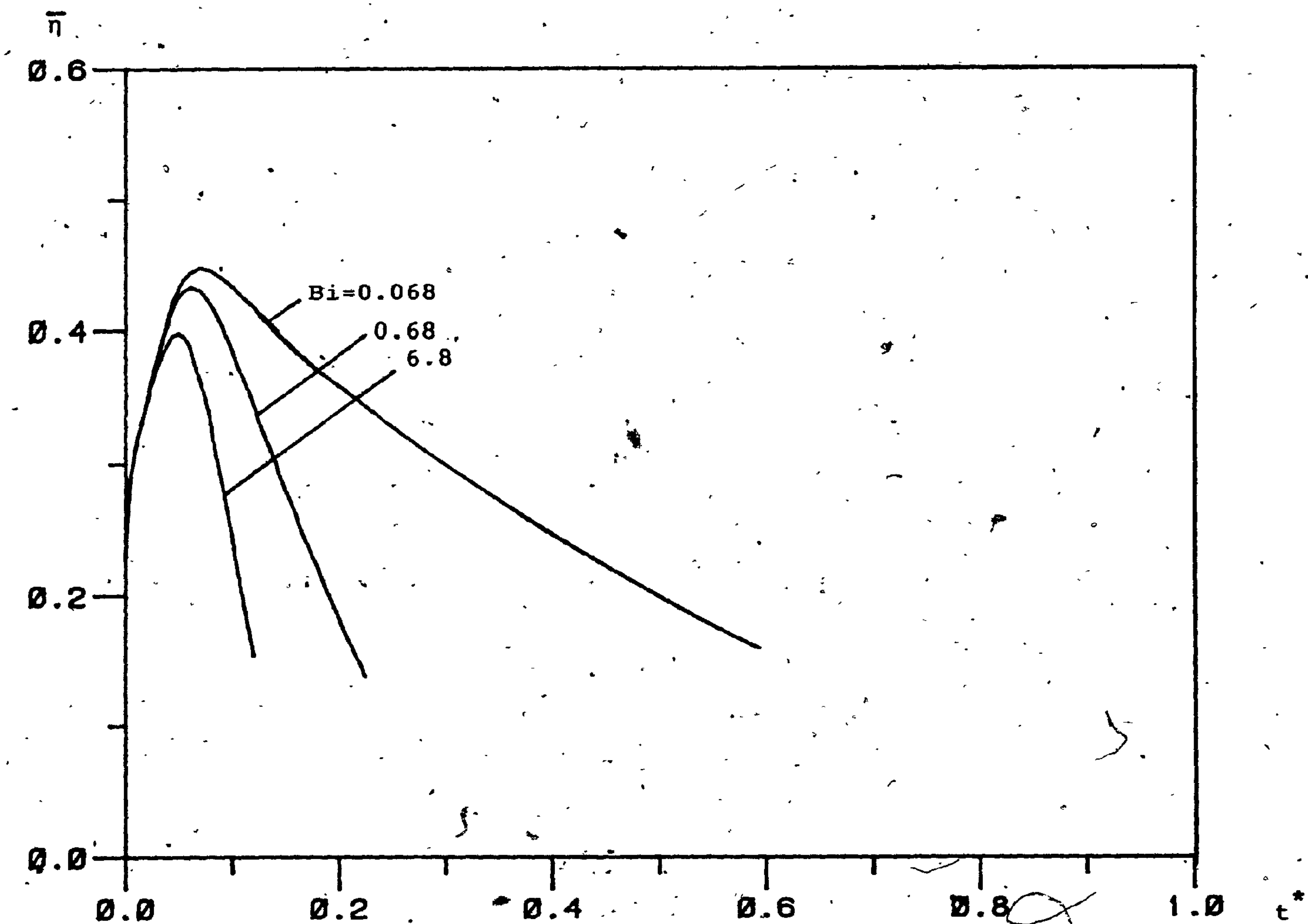

Figure 18. Dependence of the average value of the moving interface upon Bi for the aluminium fusion welding.

5.4 Effect of ϕ_c and ϕ_h

The effects of the values of ϕ_c and ϕ_h on the average value of the movement of the liquid-solid interface are presented in figs.19 and 20, respectively. A higher value of ϕ_c ($=[T_{so}-T_a]/[T_m-T_a]$) may be considered to have higher initial temperature in the solid region. It can be expected (as shown in fig.19) that a larger part of the parent plate will be melted. Furthermore, a longer time will be needed to cool the entire liquid region. Also as shown in fig.19, when the value of ϕ_c decreases below a certain value, the melting process will tend no longer to exist while sole solidification process will presence. Fig.20 indicates the tendency that, as the value of ϕ_h ($=[T_{lo}-T_a]/[T_m-T_a]$) decreases below a certain value, only solidification process will be found. As the value of ϕ_h increases, it can be seen from fig.20 that the rate of the movement of the liquid-solid interface increases. Since a large value of ϕ_h implies a higher value of the superheat in the liquid region, an increase in the melting rate is expected. Hence a large part of the parent plate will be melted, and a longer time is required to cool down the entire liquid region.

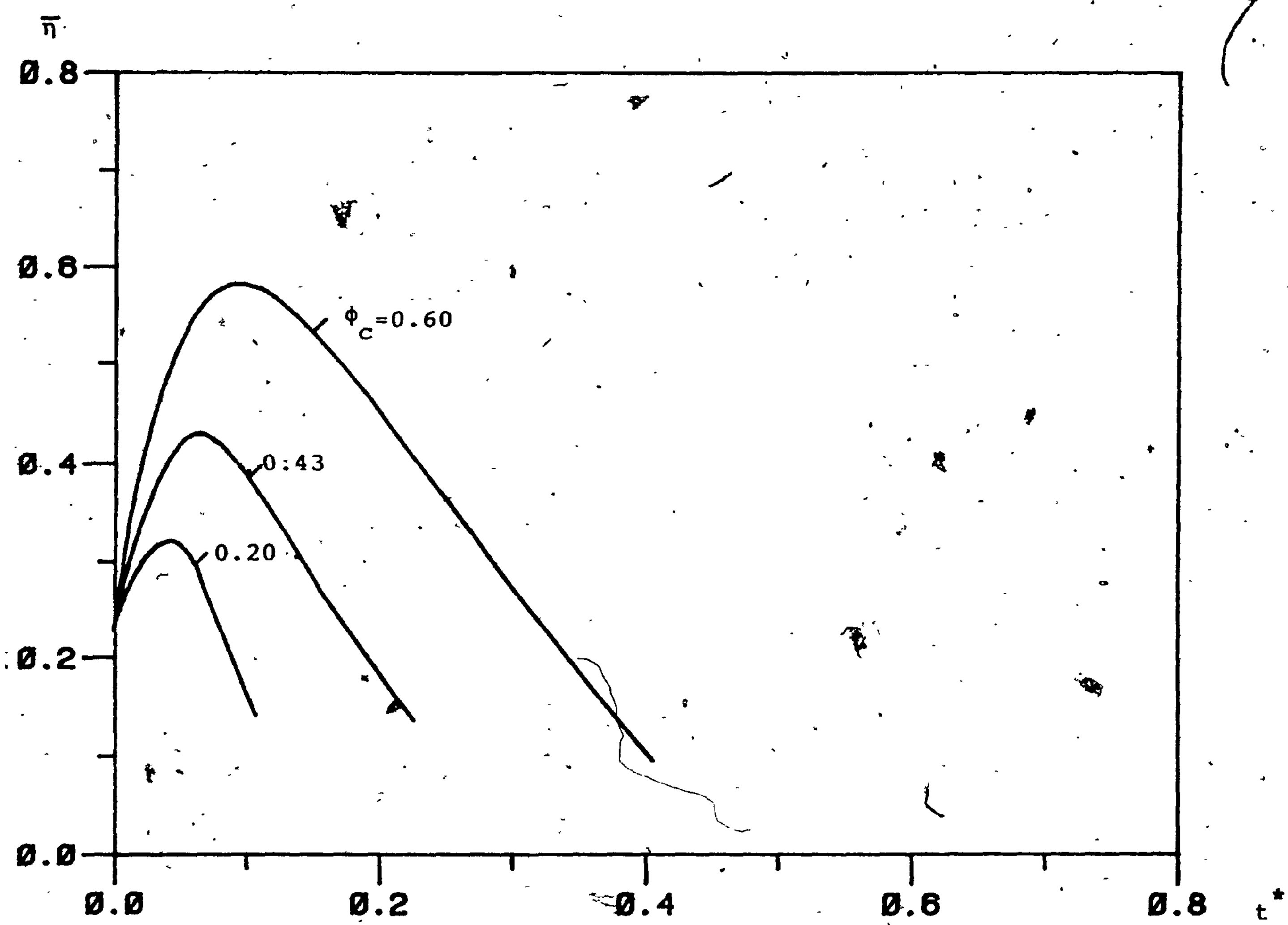

Figure 19. Dependence of the average value of the moving interface upon upon ϕ_c for the aluminium fusion welding.

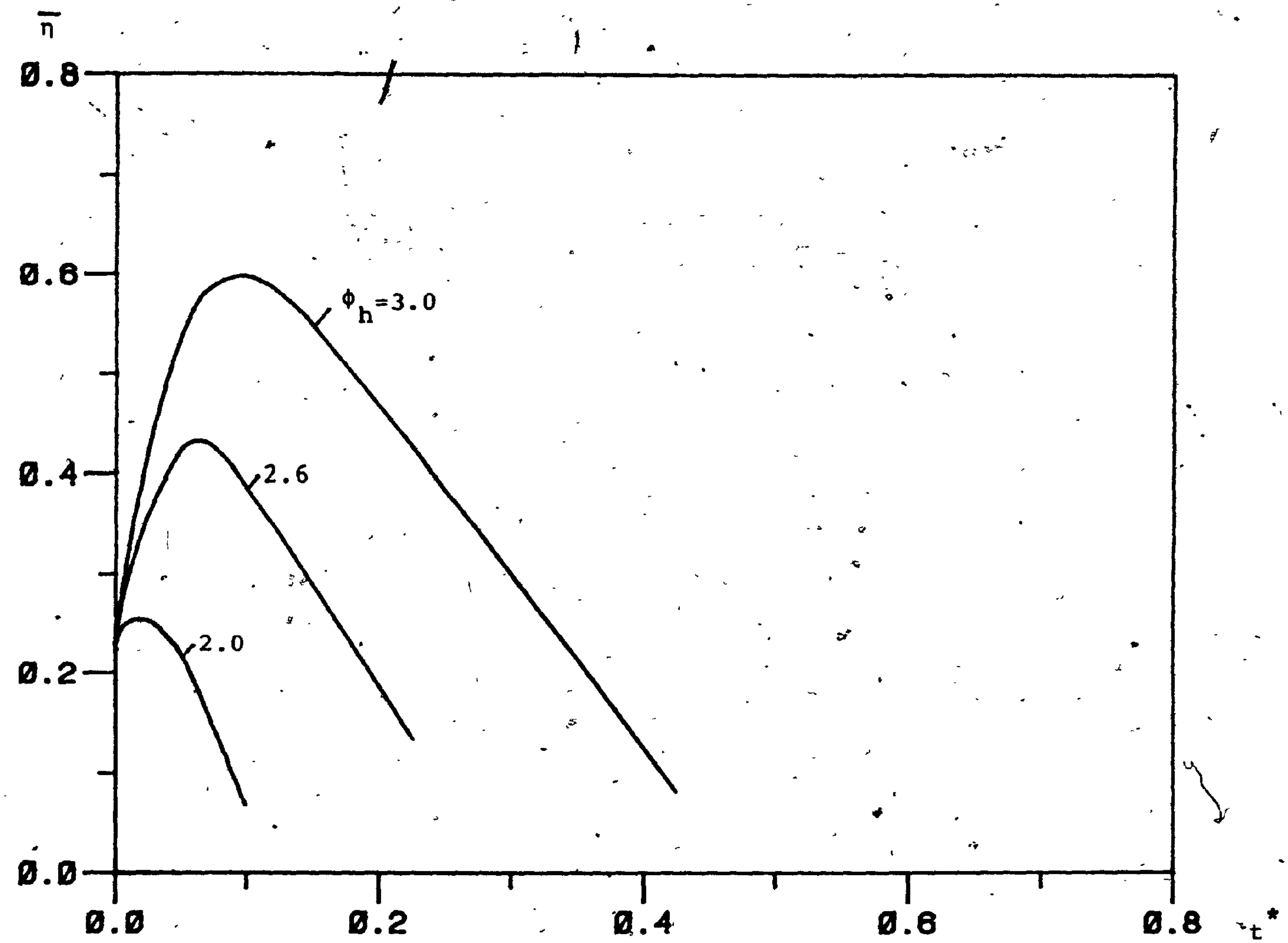

Figure 20. Dependence of the average value of the moving interface upon ϕ_h for the aluminium fusion welding.

5.5 Effect of the Geometric Dimensionless Parameter Rs

The effect of Rs ($=d_1/D$) on the movement of the liquid-solid interface are illustrated in fig.21. In fixing the value of the aspect ratio R ($=H/D$), a change in the value of Rs implies a change in the ratio d_1/H, i.e., the geometric shape of the liquid enclosure. The smaller is the value of Rs, the narrower is the liquid region. It is shown in fig.21 that, a small value of Rs will give a small value for the maximum position of the liquid-solid interface.

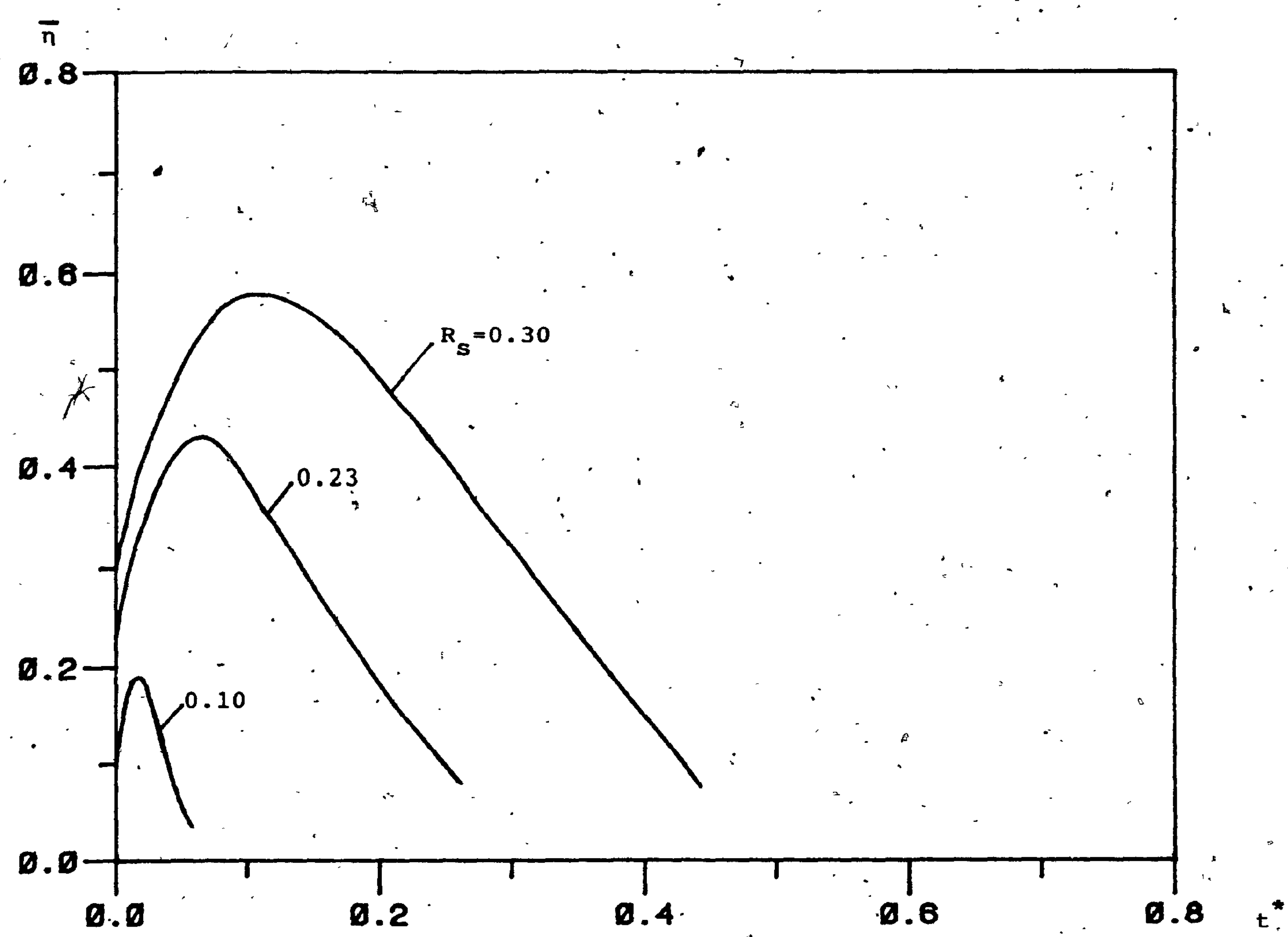

Figure 21. Dependence of the average value of the moving interface upon Rs for the aluminium fusion welding.

CHAPTER SIX

CONCLUSIONS AND SUGGESTIONS

Fusion welding involving, as it does, natural convection in the liquid region, containing both melting and solidification processes, and superheating in the liquid region and subcooling in the solid region, is both a challenging and difficult problem due to the complexities in mathematical formulation and numerical solution. The work discussed in this thesis is aimed at overcoming these difficulties and making it possible to design a solution procedure with satisfactory performance when applied to simulate such fusion-welding process.

A solution procedure incorporating the cubic spline interpolation technique was designed and applied to solve the fusion-welding problem. The accuracy of the cubic spline scheme was tested by comparing its results with those obtained via a simplified one-dimensional model in [2]. Comparing with the results given by a 20×20 uniform grid, it was found that a larger spatial interval (15×15 non-uniform mesh) could still result in a reasonable solution. This offers the opportunity to obtain a satisfactory result with very economic use of computer time and space.

The results obtained using the cubic spline technique show that the fusion-welding problem examined in this thesis is very sensible with the value of Ra number. A higher value of Ra will give a larger value of slope of the liquid-solid interface, that is, a stronger nonlinear ~~moving~~ interface. Results also indicate that the change of the slope of the liquid-solid interface happens only during the melting stage and a small lag after the start of solidification. During the remainder of the solidification process, the moving interface is almost paralell in progression.

The various results show that the cubic spline technique is a good approach to solve such complex problems. The ease of using a non-uniform grid, the high order of accuracy for the function itself, its first derivative, and even second derivative, along with the lower cost in computational time and computer storage, all show the efficiency of the cubic spline techniques. It can be expected that the cubic spline approximation technique will receive even greater application in the solution of engineering problems in the near future.

This thesis will end by pointing to the future, and making several suggestions as to the direction such work might take.

1). The assumption specified in section 2.1, which the thermal conductivity, specific heat, and viscosity are independent of the temperature, should be released in order to coincide with high values of superheating and subcooling.

2). The assumption made in section 2.3, which the slope of moving interface is minimal, should be reconsidered because a large value of slope of moving interface for metal fusion welding process was found in this thesis.

3). An experimental work should be initiated in order to assess the validity of the numerical results.

4). In order to improve the efficiency, a parallel process algorithem could be incorporated with the characteristic of cubic spline approximation technique.

REFERENCES

1. Udin, H., Frank, E.R., and Wulff, J., Welding for engineerings, John Wiley and Sons, New York, 1954.
2. Wang, P., Lin, S. and Kahawita, R., The cubic spline integration technique for solving fusion welding problems, J. of Heat Transfer, Vol.107, pp.485-489, May 1985.
3. Eckert, E.R.G., Goldstein, R.J., Patankar, S.V., Pfender, E., Ramsey, J.W., Simon, T.W., Decker, N. And Kuehn, T.H., Heat transfer --- a review of 1983 literature, Int. J. Heat Mass Transfer, Vol.27, No.12, pp.2179-2214, 1984.
4. Sparrow, E.M., Patankar, S.V., and Ramadhyani, S., Analysis of melting in the presence of natural convection in the melt region, J. of Heat Transfer, Trans. ASME, Vol.99, pp.520-526, 1977.
5. Ramachandran, N., Guptn, J.P., and Jaluria, Y., Thermal and flow effects during solidification in a rectangular enclosure, Int. J. Heat Mass Transfer, Vol.25, pp.187-194, 1982.
6. Rieger, H., Projahn, U. and Beer, H., Analysis of the heat transport mechanisms during melting around a horizontal circular cylinder, Int. J. Heat Mass Transfer, Vol.25, pp.137-147, 1982.
7. Rubin, S.G., and Graves, R.A., A cubic spline approximation for problems in fluid mechanics, NASA TR R-436, Oct. 1975.
8. Pauton, R.L. and Sallee, M.B., Spline function representation for computer solutions to fluid problems, Computers and Fluids, Vol.3, pp.257-269, 1975.

9. Wang, P. and Kahawita, R., The numerical solution of Burger's equation using splines, Presented at the Third Asian Congress of Fluid Mechanics, Beigin, PRC, Oct., 1983.

10. Patrick, J.R., Computational fluid dynamics, Hermosa publishers, 1976.

11. Shamsundar, N., Multidimensional conduction phase change with density change and application to thermal energy storage, Ph.D. Thesis, University of Minnesota, 1976.

12. Bose, A., Experimental and numerical investigation of melting in the presence of natural convection, a master thesis in McGill university, 1983.

13. White, F.M., Viscous fluid flow, McGraw-Hill, New York, 1974.

14. Ahlber, J.H., Nilson, E.N., and Walsh, J.L., The theory of splines and their applications, Academic Press, 1967.

15. Wang, P., Numerical Solution of Second Order Partial Differential Equation Using a Cubic Spline Approximation, Thesis, Dept. of Civil Engineering, Ecole Polytechnical of University of Montreal, July 1983.

16. Rubin, S.G., and Khosla, P.K., High-order numerical solutions using cubic splines, AIAA Journal, Vol.14, No.7, 1976.

17. Carslow, H.S. and Jaeger, J.C., Conduction of heat transfer in solids, Second edition, 1959.

18. Carnahan, B., Lutter, H.A., and Wilkes, J.O., Applied numerical methods, John Wiley and Sons, 1969.

19. Hicks, D.L., One-dimensional Lagrangian hydrodynamics and the IDLH hydrocode, SC-RR-69-728, Snadia laboratories, Albuquerque, New Mexico, 1969.

20. Smithells, C.J., Metals reference book (4th ed.), London, Butterworths, Vol.VI, pp.224-225 and Vol.VIII, pp.685-689, 1967.

21. Paul, R.F., College chemistry (2ed ed.), Prentice Hall Inc., 1958.

22. Lapidus, L., and Pinder, G.F., Numerical solution of partial differential equations in science and engineering, John Wiley and Sons, 1982.

23. Hsu, C.F., Sparrow, E.M., and Patarkar, S.U., Numerical solution of moving boundary problem by boundary immobilization and a control-volume-based finite difference scheme, Int. J. Heat Mass Transfer, Vol.24, pp.1335-1345, 1981.

24. Sparrow, E.M., and Hsu, C.F., Analysis of two-dimensional freezing on the outside of a coolant-carrying tube, Int. J. Heat Mass Transfer, Vol.24, pp.1345-1357, 1981.

25. Ockendon, J.R., and Hodgkins, W.R., Moving boundary problems in heat flow and diffusion, Clarendon Press, 1975.

26. Voller, V. and Cross, M., Accurate solution of melting boundary problems using the enthapy method, Int. J. Heat Mass Transfer, Vol.24, pp.545-556, 1981.

27. Morgar, L., Numerical Methods in thermal problems, Dineridge Press, 1979.

28. Vichevesky, R., Computer methods for partial differential equations, Vol.1, Prentice-Hall, 1981.

29. Shih, T.M., Numerical heat transfer, Hemisphere Publishing Cop., 1984.